DESY 14-026
BONN-TH-2014-05

Probing the Standard Model with Higgs signal rates from the Tevatron, the LHC and a future ILC

P. Bechtle[1,*], S. Heinemeyer[2,†], O. Stål[3,‡], T. Stefaniak[1,4,§], G. Weiglein[5,¶]

[1] *Physikalisches Institut der Universität Bonn*
Nußallee 12, D-53115 Bonn, Germany

[2] *Instituto de Física de Cantabria (CSIC-UC), Santander, Spain*

[3] *The Oskar Klein Centre, Department of Physics*
Stockholm University, SE-106 91 Stockholm, Sweden

[4] *Bethe Center for Theoretical Physics, Bonn University, Germany*

[5] *Deutsches Elektronen-Synchrotron DESY*
Notkestraße 85, D-22607 Hamburg, Germany

Abstract

We explore the room for possible deviations from the Standard Model (SM) Higgs boson coupling structure in a systematic study of Higgs coupling scale factor (κ) benchmark scenarios using the latest signal rate measurements from the Tevatron and LHC experiments. We employ a profile likelihood method based on a χ^2 test performed with `HiggsSignals`, which takes into account detailed information on signal efficiencies and major correlations of theoretical and experimental uncertainties. All considered scenarios allow for additional non-standard Higgs boson decay modes, and various assumptions for constraining the total decay width are discussed. No significant deviations from the SM Higgs boson coupling structure are found in any of the investigated benchmark scenarios. We derive upper limits on an additional (undetectable) Higgs decay mode under the assumption that the Higgs couplings to weak gauge bosons do not exceed the SM prediction. We furthermore discuss the capabilities of future facilities for probing deviations from the SM Higgs couplings, comparing the high luminosity upgrade of the LHC with a future International Linear Collider (ILC), where for the latter various energy and luminosity scenarios are considered. At the ILC model-independent measurements of the coupling structure can be performed, and we provide estimates of the precision that can be achieved.

[*] Electronic address: bechtle@physik.uni-bonn.de
[†] Electronic address: Sven.Heinemeyer@cern.ch
[‡] Electronic address: oscar.stal@fysik.su.se
[§] Electronic address: tim@th.physik.uni-bonn.de
[¶] Electronic address: Georg.Weiglein@desy.de

Contents

1 Introduction

On July 4, 2012 the discovery of a narrow resonance, with a mass near 125.7 GeV, in the search for the Standard Model (SM) Higgs boson at the Large Hadron Collider (LHC) was announced at CERN by both the ATLAS and CMS experiments [1,2]. The initial discovery was based on the data collected at the LHC until June 2012, and these results have since been confirmed and refined using the full 2012 data set [3–6]. Results from the Tevatron experiments [7] support the findings. Within the current experimental and theoretical uncertainties the properties of the newly discovered particle are thus far in very good agreement with the predictions for a SM Higgs boson, including the measurements of signal rates as well as further properties such as spin.

In order to test the compatibility of the newly observed boson with the predictions for the SM Higgs boson based on the data accumulated up to 2012, the LHC Higgs Cross Section Working Group (LHCHXSWG) proposed several benchmark scenarios within an "interim framework" comprising *coupling scale factors* (or *coupling strength modifiers*) [8, 9]. Those have been analyzed by the experimental collaborations [3,5] as well as in further phenomenological studies where Higgs coupling fits have been carried out [10–14]. The results of those analyses show no significant deviations from SM Higgs couplings.

The total Higgs decay width for a Higgs boson mass around 125.7 GeV is not expected to be directly observable at the LHC. In the SM, a total width around 4 MeV is predicted, which is several orders of magnitude below the experimental mass resolution. Suggestions to achieve more sensitive constraints on the total width than the ones limited by the experimental mass resolution have been made based on the analysis of off-shell contributions from above the Higgs resonance in Higgs decays to ZZ^* or WW^* final states [15–18] and of interference effects between the $H \to \gamma\gamma$ signal and the background continuum [19], but the ultimate sensitivities are expected to remain about one order of magnitude above the level of the SM width. The limited access of the LHC to the Higgs width implies that only ratios of couplings can be determined at the LHC—rather than couplings themselves—without additional theory assumptions (see the next section).

Looking beyond the SM, a generic property of many theories with extended Higgs sectors is that the lightest scalar can have nearly identical properties to the SM Higgs boson. In this so-called decoupling limit, additional states of the Higgs sector are heavy and may be difficult to detect in collider searches. Deviations from the Higgs properties in the SM can arise from an extended structure of the Higgs sector, for instance if there is more than one Higgs doublet. Another source of possible deviations from the SM Higgs properties are loop effects from new particles. The potential for deciphering the physics of electroweak symmetry breaking is directly related to the sensitivity for verifying deviations from the SM. Given the far-reaching consequences for our understanding of the fundamental structure of matter and the basic laws of nature, it is of the highest priority to probe the properties of the discovered new particle with a comprehensive set of high-precision measurements and in particular to determine its couplings to other particles with highest precision.

The aim of this paper is to investigate whether there are hints of deviations from the SM Higgs couplings based on a combined picture of all the latest results from the Tevatron and LHC experiments. By investigating the whole spectrum of parametrizations of Higgs coupling strengths ranging from highly constrained to very generic (higher-dimensional) parametrizations, we systematically study potential tendencies in the signal rates and correlations among the fit parameters. In all considered scenarios we allow for an additional Higgs decay mode (or more than one) that is either assumed to be an *invisible* Higgs decay mode, thus yielding a missing energy collider signature, or considered as an *undetectable* decay mode. In the latter case, additional model assumptions have to be imposed to

constrain the total width at the LHC. Based on those assumptions an upper limit on the branching ratio of the undetectable decay mode can be derived for each parametrization.

Going beyond the present status, we analyze the prospects of Higgs coupling determination with future LHC measurements with 300 fb^{-1} and 3000 fb^{-1} of integrated luminosity, as well as with a future e^+e^- International Linear Collider (ILC). The estimated ILC capabilities are presented both for a model-dependent and model-independent fit framework. In the first case, the total width is constrained by imposing the same assumptions as required for the LHC, and we compare the ILC capabilities directly with those of the high-luminosity LHC (HL–LHC) with 3000 fb^{-1}. In the latter case, the total width is only constrained by the total cross section measurement of the $e^+e^- \to ZH$ process at the ILC, thus enabling measurements of coupling scale factors free from theoretical prejudice.

Finding significant deviations in certain Higgs coupling scale factors would provide a strong motivation for studying full models which exhibit a corresponding coupling pattern. However, the fit results obtained within the framework of coupling scale factors can in general *not* be directly translated into realistic new physics models, see Sect. 2.1 for a discussion. Concerning the investigation of particular models of new physics, the most reliable and complete results are obtained by performing a dedicated fit of the Higgs signal rates within the considered model. Such model-dependent fits (for recent examples, see [20–23]), can easily be performed with the generic code `HiggsSignals` [13, 24] that has been used to perform this work.

This paper is organized as follows. Section 2 introduces the fit methodology and the statistical treatment employed in `HiggsSignals`. This section also contains a discussion of the experimental input and and the treatment of theoretical uncertainties, with further details given in the Appendix. In Sect. 3 we present the fit results for the various benchmark parametrizations of Higgs coupling scale factors using all the currently available data from the LHC and the Tevatron. Results for future expectations are presented in Sect. 4. Here the current data is replaced by the projections for the future precisions at the HL–LHC and the ILC, and we discuss to which accuracy the Higgs coupling scale factors can be determined in the various scenarios. The conclusions are given in Sect. 5. Additional information can be found in the three appendices. Appendix A presents the experimental dataset that is used (and its validation). Appendix B contains a discussion of the statistical $\mathcal{P}$-value derived from χ^2 tests of model predictions against measurements of Higgs boson signal rates. Finally, Appendix C contains further details on how we treat the theoretical uncertainties of Higgs production and decay rates.

2 Methodology

2.1 Coupling scale factors

The SM predicts the couplings of the Higgs boson to all other known particles. These couplings directly influence the rates and kinematic properties of production and decay of the Higgs boson. Therefore, measurements of the production and decay rates of the observed state, as well as their angular correlations, yield information that can be used to probe whether data is compatible with the SM predictions.

In the SM, once the numerical value of the Higgs mass is specified, all the couplings of the Higgs boson to fermions, gauge bosons and to itself are specified within the model. It is therefore in general not possible to perform a fit to experimental data within the context of the SM where Higgs couplings are treated as free parameters [25, 26]. In order to test the compatibility of the newly observed boson with the predictions for the SM Higgs boson and potentially to find evidence for deviations in the

2012 data, the LHC Higgs Cross Section Working Group (LHCHXSWG) proposed several benchmark scenarios containing "coupling scale factors" (or "coupling strength modifiers") [8,9]. The idea behind this framework is that all deviations from the SM are computed assuming that there is only one underlying state at 125.7 GeV. It is assumed that this state is a Higgs boson, and that it is SM-like, in the sense that the experimental results so far are compatible with the SM Higgs boson hypothesis. Also the coupling tensor structures are assumed to be as in the SM, meaning in particular that the state is CP-even scalar. Furthermore, the zero width approximation is assumed to be valid, allowing for a clear separation and simple handling of production and decay of the Higgs particle.

In order to take into account the currently best available SM predictions for Higgs cross sections and partial widths, which include higher-order QCD and EW corrections [9,27,28], while at the same time introducing possible deviations from the SM values of the couplings, the predicted SM Higgs cross sections and partial decay widths are dressed with scale factors κ_i. The scale factors κ_i are defined in such a way that the cross sections σ_{ii} or the partial decay widths Γ_{ii} associated with the SM particle i scale with the factor κ_i^2 when compared to the corresponding SM prediction.[1] The most relevant coupling strength modifiers are κ_t, κ_b, κ_τ, κ_W, κ_Z, ... In the various benchmark scenarios defined in Ref. [8,9] several assumptions are made on the relations of these scale factors in order to investigate certain aspects of the Higgs boson couplings, as will be discussed here in Sect. 3.

One should keep in mind that the inherent simplifications in the κ framework make it rarely possible to directly map the obtained results onto realistic models beyond the SM (BSM). The scale factor benchmark scenarios typically have more freedom to adjust the predicted signal rates to the measurements than realistic, renormalizable models. The latter generally feature specific correlations among the predicted rates, which furthermore can depend non-trivially (and non-linearly) on the model parameters. Moreover, constraints from the electroweak precision data and possibly other sectors (dark matter, collider searches, vacuum stability, etc.) can further restrict the allowed parameter space and thus the room for Higgs coupling deviations. Preferred values (and C.L. regions) of the scale factors obtained from profiling over regions in the κ parameter space, which are not covered by the allowed parameter space of the full model, cannot be transferred to the full model. The implications of the Higgs signal rate measurements for the full model can then only be investigated consistently in a dedicated, model-dependent analysis. In that sense, such analyses of realistic BSM models are complementary to the approach followed here, and can easily be performed with the same tools and statistical methods as employed here.

One limitation at the LHC (but not at the ILC) is the fact that the total width cannot be determined experimentally without additional theory assumptions. In the absence of a total width measurement only ratios of κ's can be determined from experimental data. In order to go beyond the measurement of ratios of coupling scale factors to the determination of absolute coupling scale factors κ_i additional assumptions are necessary to remove one degree of freedom. One possible and simple assumption is that there are no new Higgs decay modes besides those with SM particles in the final state. Another possibility is to assume the final state of potentially present additional Higgs decay(s) to be purely invisible, leading to a Z boson recoiling against missing transverse energy in the Higgs-strahlung process at the LHC. By employing constraints from dedicated LHC searches for this signature the total width can be constrained. In both cases, further assumptions need to be imposed

[1] Note, that in this interim framework, slight dependencies of the derived collider observables (cross sections σ_{ii}, partial widths Γ_{ii}) on the remaining Higgs coupling scale factors, κ_j ($j \neq i$), are often neglected. For instance, the cross section of the Higgs-strahlung process $pp \to ZH$ features a small dependence on the top-Yukawa coupling scale factor entering via the NNLO process $gg \to Z^* \to HZ$ [29]. However, for scale factor ranges, $\kappa_t \lesssim 3$, this effect is negligible. Hence, the $pp \to ZH$ cross section can be simply rescaled by κ_Z^2.

on the partial widths of Higgs decays to SM particles which are unobservable at the LHC, like for instance $H \to gg, cc, ss$. As a third possibility, an assumption can be made on the couplings of the Higgs to the SM gauge bosons, $\kappa_{W,Z} \leq 1$ [30]. This assumption is theoretically well-motivated as it holds in a wide class of models, such as any model with an arbitrary number of Higgs doublets, with and without additional Higgs singlets, or in certain classes of composite Higgs models. We will partly make use of these assumptions in our analysis below. More details will be given in Sect. 3.

2.2 The profile likelihood analysis using `HiggsSignals`

We use the public computer program `HiggsSignals` [13,24] (based on the `HiggsBounds-4` library [31–34]), which is a dedicated tool to test model predictions of arbitrary Higgs sectors against the mass and signal rate measurements from Higgs searches at the LHC and the Tevatron. For both types of measurement a statistical χ^2 value can be evaluated, denoted as χ^2_μ (for the signal rates) and χ^2_m (for the Higgs mass). In this work we are only interested in the contribution from the signal rates and fix the Higgs mass to $m_H = 125.7$ GeV.

The Higgs signal rate measurement performed in an analysis i, denoted by $\hat{\mu}_i$, is given by the experiments as a SM normalized quantity. It contains all relevant Higgs collider processes (each comprised of production mode $P_j(H)$ with decay mode $D_j(H)$), and their efficiencies ϵ_j. The observed signal strength modifier can thus be understood as a universal scale factor for the SM predicted signal rates of all involved Higgs processes. The corresponding model-predicted signal rates are calculated as

$$\mu_i = \frac{\sum_j \epsilon^{i,j}_{\rm model}\, \sigma_{\rm model}(P_j(H)) \times {\rm BR}_{\rm model}(D_j(H))}{\sum_j \epsilon^{i,j}_{\rm SM}\, \sigma_{\rm SM}(P_j(H)) \times {\rm BR}_{\rm SM}(D_j(H))}. \tag{1}$$

In general, the efficiencies $\epsilon^{i,j}$ can be different from the SM for models where the influence of Higgs boson interaction terms with a non-standard (higher-dimensional or CP-odd) tensor-structure cannot be neglected [35–41]. In this paper, the efficiencies $\epsilon^{i,j}$ are assumed to be identical for the SM and the (unknown) model predicting the rescaled signal rates. This assumption is valid for *small* deviations from the SM Higgs couplings, where kinematic effects changing the efficiencies can be neglected. However, if significant deviations from the SM are found from the analysis, a more careful investigation of anomalous Higgs couplings [42–44] becomes necessary, including a detailed study of their effects on the efficiencies.

In this work we employ profile likelihood fits based on the χ^2 value derived from `HiggsSignals`. A "naive" $\mathcal{P}$-value, i.e. the probability of a false model rejection, is quoted based on the agreement between the minimal χ^2 value found in the fit and the number of degrees of freedom (ndf). However, the χ^2 value evaluated by `HiggsSignals` does not generically fulfill the prerequisite for this simple $\mathcal{P}$-value estimation: Firstly, `HiggsSignals` uses asymmetric uncertainties in order to take into account remaining non-Gaussian effects in the measurements. Secondly, the signal rate uncertainties are comprised of constant and relative parts. To the latter belong theoretical uncertainties on the cross sections and branching ratios, which are proportional to the signal rate prediction, as well as the luminosity uncertainty, which is proportional to the measured signal rate. These features are necessary in order to effectively reproduce the properties of the full likelihood implementation as done by the experimental collaborations and ensure the correct scaling behavior when testing models different from the SM [13].

These features potentially introduce deviations from the naive χ^2 behavior, which could affect both the extraction of preferred parameter ranges at a certain confidence level (C.L.) from the profiling of

the obtained χ^2 distribution, as well as the calculation of the $\mathcal{P}$-value. In order to estimate the impact of these effects, we performed a Monte Carlo (MC) toy study for a simple one-dimensional scale factor model, which is presented in Appendix B. From this study two important conclusions can be drawn: Firstly, the central value and uncertainties of the estimated fit parameter extracted from the full toy study do indicate a small variation from the naive values extracted from profiling. However, these variations are each within less than 2%. Hence, we are confident that the uncertainties and best fit values quoted later for the profile likelihood scans are valid to a good approximation. Secondly, the $\mathcal{P}$-value obtained in the full MC toy study can be different to the naive χ^2 distribution. For an example of a change in the shape of the observed χ^2 probability density function in toy experiments, see Fig. 23 in Appendix B, which indicates that the actual $\mathcal{P}$-value may be higher than expected when assuming an ideal χ^2 distribution. This effect could be significant and should be taken into account once this technique is used to exclude models, e.g. once the χ^2 probability comes close to 5%. Here, we find naive $\mathcal{P}$-values in the range of 25 – 35%, which are far away from any critical border. Therefore, we are confident that the conclusions drawn from the naive $\mathcal{P}$-values in the remainder of the paper would not change in any significant way if a full toy study or, even better, a full likelihood analysis by the experimental collaborations, was done for every fit.

Within `HiggsSignals` the correlations of theoretical cross section, branching ratio and luminosity uncertainties among different observables are taken into account [13]. For this work, we further develop this implementation to also take into account major correlations of experimental systematic uncertainties for a few important analyses where the necessary information is provided. Specifically, this is the case for the CMS $H \to \gamma\gamma$ analysis [45] and the ATLAS $H \to \tau^+\tau^-$ analysis [46]. More details are given in Sect. 2.3 and Appendix A, including a comparison with official results.

We want to note that an alternative approach for transferring the experimental results into global Higgs coupling or model fits exists [14, 47]. This approach suggests that the experiments provide combined (higher-dimensional) likelihood distributions for scale factors of the Higgs boson production modes. On first sight, an appealing feature is that correlations among the combined analyses of the experimental and theoretical uncertainties for the model investigated by the analysis (usually the SM) are automatically taken care of by the collaborations. However, when going beyond the combination of that specific selection of analyses (e.g. when combining ATLAS and CMS results), or already when combining the likelihoods of different decay modes, detailed knowledge of the correlations of common uncertainty sources is again required. Moreover, a careful treatment of these correlations in a combination (as is done for the simple one-dimensional signal strength measurements in `HiggsSignals`) is far more complicated for higher-dimensional likelihoods. We therefore advise the collaborations to continue providing one-dimensional signal strength measurements, including detailed information on signal efficiencies and correlations, since then the amount of model-dependence in the experimental results is rather minimal [48]. Nevertheless, we also support the suggestions made in Refs. [47], since these higher-dimensional likelihoods are still useful on their own and for validation. Note also recently proposed attempts to disentangle theoretical uncertainties from signal strength measurements [49].

The technical details of the profiled likelihood scans performed in this work are as follows. For an efficient sampling of the parameter space the scans are performed with an adaptive Metropolis (AM) algorithm [50] with flat prior probability distributions using the Markov-Chain Monte Carlo (MCMC) python package `PyMC` [51]. Appropriate initial values for the MCMC chains are found using the maximum a posteriori estimate (MAP) class of `PyMC`. The results are presented in a purely frequentist's interpretation based on the global χ^2 derived from `HiggsSignals` and, optionally, further χ^2 contributions from constraints from invisible Higgs searches at the LHC. This (higher-dimensional) χ^2 distribution is then profiled in order to obtain one- and two-dimensional likelihoods for the fit

parameters and related quantities. The $\{1, 2, 3\}\,\sigma$ parameter regions around the best-fit point are then obtained for values of the χ^2 difference to the minimal value, $\Delta\chi^2 = \chi^2 - \chi^2_{\rm min}$, of $\Delta\chi^2 \leq \{1.0, 4.0, 9.0\}$ for the one-dimensional, and $\Delta\chi^2 \leq \{2.30, 5.99, 11.90\}$ for the two-dimensional profiles, respectively. As discussed above, we also quote for each benchmark scenario the fit quality at the best-fit point, given by $\chi^2_{\rm min}$/ndf, and the corresponding (naively estimated) $\mathcal{P}$-value.

2.3 Experimental input from the Tevatron and the LHC

In the analysis of the present status of potential deviations in the Higgs couplings, presented in Sect. 3, we use the latest available signal strength measurements from the Tevatron and LHC experiments, which are included in `HiggsSignals-1.2.0`. Detailed information on these in total 80 signal strength measurements and the (assumed) signal composition of the production modes is given in Appendix A. Notably, these measurements include the recently published results from ATLAS in the $H \to \tau^+\tau^-$ channel [46], for which we implement correlations of experimental systematic uncertainties in `HiggsSignals`, cf. Appendix A. Based on the comparison of a six-dimensional scale factor fit to the official CMS results [5], we perform an approximate rescaling of the CMS $H \to \gamma\gamma$ measurements [45] from the published Higgs mass value of 125.0 GeV to the best-fit combined mass of 125.7 GeV. Using the rescaled measurements, we find very good agreement with the official CMS fit results, see Appendix A.2 for details.

2.4 Treatment of theoretical uncertainties

We attempt to account for various correlations among the theoretical uncertainties of the cross section and branching ratio predictions. Correlations of theoretical uncertainties among different signal strength observables, as well as correlations among the theoretical uncertainties themselves induced by e.g. common parametric dependencies, are taken into account in `HiggsSignals` since version `1.1.0` [52]. Here we outline how the latter type of correlations is evaluated. More details are given in Appendix C.

The contributions of the major parametric and theoretical (higher-order) uncertainty sources to the total uncertainties of the partial decay widths and production cross sections are given separately by the LHCHXSWG in Refs. [9,53]. However, there is unfortunately no consensus on how these contributions can be properly combined since the shapes of the underlying probability distributions are unknown. Hence, thus far, the use of conservative maximum error estimates is recommended. Nevertheless, such a prescription is needed in order to account for the correlations. In this work we employ covariance matrices evaluated by a Monte Carlo (MC) simulation, which combines the parametric and theoretical uncertainties in a correlated way. The importance of a combination prescription for precision Higgs coupling determination in the future ILC era is briefly discussed in Appendix C.

The relative parametric uncertainties (PU) on the partial Higgs decay widths, $\Delta\Gamma^i_{\rm PU}(H \to X_k)$, from the strong coupling, α_s, and the charm, bottom and top quark mass, m_c, m_b and m_t, respectively, as well as the theoretical uncertainties (THU) from missing higher order corrections, $\Delta\Gamma_{\rm THU}(H \to X_k)$, are given in Tab. 1 of Ref. [9]. The PUs are given for each decay mode for both positive and negative variation of the parameter. From this response to the parameter variation we can deduce the correlations among the various decay modes resulting from the PUs. More importantly, correlations between the branching ratio uncertainties are introduced by the total decay width, $\Gamma^{\rm tot} = \sum_k \Gamma(H \to X_k)$.

The covariance matrix for the Higgs branching ratios is then evaluated with a toy MC: all PUs are smeared by a Gaussian of width $\Delta\Gamma^i_{\rm PU}(H \to X_k)$, where the derived correlations are taken into

account. Similarly, the THUs are smeared by a Gaussian or a uniform distribution within their uncertainties. We find that both probability distributions give approximately the same covariance matrix. A detailed description of our procedure is given in Appendix C, including a comparison of different implementations and assumptions on the theoretical uncertainties in the light of future data from the high luminosity LHC and ILC. Overall, we find slightly smaller estimates for the uncertainties than those advocated by the LHCHXSWG, cf. Appendix C. This is not surprising, since the (very conservative) recommendation is to combine the uncertainties linearly.

Using the present uncertainty estimates [9], the correlation matrix for the branching ratios in the basis $(H \to \gamma\gamma, WW, ZZ, \tau\tau, bb, Z\gamma, cc, \mu\mu, gg)$ is given by

$$(\rho^{\rm SM}_{{\rm BR},ij}) = \begin{pmatrix} 1 & 0.91 & 0.91 & 0.71 & -0.88 & 0.41 & -0.13 & 0.72 & 0.60 \\ 0.91 & 1 & 0.96 & 0.75 & -0.94 & 0.43 & -0.14 & 0.76 & 0.64 \\ 0.91 & 0.96 & 1 & 0.75 & -0.93 & 0.43 & -0.13 & 0.76 & 0.64 \\ 0.71 & 0.75 & 0.75 & 1 & -0.79 & 0.34 & -0.12 & 0.59 & 0.50 \\ -0.88 & -0.94 & -0.93 & -0.79 & 1 & -0.42 & 0.11 & -0.73 & -0.79 \\ 0.41 & 0.43 & 0.43 & 0.34 & -0.42 & 1 & -0.05 & 0.34 & 0.29 \\ -0.13 & -0.14 & -0.13 & -0.12 & 0.11 & -0.05 & 1 & -0.12 & -0.50 \\ 0.72 & 0.76 & 0.76 & 0.59 & -0.73 & 0.34 & -0.12 & 1 & 0.50 \\ 0.60 & 0.64 & 0.64 & 0.50 & -0.79 & 0.29 & -0.50 & 0.50 & 1 \end{pmatrix}. \tag{2}$$

As can be seen, strong correlations are introduced via the total width. As a result, the $H \to b\bar{b}$ channel, which dominates the total width, as well as the $H \to c\bar{c}$ channel are anti-correlated with the remaining decay modes.

For the production modes at the LHC with a center-of-mass energy of 8 TeV the correlation matrix in the basis (ggH, VBF, WH, ZH, $t\bar{t}H$) is given by

$$(\rho^{\rm SM}_{\sigma,ij}) = \begin{pmatrix} 1 & -2.0 \cdot 10^{-4} & 3.7 \cdot 10^{-4} & 9.0 \cdot 10^{-4} & 0.524 \\ -2.0 \cdot 10^{-4} & 1 & 0.658 & 0.439 & 2.5 \cdot 10^{-4} \\ 3.7 \cdot 10^{-4} & 0.658 & 1 & 0.866 & -9.8 \cdot 10^{-5} \\ 9.0 \cdot 10^{-4} & 0.439 & 0.866 & 1 & 2.8 \cdot 10^{-4} \\ 0.524 & 2.5 \cdot 10^{-4} & -9.8 \cdot 10^{-5} & 2.8 \cdot 10^{-4} & 1 \end{pmatrix}. \tag{3}$$

Significant correlations appear between the gluon fusion (ggH) and $t\bar{t}H$ production processes due to common uncertainties from the parton distributions and QCD-scale dependencies, as well as among the vector boson fusion (VBF) and associate Higgs-vector boson production (WH, ZH) channels.

These correlations are taken into account in all fits presented in this work. The numerical values presented in Eqs. (2) and (3) are evaluated for the setting used in the fits to current measurements, cf. Sect. 3, as well as in the conservative future LHC scenario (S1), see Sect. 4.1. For the other future scenarios discussed in Sect. 4, we re-evaluate the covariance matrices based on the assumptions on future improvements of parametric and theoretical (higher-order) uncertainties. However, while the magnitude of the uncertainties changes in the various scenarios discussed later, we find that the correlations encoded in Eqs. (2) and (3) are rather universal. A comparison of uncertainty estimates among all future scenarios we discuss, as well as with the recommended values from the LHCHXSWG, can be found in Appendix C.

3 Current status of Higgs boson couplings

In this section we explore the room for possible deviations from the SM Higgs boson couplings for various benchmark models, each targeting slightly different aspects of the Higgs sector. We follow

the LHCHXSWG interim framework [8, 9] for probing (small) deviations from the SM Higgs boson couplings by employing simple scale factors for the production and decay rates. Hereby, we assume that the LHC Higgs signal is due to a single narrow resonance with a mass of ~ 125.7 GeV. The experimental signal efficiencies of the various analyses are assumed to be unchanged with respect to the SM Higgs signal. This corresponds to the underlying assumption that the tensor structure of the couplings is the same as in the SM, i.e. we investigate the coupling structure of a $\mathcal{CP}$-even, scalar boson.

The LHC signal rate measurements, i.e. measurements of the product of a production cross section times the branching ratio to a certain final state, do not provide direct information about the total width of the Higgs boson. Hence, the LHC is regarded to be insensitive to probe the total Higgs width, Γ_H, unless it features a very broad resonance, $\Gamma_H \sim \mathcal{O}(\text{few GeV})$. The current best limit, $\Gamma_H < 3.4$ GeV at 95% C.L., is obtained by CMS using the $H \to ZZ^{(*)} \to 4\ell$ channel [54]. An even more recent proposal is to exploit the ZZ invariant mass spectrum in the process $gg \to ZZ^{(*)} \to 4\ell$, where the total Higgs decay width can be constrained due to strongly enhanced contributions from off-shell Higgs production. This has been projected to yield a 95% C.L. upper limit of $\Gamma_H \lesssim 40 \times \Gamma_H^{\text{SM}}$ using current data, and a potential future sensitivity of $\sim 10 \times \Gamma_H^{\text{SM}}$ is claimed for increased integrated luminosity [15, 18]. A total width of that order still allows for a significant branching fraction to undetectable/invisible final states and sizable coupling modifications. SM-like signal rates for a Higgs boson with an increased total width can always be obtained by a simultaneous increase of the branching fraction to undetectable particles and the Higgs couplings to SM particles, if both are allowed to vary and no further assumptions are imposed [30, 55].[2] Given the signal rate measurements from the experiments at the Tevatron and the LHC, this degeneracy can only be overcome by additional model assumptions and constraints.

In our analysis, we generally allow for an additional branching fraction to new physics, BR($H \to$ NP). Concerning the assumptions needed to constrain the total width, we distinguish the two cases of the additional branching fraction being comprised of either *invisible* or *undetectable* Higgs decays. The *invisible* decays are considered to measurable/detectable via e.g. the Higgs-strahlung process, leading to a Z boson recoiling against missing transverse energy at the LHC. Invisible Higgs decays can appear in models where the Higgs boson couples to a light dark matter (DM) candidate, as for instance in light singlet DM models [56] or supersymmetry with a stable neutralino as the lightest supersymmetric particle (LSP). In contrast, the *undetectable* decays cannot be constrained by any present LHC analysis. Possible examples are $H \to gg, cc, ss$ or other light flavored hadronic Higgs decays as these signatures are considered indistinguishable from the background. Other examples can be found in theories beyond the SM, like for instance, the decay to supersymmetric particles that further decay via subsequent SUSY cascades or via $\mathcal{R}$-parity violating interactions [57], also potentially leading to detached vertices. In this work we investigate the following two options to overcome the above discussed degeneracy:

(i) The additional Higgs decay mode(s) feature to 100% an *invisible* final state, BR($H \to$ NP) $\equiv$ BR($H \to$ inv.). Hence, results from ATLAS and CMS searches measuring the recoil of a Z

[2] Although the κ scale factor framework technically features a perfect degeneracy between an increasing BR($H \to$ NP) and increasing scale factors of the Higgs couplings to SM particles if no additional constraints are imposed, the validity of the underlying model assumptions — in particular the assumption of identical signal efficiencies as in the SM — need to be scrutinized carefully in parameter regions with significant deviations from the SM Higgs couplings. In general, effects leading to such large coupling deviations within the underlying (unknown) model may potentially also lead to different kinematical distributions and hence to changed signal efficiencies. Furthermore, the narrow width approximation will become worse for an increasing total width.

boson against missing transverse energy in the $pp \to ZH$ production can be used to constrain $\kappa_Z^2\,\mathrm{BR}(H \to \mathrm{NP})$.

(ii) The Higgs-vector boson coupling scale factor is required to be $\kappa_V \leq 1$ ($V = W, Z$). The Higgs production in the VH and VBF channels is then constrained from above [30]. In this case, no assumption on additional Higgs decay modes needs to be imposed. Hence, an upper limit on $\mathrm{BR}(H \to \mathrm{NP})$ can be derived from the fit result. This assumption is valid for models that contain only singlet and doublet Higgs fields. However, in models with higher Higgs field representations [58, 59] this assumption does generally not hold.

As will be discussed in Section 4.2, both assumptions become obsolete once the direct cross section measurement for $e^+e^- \to HZ$ becomes available from the ILC.

In the following Sections 3.1–3.6 we discuss several fits to benchmark parametrizations of Higgs coupling deviations, where we also allow for an additional Higgs boson decay mode $\mathrm{BR}(H \to \mathrm{NP})$ leading to an invisible final state (*i*). In this case, we further constrain the product $\kappa_Z^2\,\mathrm{BR}(H \to \mathrm{NP})$ by adding the profile likelihood, $-2\log\Lambda$, from the ATLAS search $pp \to ZH \to Z(\mathrm{inv.})$ [60] to the global χ^2 obtained from `HiggsSignals`.[3] In Section 3.7 we instead employ the theoretical constraint $\kappa_V \leq 1$ (*ii*) to constrain the total width. Under this condition we derive for each benchmark parametrization upper limits on a new Higgs decay mode, which apply irrespectively of whether the final state is truly invisible or just undetectable.

If the individual scale factors for the loop-induced Higgs couplings to gluons and photons, κ_g and κ_γ, respectively, are not treated as individual free parameters in the fit, they can be derived from the fundamental Higgs coupling scale factors. We generally denote such *derived* scale factors as $\overline{\kappa}$. Additional genuine loop contributions from new, non-SM particles to these effective couplings are then assumed to be absent. The Higgs-gluon scale factor is then given in terms of κ_t and κ_b as [8, 9]

$$\overline{\kappa}_g^2(\kappa_b, \kappa_t, m_H) = \frac{\kappa_t^2 \cdot \sigma_{\mathrm{ggH}}^{tt}(m_H) + \kappa_b^2 \cdot \sigma_{\mathrm{ggH}}^{bb}(m_H) + \kappa_t\kappa_b \cdot \sigma_{\mathrm{ggH}}^{tb}(m_H)}{\sigma_{\mathrm{ggH}}^{tt}(m_H) + \sigma_{\mathrm{ggH}}^{bb}(m_H) + \sigma_{\mathrm{ggH}}^{tb}(m_H)}. \tag{4}$$

Here, $\sigma_{\mathrm{ggH}}^{tt}(m_H)$, $\sigma_{\mathrm{ggH}}^{bb}(m_H)$ and $\sigma_{\mathrm{ggH}}^{tb}(m_H)$ denote the contributions to the cross section from the top-quark loop, the bottom-quark loop and the top-bottom interference, respectively. For a Higgs mass around 125.7 GeV the interference term is negative (for positive scale factors). Details about state-of-the-art calculations have been summarized in Refs. [9, 27, 28]. We use numerical values for the different contributions to Eq. (4) extracted from `FeynHiggs-2.9.4` [63, 64] for a center-of-mass energy of 8 TeV. These evaluations are based on the calculations presented in Ref. [65, 66]. The top Yukawa contributions are calculated up to NNLO, whereas the bottom Yukawa contributions are evaluated up to NLO. These calculations agree well with the numbers used so far by the experimental collaborations [27].

Similarly to $\overline{\kappa}_g$, the scale factor for the loop-induced Higgs-photon coupling, $\overline{\kappa}_\gamma$, is derived from the coupling scale factors and contributions to the partial width of the involved particles in the loop,

$$\overline{\kappa}_\gamma^2(\kappa_b, \kappa_t, \kappa_\tau, \kappa_W, m_H) = \frac{\sum_{i,j} \kappa_i\kappa_j \cdot \Gamma_{\gamma\gamma}^{ij}(m_H)}{\sum_{i,j} \Gamma_{\gamma\gamma}^{ij}(m_H)}, \tag{5}$$

[3] CMS carried out similar searches for the $pp \to ZH \to Z(\mathrm{inv.})$ process and obtained 95% C.L. upper limits corresponding to $\kappa_Z^2\,\mathrm{BR}(H \to \mathrm{inv.}) \leq 0.75$ (for $Z \to \ell^+\ell^-$) [61] and ≤ 1.82 (for $Z \to b\bar{b}$) [62]. However, unlike ATLAS, CMS does not provide a profile likelihood that can be incorporated into our fit.

where (i,j) loops over the particles tt, bb, $\tau\tau$, WW, tb, $t\tau$,tW, $b\tau$, bW, τW. The Γ^{ij} have been evaluated with HDECAY [67]. The partial widths $\Gamma^{ii}_{\gamma\gamma}$ are derived by setting $\kappa_i = 1$, $\kappa_j = 0$ $(i \neq j)$. Then the cross terms are derived by first calculating $\Gamma_{\gamma\gamma}$ with $\kappa_i = \kappa_j = 1$ and $\kappa_k = 0$ $(k \neq i,j)$, and then subtracting $\Gamma^{ii}_{\gamma\gamma}$ and $\Gamma^{jj}_{\gamma\gamma}$. Despite the absence of a sensitive observable probing the Higgs coupling to $Z\gamma$ directly, we also derive the coupling scale factor $\overline{\kappa}_{Z\gamma}$ in order to infer indirect constraints on this quantity and to evaluate its contribution to the total decay width. This scale factor coupling is derived in complete analogy to $\overline{\kappa}_\gamma$.

In the following benchmark fits, we choose to parametrize our results in terms of the absolute scale factors, κ_i, and an additional branching ratio to new particles, $\mathrm{BR}(H \to \mathrm{NP})$. These parameters can be transformed into the total width scale factor κ_H^2 used in the benchmark model proposals of the LHCHXSWG [8,9],

$$\kappa_H^2 = \frac{\overline{\kappa}_H^2(\kappa_i)}{1 - \mathrm{BR}(H \to \mathrm{NP})}, \tag{6}$$

where $\overline{\kappa}_H^2(\kappa_i)$ is the derived scale factor for the SM total width as induced by the modified Higgs couplings to SM particles, κ_i (both including the fundamental and loop-induced couplings). For an allowed range $\mathrm{BR}(H \to \mathrm{NP}) \in [0,1]$, the total width scale factor, κ_H^2, thus ranges from $\overline{\kappa}_H^2$ to ∞.

Before we study potential deviations from the SM Higgs couplings it is worthwhile to look at the fit quality of the SM itself: Tested against the 80 signal rate measurements we find $\chi^2/\mathrm{ndf} = 84.3/80$ which corresponds to a (naive) $\mathcal{P}$-value of $\sim 35.0\%$.[4] Thus, the the measurements are in good agreement with the SM predictions. However, coupling variations may be able to improve the fit quality if the signal rates actually feature systematic under- or over-fluctuations, indicating deviations in (some of) the Higgs couplings from their SM values. It is the goal of the next sections to systematically search for such tendencies as well as to determine the viable parameter space of possible deviations. Note that, if we slightly modify the SM by only adding a new Higgs decay mode while keeping the couplings at their SM predictions ($\kappa_i = 1$), we obtain 95% C.L. upper limits of $\mathrm{BR}(H \to \mathrm{inv.}) \leq 17\%$ in the case of purely invisible final states of the additional decay mode, and $\mathrm{BR}(H \to \mathrm{NP}) \leq 20\%$ in the case of an undetectable (but not necessarily invisible) decay mode.

3.1 Universal coupling modification

The first benchmark model that we consider contains only one universal Higgs coupling scale factor, κ, in addition to the invisible Higgs decay mode. Hence, all Higgs production cross sections and partial widths to SM particles are universally scaled by κ^2. Although this scenario seems to be overly simplistic it actually represents realistic physics models, such as the extension of the SM Higgs sector by a real or complex singlet [56, 68]. In the presence of singlet-doublet mixing κ can be identified with the mixing angle. Both undetectable and invisible Higgs decays are potentially present in these models.

We show the fit results obtained under the assumption of a fully invisible additional Higgs decay mode as one- and two-dimensional (profiled) $\Delta\chi^2$ distributions in Figs. 1 and 2(a), respectively. The best fit point is found at $\kappa = 1.01^{+0.10}_{-0.08}$ with a $\chi^2_{\mathrm{min}}/\mathrm{ndf} = 84.3/79$, which corresponds to a $\mathcal{P}$-value of $\sim 32.2\%$. The 68% and 95% C.L. ranges are also listed in Tab. 1, along with the corresponding range for the total width scale factor κ_H^2. The two-dimensional $\Delta\chi^2$ distribution in Fig. 2(a) shows

[4] For the SM, where we have no additional invisible or undetectable decay modes, we do not count the ATLAS $\mathrm{BR}(H \to \mathrm{inv.})$ limit into the ndfs.

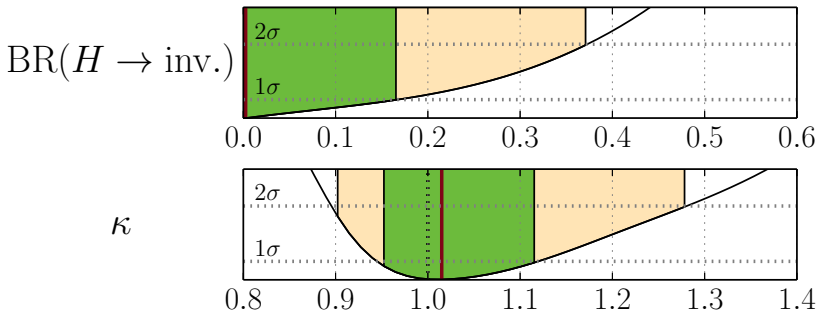

Figure 1: One-dimensional $\Delta\chi^2$ profiles for the parameters in the $(\kappa, \mathrm{BR}(H \to \mathrm{inv.}))$ fit. The best-fit point is indicated by the red line. The 68% (95%) C.L. regions are illustrated by the green (pale yellow) bands.

Fit parameter	best-fit value	68% C.L. range (1D)	95% C.L. range (1D)
$\mathrm{BR}(H \to \mathrm{inv.})$	0.00	$^{+0.17}_{-0.00}$	$^{+0.37}_{-0.00}$
κ	1.01	$^{+0.10}_{-0.08}$	$^{+0.26}_{-0.13}$
κ_H^2	1.03	$^{+0.43}_{-0.13}$	$^{+1.55}_{-0.23}$

Table 1: Best-fit values and 68% and 95% C.L. ranges for the fit parameters obtained from the one-dimensional $\Delta\chi^2$ profiles in the $(\kappa, \mathrm{BR}(H \to \mathrm{inv.}))$ fit.

a strong positive correlation between κ and $\mathrm{BR}(H \to \mathrm{inv.})$. This reflects the fact that a suppression of the branching ratios to SM particles introduced by an additional invisible decay mode needs to be compensated by an increase of the production rates. The allowed region is however bounded at increasing $\mathrm{BR}(H \to \mathrm{inv.})$ by the limit from the invisible Higgs search from ATLAS.

In Fig. 2(b) we illustrate what happens if this constraint is absent, i.e. if no assumptions on the additional Higgs decay mode or model parameters, such as $\kappa_V \leq 1$, are imposed. The allowed parameter range then extends towards arbitrarily large values of κ, and $\mathrm{BR}(H \to \mathrm{NP}) \to 1$ due to the perfect degeneracy mentioned above. In the same figure we indicate present ($\kappa_H^2 \leq 40$) and potential future ($\kappa_H^2 \leq 10$) LHC constraints on the total width that could be derived from off-shell Higgs production in $gg \to ZZ^{(*)} \to 4\ell$ [15, 18]. Such upper limits on the total width scale factor, $\kappa^2_{H,\mathrm{limit}}$, can be used to infer indirect bounds on $\mathrm{BR}(H \to \mathrm{NP})$ and the coupling scale factor κ.[5] Using Eq. (6), the limit can be parametrized by

$$\frac{\kappa^2}{1 - \mathrm{BR}(H \to \mathrm{NP})} \leq \kappa^2_{H,\mathrm{limit}}, \tag{7}$$

while SM signal rates are obtained for

$$\kappa^2 \cdot [1 - \mathrm{BR}(H \to \mathrm{NP})] = 1. \tag{8}$$

[5]Note, that this argument applies also for more general, higher-dimensional scale factor models since all scale factors κ_i are identical in the degenerate case.

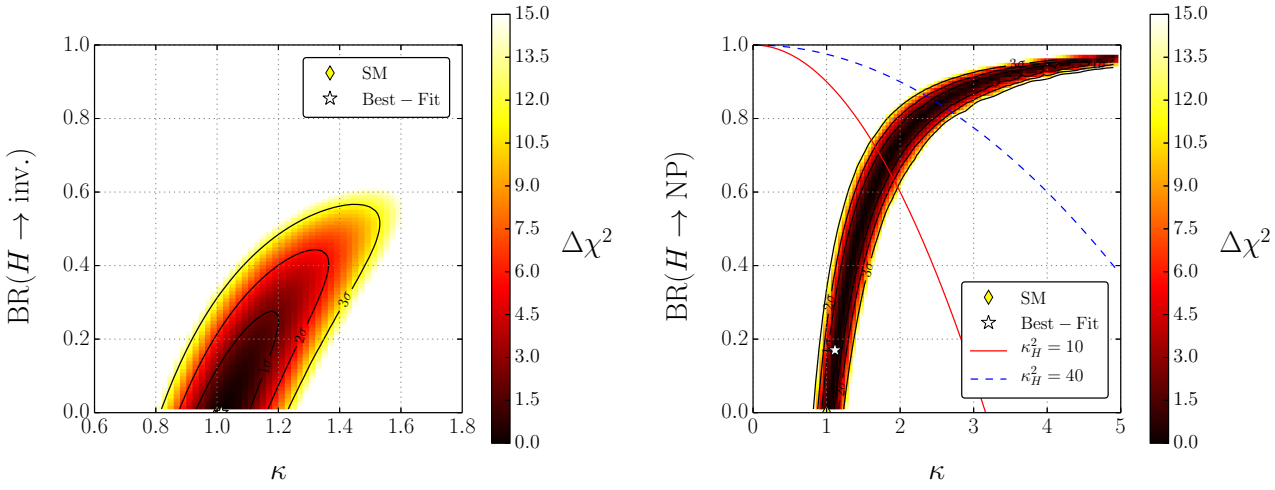

(a) Assuming $\mathrm{BR}(H \to \mathrm{NP}) \equiv \mathrm{BR}(H \to \mathrm{inv.})$

(b) No assumptions. The blue and red contours indicate current and prospective limits, respectively, on the total width from off-shell Higgs production at the LHC [15, 18].

Figure 2: Two-dimensional $\Delta\chi^2$ profiles for the fit parameters in the $(\kappa, \mathrm{BR}(H \to \mathrm{NP}))$ fit.

For a given upper limit of the total width scale factor, $\kappa^2_{H,\mathrm{limit}}$, we can thus infer the indirect bounds

$$\kappa \leq \sqrt{\kappa_{H,\mathrm{limit}}}, \qquad \mathrm{BR}(H \to \mathrm{NP}) = 1 - \kappa^{-1}_{H,\mathrm{limit}}. \tag{9}$$

For a current (prospective) upper limit of $\kappa^2_{H,\mathrm{limit}} = 40$ (10) at the (high-luminosity) LHC, this would translate into $\kappa \leq 2.51$ (1.78) and $\mathrm{BR}(H \to \mathrm{NP}) \leq 84\%$ (68%). However, even when taking these constraints into account there remains a quite large parameter space with possibly sizable $\mathrm{BR}(H \to \mathrm{NP})$. Hence, the LHC will not be capable to determine absolute values of the Higgs couplings in a model-independent way. This is reserved for future e^+e^- experiments like the ILC, which will be discussed in Sect. 4.2.

Returning to the current fit results displayed in Fig. 2, we can also infer from this fit a lower limit on the total signal strength into known final states (normalized to the SM):

$$\kappa^2 \cdot [1 - \mathrm{BR}(H \to \mathrm{NP})] \geq 0.81 \quad (\text{at } 95\% \text{ C.L.}). \tag{10}$$

Note, that this limit is irrespective of the final state(s) of the additional Higgs decay mode(s).

3.2 Couplings to gauge bosons and fermions

The next benchmark model contains one universal scale factor for all Higgs couplings to fermions, κ_F, and one for the $SU(2)$ gauge bosons, κ_V ($V = W, Z$). This coupling pattern occurs, for example, in minimal composite Higgs models [69], where the Higgs couplings to fermions and vector bosons can be suppressed with different factors. The loop-induced coupling scale factors are scaled as expected from the SM structure, Eqs. (4) and (5). Note that $\overline{\kappa}_g$ scales trivially like κ_F in this case, whereas $\overline{\kappa}_\gamma$ depends on the relative sign of κ_V and κ_F due to the W boson-top quark interference term, giving a negative contribution for equal signs of the fundamental scale factors. Due to this sign dependence we allow for negative values of κ_F in the fit, while we restrict $\kappa_V \geq 0$. The assumption of universality

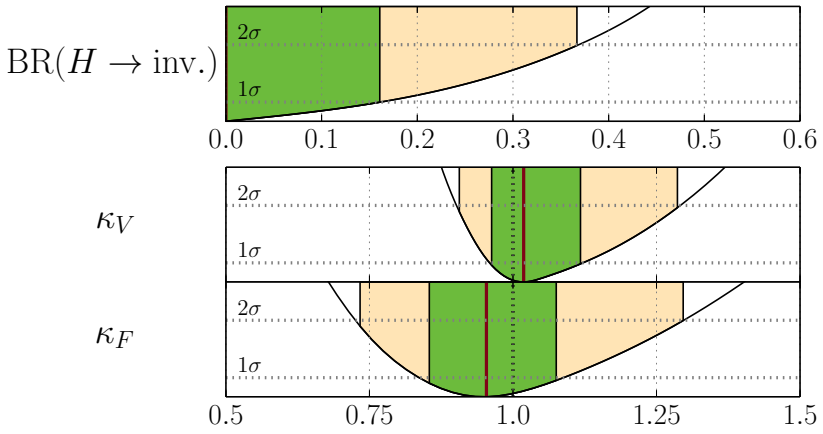

Figure 3: One-dimensional $\Delta\chi^2$ profiles for the parameters in the $(\kappa_V, \kappa_F, \mathrm{BR}(H \to \mathrm{inv.}))$ fit.

Fit parameter	best-fit value	68% C.L. range (1D)	95% C.L. range (1D)
BR($H \to$ inv.)	0.00	$^{+0.16}_{-0.00}$	$^{+0.37}_{-0.00}$
κ_V	1.02	$^{+0.11}_{-0.06}$	$^{+0.27}_{-0.12}$
κ_F	0.95	$^{+0.14}_{-0.12}$	$^{+0.34}_{-0.22}$
κ_H^2	0.95	$^{+0.40}_{-0.20}$	$^{+1.51}_{-0.30}$
$\overline{\kappa}_g$	0.95	$^{+0.14}_{-0.12}$	$^{+0.34}_{-0.23}$
$\overline{\kappa}_\gamma$	1.04	$^{+0.11}_{-0.07}$	$^{+0.28}_{-0.14}$
$\overline{\kappa}_{Z\gamma}$	1.03	$^{+0.10}_{-0.06}$	$^{+0.27}_{-0.12}$

Table 2: Best-fit values and 68% and 95% C.L. regions for the fit parameters obtained from the one-dimensional $\Delta\chi^2$ profiles in the $(\kappa_V, \kappa_F, \mathrm{BR}(H \to \mathrm{inv.}))$ fit.

of the Higgs-gauge boson couplings, $\kappa_W = \kappa_Z$, corresponds to the (approximately fulfilled) custodial global $SU(2)$ symmetry of the SM Higgs sector. We will explore the possibility of non-universal Higgs-gauge boson couplings in the next section.

We show the one- and two-dimensional profiled $\Delta\chi^2$ distributions in Figs. 3 and 4, respectively. At the best-fit point we have $\chi^2_{\mathrm{min}}/\mathrm{ndf} = 84.0/78$, corresponding to a $\mathcal{P}$-value of $\sim 30.1\%$. The best-fit values of the fit parameters and the (derived) scale factors for the total width and loop-induced couplings are listed in Tab. 2 including the one-dimensional 68% and 95% C.L. ranges. Both the Higgs-fermion couplings and Higgs-gauge boson couplings are very close to their SM values. At most, κ_F indicates a very weak tendency to a slight suppression. We can obtain 95% C.L. upper limits on the branching ratio to invisible final states, $\mathrm{BR}(H \to \mathrm{inv.}) \leq 37\%$, and the total decay width $\Gamma^{\mathrm{tot}} \leq 2.46 \cdot \Gamma^{\mathrm{tot}}_{\mathrm{SM}} \approx 10.3$ MeV.

From the two-dimensional χ^2 profiles, shown in Fig. 4, we see that the sector with negative κ_F is disfavored by more than 2σ. In the positive κ_F sector, κ_V and κ_F show a strong positive correlation to preserve SM-like relations among the production cross sections and branching ratios. At this stage, due to the assumed scaling universality of all Higgs couplings to fermions and gauge bosons, the fit

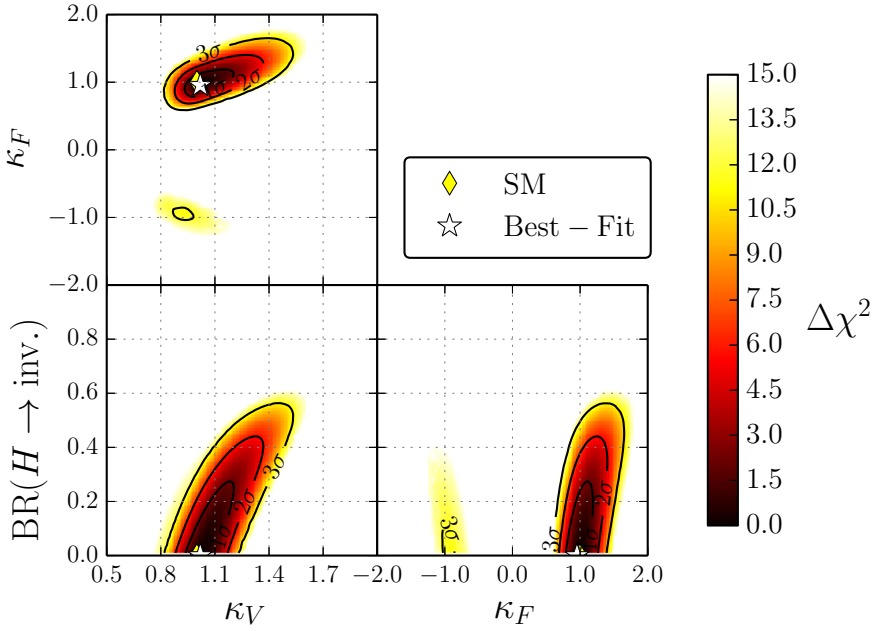

Figure 4: Two-dimensional $\Delta\chi^2$ profiles for the parameters in the $(\kappa_V, \kappa_F, \mathrm{BR}(H \to \mathrm{inv.}))$ fit.

does not have enough freedom to resolve small potentially present tendencies in the Higgs signal rates, but rather reflects the overall global picture. Hence, we expect the correlation of κ_V with the Higgs fermion coupling scale factor(s) to diminish once more freedom is introduced in the Yukawa coupling sector. This will be discussed in Section 3.4. Furthermore, Fig. 4 shows that both κ_V and κ_F are positively correlated with $\mathrm{BR}(H \to \mathrm{inv.})$, similarly to the case with an overall coupling scale factor (cf. Fig. 2).

3.3 Probing custodial symmetry

Experimentally, deviations from the custodial global $SU(2)$ symmetry are strongly constrained by the oblique (Peskin-Takeuchi) T parameter [70] obtained in global electroweak fits [71]. Nevertheless, as an independent and complementary test, it is important to investigate the universality of the Higgs-gauge boson couplings directly using the signal rate measurements.

Here, we restrict the analysis to the simplest benchmark model probing the custodial symmetry, consisting of individual scale factors for the Higgs couplings to W and Z-bosons, κ_W and κ_Z, respectively, and a universal scale factor for the Higgs-fermion couplings, κ_F. Again, we also allow for an additional invisible decay mode, $\mathrm{BR}(H \to \mathrm{inv.})$. Note that, besides the direct signal rate measurements in the channels $H \to WW^{(*)}$ and $H \to ZZ^{(*)}$, different constraints apply to the scale factors κ_W and κ_Z: The loop-induced coupling scale factors $\overline{\kappa}\gamma$ and $\overline{\kappa}_{Z\gamma}$ are only affected by κ_W and κ_F, hence κ_Z plays a subdominant role in the important channel $H \to \gamma\gamma$ by only affecting the (subdominant) production modes HZ and VBF. In contrast, the invisible Higgs search does not constrain κ_W at all, but only the product $\kappa_Z^2 \mathrm{BR}(H \to \mathrm{inv.})$. Since the WZ boson interference term in the vector boson fusion channel is neglected, we can impose $\kappa_Z \geq 0$ without loss of information. As in Sect. 3.2, we furthermore impose $\kappa_W \geq 0$ and accommodate the sign dependence in the loop-induced couplings by

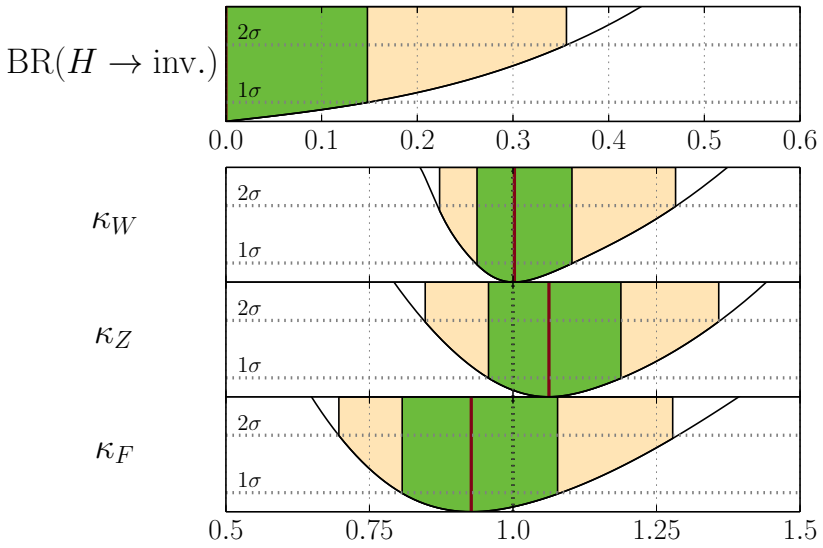

Figure 5: One-dimensional $\Delta\chi^2$ profiles for the parameters in the $(\kappa_W, \kappa_Z, \kappa_F, \mathrm{BR}(H \to \mathrm{inv.}))$ fit.

Fit parameter	best-fit value	68% C.L. range (1D)	95% C.L. range (1D)
BR($H \to$ inv.)	0.00	$^{+0.15}_{-0.00}$	$^{+0.36}_{-0.00}$
κ_W	1.00	$^{+0.10}_{-0.07}$	$^{+0.28}_{-0.14}$
κ_Z	1.06	$^{+0.13}_{-0.11}$	$^{+0.30}_{-0.22}$
κ_F	0.93	$^{+0.16}_{-0.12}$	$^{+0.36}_{-0.23}$
κ_H^2	0.90	$^{+0.41}_{-0.18}$	$^{+1.45}_{-0.31}$
$\overline{\kappa}_g$	0.93	$^{+0.15}_{-0.12}$	$^{+0.35}_{-0.23}$
$\overline{\kappa}_\gamma$	1.02	$^{+0.11}_{-0.08}$	$^{+0.29}_{-0.16}$
$\overline{\kappa}_{Z\gamma}$	1.00	$^{+0.11}_{-0.07}$	$^{+0.29}_{-0.13}$

Table 3: Best-fit parameter values and 68% and 95% C.L. regions obtained from the one-dimensional $\Delta\chi^2$ profiles in the $(\kappa_W, \kappa_Z, \kappa_F, \mathrm{BR}(H \to \mathrm{inv.}))$ fit.

allowing κ_F to take on negative values.

The results of the fit are shown in Figs. 5 and 6 as one- and two-dimensional χ^2 profiles in the fit parameters. The best-fit values and the (1D) 68% and 95% C.L. intervals of the fit parameters and derived scale factors are listed in Tab. 3. The best fit point features $\chi^2_{\mathrm{min}}/\mathrm{ndf} = 83.7/77$, corresponding to a $\mathcal{P}$-value of $\sim 28.2\%$. Similar as in the previous fit, a very small (non-significant) suppression of the Higgs-fermion coupling scale factor $\kappa_F \sim 0.93$ can be observed. The fit has furthermore a small tendency towards slightly enhanced $\kappa_Z \sim 1.06$, whereas κ_W is very close to the SM value.[6] Both Higgs-gauge boson coupling scale factors agree well within $1\,\sigma$ with the SM, and also with being equal

[6] A stronger tendency like this was also seen in the official ATLAS result [3]. Due to the combination with the measurements from other experiments, the tendency observed in our fit is much weaker.

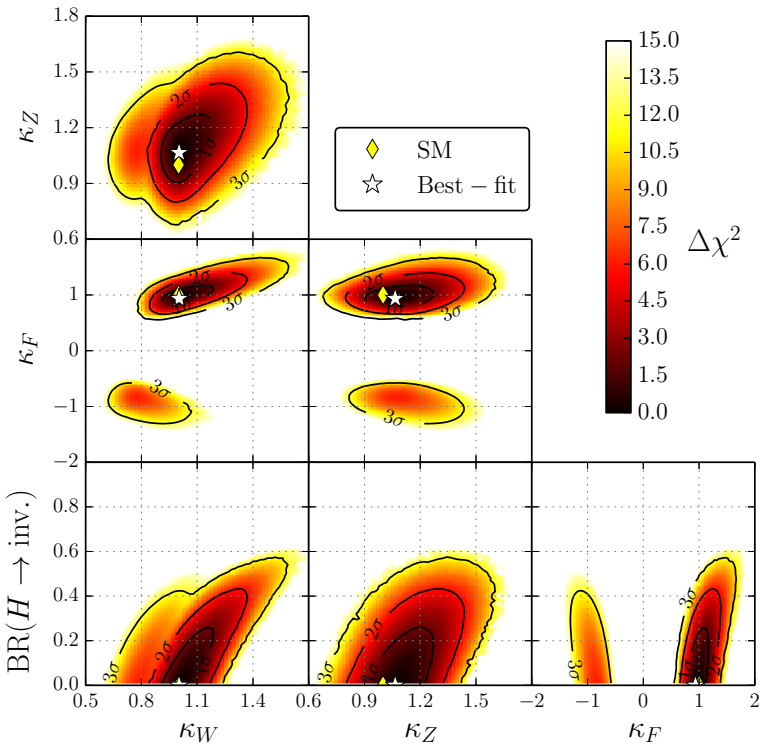

Figure 6: Two-dimensional $\Delta\chi^2$ profiles for the parameters in the $(\kappa_W, \kappa_Z, \kappa_F, \mathrm{BR}(H \to \mathrm{inv.}))$ fit.

to each other. Since the fit shows excellent agreement of the data with the assumption of custodial symmetry, we will assume $\kappa_W = \kappa_Z \equiv \kappa_V$ in the following.

As can be seen from the two-dimensional $\Delta\chi^2$ profiles, Fig. 6, the sector with negative κ_F is less disfavored than in the previous fit, albeit still by more than $2\,\sigma$. Since the connection between κ_W and κ_Z is dissolved, the signal rates of $H \to \gamma\gamma$ can be accommodated more easily in the negative κ_F sector than before. It can be seen in Fig. 6 that the least constrained region for negative κ_F favors values of $\kappa_W \sim 0.70 - 0.85$ and $\kappa_Z \sim 0.95 - 1.20$, i.e. a much larger discrepancy between κ_W and κ_Z than in the positive κ_F sector (which gives the overall best fit).

3.4 Probing the Yukawa structure

We will now have a closer look at the Higgs-fermion coupling structure. In fact, assuming that all Higgs-fermion couplings can be described by one common scale factor—as we have done until now—is motivated in only a few special BSM realizations. A splitting of up- and down-type Yukawa couplings appears in many BSM models, e.g. Two-Higgs-Doublet Models (2HDM) [72, 73] of Type II or in the minimal supersymmetric extension of the SM (MSSM) [74]. Moreover, realistic 2HDMs with even more generic Yukawa couplings (denoted as Type III)—thus featuring additional freedom for the Higgs-charged lepton coupling—can be constructed to be consistent with constraints from flavor-changing neutral currents (FCNCs) [73, 75]. Also in the MSSM, the degeneracy of bottom-type quarks and leptons can be abrogated by radiative SUSY QCD corrections (so-called Δ_b corrections) [76]. Therefore, we now relax the assumption of a universal Higgs-fermion coupling scale factor and in-

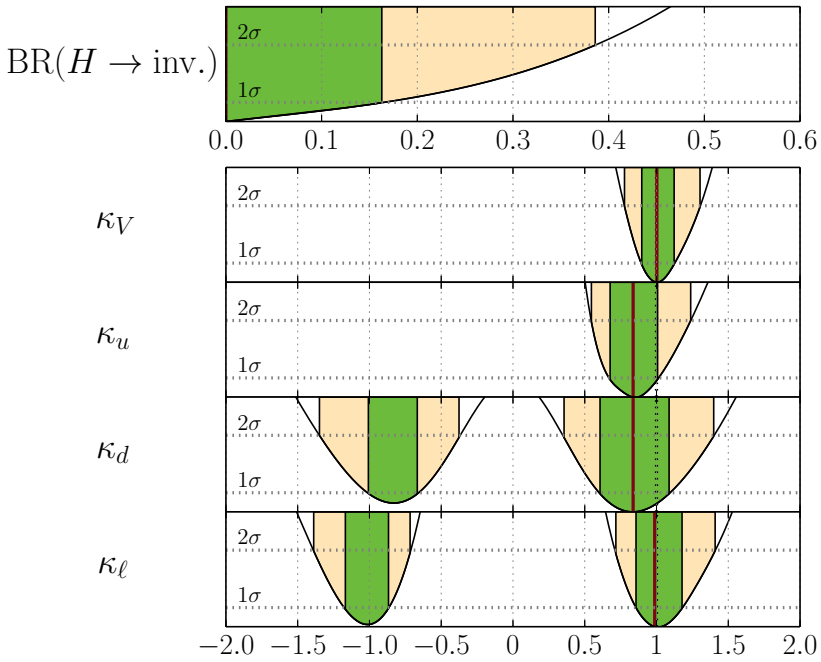

Figure 7: One-dimensional $\Delta\chi^2$ profiles for the parameters in the $(\kappa_V, \kappa_u, \kappa_d, \kappa_\ell, \mathrm{BR}(H \to \text{inv.}))$ fit.

Fit parameter	best-fit value	68% C.L. range (1D)	95% C.L. range (1D)
BR($H \to$ inv.)	0.00	$^{+0.17}_{-0.00}$	$^{+0.39}_{-0.00}$
κ_V	1.00	$^{+0.13}_{-0.11}$	$^{+0.31}_{-0.23}$
κ_u	0.84	$^{+0.18}_{-0.17}$	$^{+0.40}_{-0.29}$
κ_d	0.84	$^{+0.26}_{-0.24}$	$^{+0.56}_{-0.49}$
κ_ℓ	0.99	$^{+0.19}_{-0.13}$	$^{+0.42}_{-0.28}$
κ_H^2	0.80	$^{+0.45}_{-0.28}$	$^{+1.53}_{-0.50}$
$\overline{\kappa}_g$	0.84	$^{+0.16}_{-0.12}$	$^{+0.38}_{-0.24}$
$\overline{\kappa}_\gamma$	1.04	$^{+0.15}_{-0.11}$	$^{+0.33}_{-0.24}$
$\overline{\kappa}_{Z\gamma}$	1.01	$^{+0.13}_{-0.10}$	$^{+0.31}_{-0.22}$

Table 4: Best-fit values and 68% and 95% C.L. regions for the fit parameters around the best fit point (positive sector only) obtained from the one-dimensional $\Delta\chi^2$ profiles in the $(\kappa_V, \kappa_u, \kappa_d, \kappa_\ell, \mathrm{BR}(H \to \text{inv.}))$ fit.

troduce common scale factors for all up-type quarks, κ_u, all down-type quarks, κ_d, and all charged leptons, κ_ℓ. All Higgs-fermion coupling scale factors are allowed to take positive and negative values. The parameters κ_V and BR($H \to$ inv.) remain from before.

The one-dimensional $\Delta\chi^2$ profiles of the fit parameters are shown in Fig. 7. The parameter values of the best-fit point, which is found in the sector with all scale factors being positive, are given in

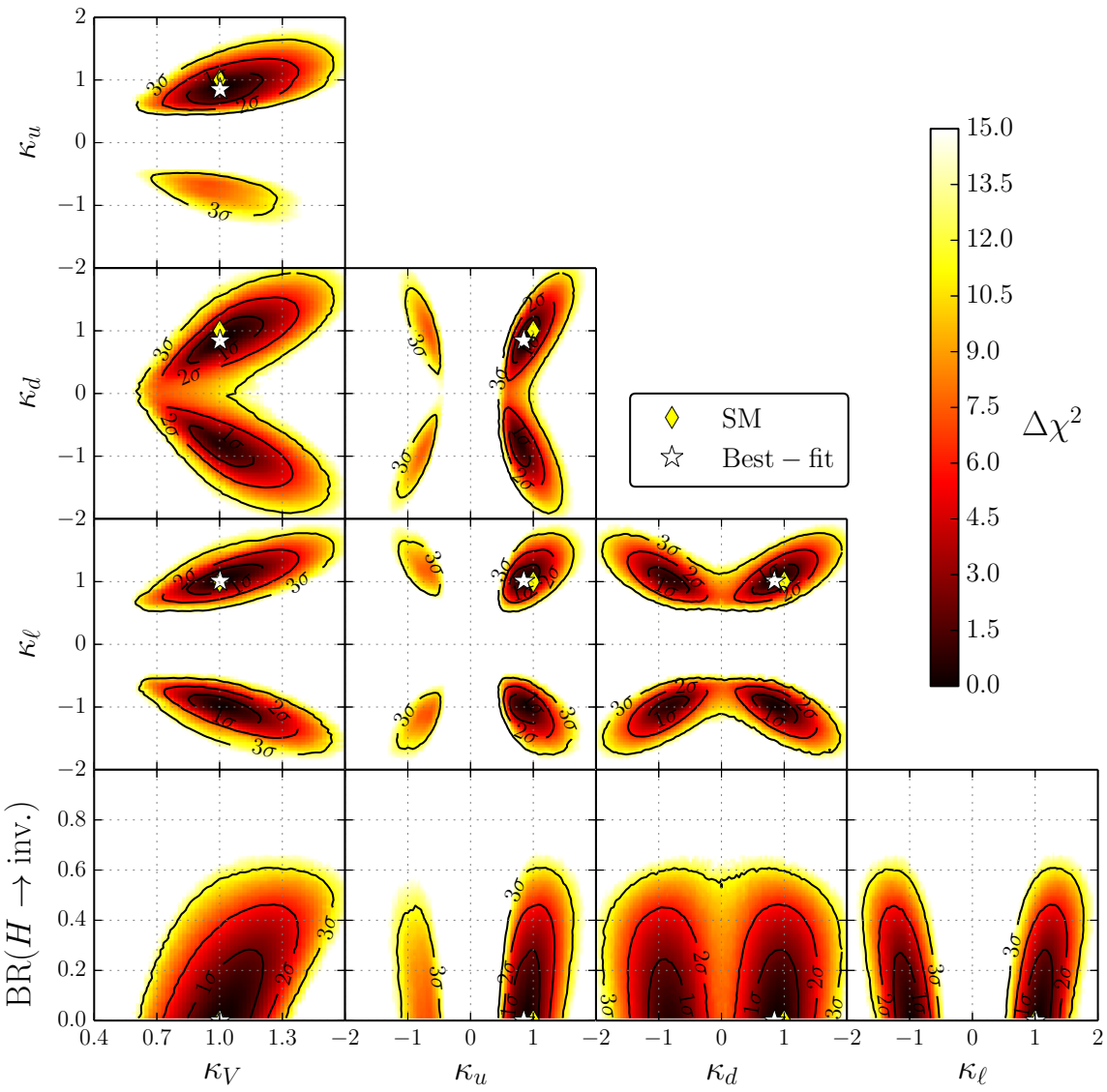

Figure 8: Two-dimensional $\Delta\chi^2$ profiles for the parameters in the $(\kappa_V, \kappa_u, \kappa_d, \kappa_\ell, \mathrm{BR}(H \to \mathrm{inv.}))$ fit.

Tab. 4 along with the (1D) 68% and 95% C.L. intervals. The fit quality is $\chi^2_{\mathrm{min}}/\mathrm{ndf} = 82.8/76$ corresponding to a $\mathcal{P}$-value of $\sim 27.8\%$. As can be clearly seen in Fig. 7, negative values of κ_d and κ_ℓ are still consistent with the measurements within 68% C.L. due to their small influence on the loop-induced Higgs couplings to gluons and/or photons. In particular the sign discrimination of κ_ℓ is very weak. In contrast, negative values of κ_u are disfavored by more than $2\,\sigma$ due to the influence on the Higgs-photon effective coupling (in the convention $\kappa_V \geq 0$). The fit prefers slightly suppressed values of $\kappa_u \sim 0.84$ since $\kappa_g \simeq \kappa_u$, Eq. (4), which is sensitively probed by the LHC measurements via the gluon fusion production mode. Due to the recent $H \to \tau^+\tau^-$ results from ATLAS [46] and CMS [77–79], κ_ℓ is determined to be very close to its SM value with a precision of $\sim 15\%$. We observe a slight (but non-signifcant) suppression of the Higgs-down type quark coupling, $\kappa_d \sim 0.84$. This scale

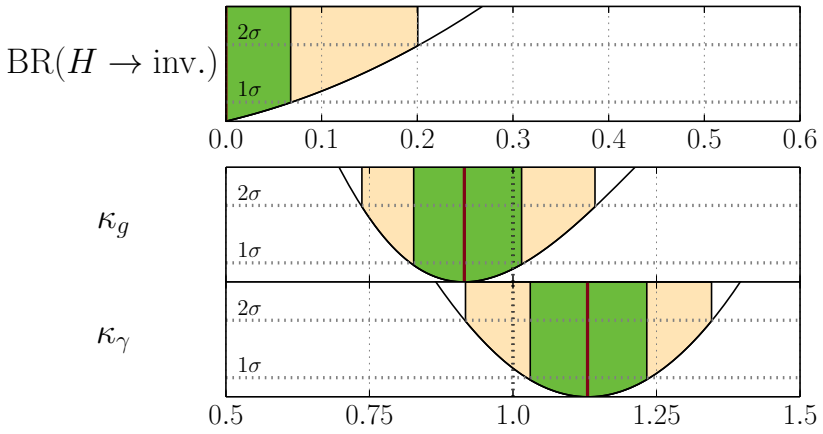

Figure 9: One-dimensional $\Delta\chi^2$ profiles for the parameters in the $(\kappa_g, \kappa_\gamma, \mathrm{BR}(H \to \text{inv.}))$ fit. The best-fit point is indicated by the red line, 68% and 95% C.L. regions are illustrated by the green and pale yellow bands.

factor has the worst precision of the fitted parameters, about $\sim 30\%$. The sign degeneracy of κ_d is slightly broken via the sensitivity of the Higgs-gluon coupling scale factor to the relative sign of κ_t and κ_b, cf. Eq. (4).

The correlation of the fitted coupling scale factors can be seen from the shape of the ellipses in the two-dimensional χ^2 profiles, shown in Fig. 8. The slope of the major axis of the ellipse in the positive sector of the $(\kappa_V,\ \kappa_u)$ plane is with $\sim 0.6 - 0.7$ much shallower than the slopes in the $(\kappa_V,\ \kappa_d)$ and $(\kappa_V,\ \kappa_\ell)$ planes, approximately given by ~ 1.7 and ~ 1.3, respectively. Therefore, this parameterization exhibits more freedom to adjust the predicted signal rates to the Tevatron and LHC measurements. Nevertheless, the best-fit point and favored region is in perfect agreement with the SM and thus the additional freedom does not improve the fit quality. Once more precise measurements of the $H \to \tau^+\tau^-$ and $H \to b\bar{b}$ channels become available, this parametrization can be expected to provide a good test of the SM due to the different correlations among κ_V and the Higgs-fermion coupling scale factors.

3.5 Probing new physics in loop-induced couplings

Up to now we have investigated possible modifications of the fundamental (tree-level) Higgs boson couplings to SM particles and derived the loop-induced couplings to gluons and photons using Eq. (4) and (5), respectively. In this section, we modify these coupling scale factors, κ_g and κ_γ, directly. Such modifications could be introduced by (unknown) new physics loop contributions, while the tree-level Higgs boson couplings are unaffected. Triggered by the hints in the experimental data for a possible $H \to \gamma\gamma$ enhancement, new physics sources for modifications of the Higgs-photon coupling have been subject to many recent studies. For instance, charged supersymmetric particles such as light staus [20,22,80,81] and charginos [82] could give (possibly substantial) contributions. In 2HDMs the Higgs-photon coupling can be altered due to contributions from the charged Higgs boson [83], and in the special case of the Inert Doublet Model [84], modifications of κ_γ and $\kappa_{Z\gamma}$ are indeed the only possible change to the Higgs coupling structure. In addition, many of these models can also feature invisible or undetectable Higgs decays. The effective Higgs-gluon coupling can be modified

Fit parameter	best-fit value	68% C.L. range (1D)	95% C.L. range (1D)
$\mathrm{BR}(H \to \mathrm{NP})$	0.00	$^{+0.07}_{-0.00}$	$^{+0.20}_{-0.00}$
κ_g	0.92	$^{+0.11}_{-0.10}$	$^{+0.23}_{-0.18}$
κ_γ	1.14	$^{+0.11}_{-0.11}$	$^{+0.21}_{-0.22}$
κ_H^2	1.01	$^{+0.08}_{-0.03}$	$^{+0.28}_{-0.03}$

Table 5: Best-fit values and 68% and 95% C.L. regions for the fit parameters around the best fit point obtained from the one-dimensional $\Delta\chi^2$ profiles in the $(\kappa_g, \kappa_\gamma, \mathrm{BR}(H \to \mathrm{inv.}))$ fit.

in supersymmetric models by stop contributions, where one can easily find rate predictions for Higgs production in gluon fusion corresponding to $\kappa_g < 1$ [81, 85].

Our fit parametrization represents the case where indirect new physics effects may be visible only in the loop-induced Higgs-gluon and Higgs-photon couplings. Direct modifications to the tree-level couplings, as introduced e.g. if the observed Higgs boson is a mixed state, are neglected. The more general case where all couplings are allowed to vary will be discussed in the next section. Due to the very small branching ratio $\mathrm{BR}(H \to Z\gamma) \times \mathrm{BR}(Z \to \ell\ell)$ in the SM, the LHC is not yet sensitive to probe $\kappa_{Z\gamma}$. We therefore set $\kappa_{Z\gamma} = \kappa_\gamma$. In addition, here we assume that any additional Higgs decay leads to an invisible final state. Undetectable Higgs decays are discussed in Sect. 3.7.

The fit results are shown as one- and two-dimensional $\Delta\chi^2$ profiles in the fit parameters in Fig. 9 and 10, respectively. The (1D) preferred parameter values are also provided in Tab. 5. In this scenario, the best fit indicates a slight suppression of the Higgs-gluon coupling, $\kappa_g = 0.92$, with a simultaneous enhancement in the Higgs-photon coupling, $\kappa_\gamma = 1.14$. The anti-correlation of these two parameters

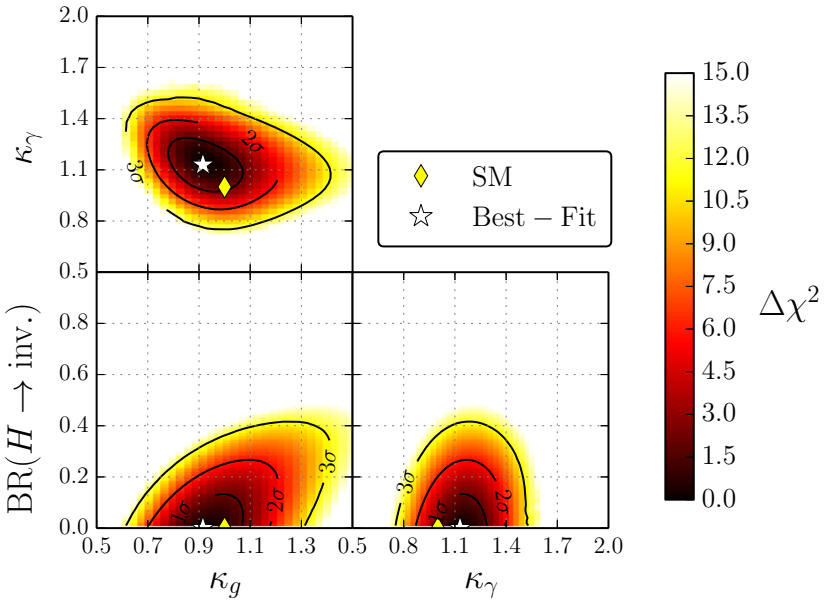

Figure 10: Two-dimensional χ^2 profiles for the fit parameters in the $(\kappa_g, \kappa_\gamma, \mathrm{BR}(H \to \mathrm{inv.}))$ fit.

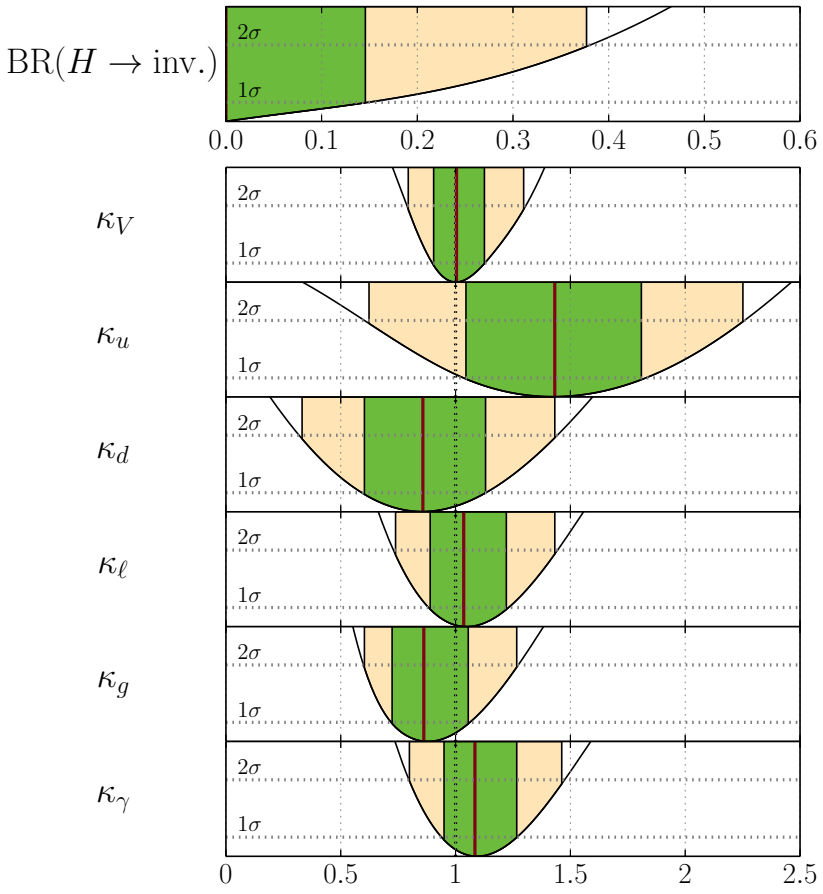

Figure 11: One-dimensional $\Delta\chi^2$ profiles for the parameters in the $(\kappa_V, \kappa_u, \kappa_d, \kappa_\ell, \kappa_g, \kappa_\gamma, \mathrm{BR}(H \to \text{inv.}))$ fit.

can be seen in Fig. 10. It is generated by the necessity of having roughly SM-like $gg \to H \to \gamma\gamma$ signal rates. The best fit point, which has $\chi^2_{\text{min}}/\text{ndf} = 82.6/78$, is compatible with the SM expectation at the 1σ level, as can be seen in Fig. 10. The estimated $\mathcal{P}$-value is $\sim 33.9\%$. Note that $\mathrm{BR}(H \to \text{inv.})$ is much stronger constrained to $\leq 20\%$ (at 95% C.L.) in this parametrization than in the previous fits. The reason being that the suppression of the SM decay modes with an increasing $\mathrm{BR}(H \to \text{inv.})$ cannot be fully compensated by an increasing production cross sections since the tree-level Higgs couplings are fixed. The partial compensation that is possible by an increased gluon fusion cross section is reflected in the strong correlation between κ_g and $\mathrm{BR}(H \to \text{inv.})$, which can be seen in Fig. 10.

3.6 General Higgs couplings

We now allow for genuine new physics contributions to the loop-induced couplings by treating κ_g and κ_γ as free fit parameters in addition to a general parametrization of the Yukawa sector as employed in Sect. 3.4. This gives in total seven free fit parameters, κ_V, κ_u, κ_d, κ_ℓ, κ_g, κ_γ and $\mathrm{BR}(H \to \text{inv.})$. Note, that this parametrization features a perfect sign degeneracy in *all* coupling scale factors, since the only derived scale factor, κ_H^2, depends only on the squared coupling scale factors. For practical

Fit parameter	best-fit value	68% C.L. range (1D)	95% C.L. range (1D)
$\mathrm{BR}(H \to \text{inv.})$	0.00	$^{+0.15}_{-0.00}$	$^{+0.39}_{-0.00}$
κ_V	1.00	$^{+0.13}_{-0.11}$	$^{+0.31}_{-0.22}$
κ_u	1.42	$^{+0.40}_{-0.39}$	$^{+0.83}_{-0.82}$
κ_d	0.86	$^{+0.28}_{-0.27}$	$^{+0.59}_{-0.54}$
κ_ℓ	1.05	$^{+0.19}_{-0.17}$	$^{+0.40}_{-0.32}$
κ_g	0.88	$^{+0.18}_{-0.16}$	$^{+0.39}_{-0.28}$
κ_γ	1.09	$^{+0.18}_{-0.15}$	$^{+0.38}_{-0.29}$
$\overline{\kappa}_H^2$	0.86	$^{+0.36}_{-0.27}$	$^{+0.90}_{-0.48}$
κ_H^2	0.88	$^{+0.43}_{-0.28}$	$^{+1.56}_{-0.50}$
$\Delta\kappa_\gamma$	0.19	$^{+0.14}_{-0.14}$	$^{+0.30}_{-0.28}$
$\Delta\kappa_g$	−0.63	$^{+0.36}_{-0.32}$	$^{+0.90}_{-0.62}$
$\overline{\kappa}_{Z\gamma}$	0.98	$^{+0.13}_{-0.13}$	$^{+0.29}_{-0.25}$

Table 6: Best-fit values and 68% and 95% C.L. regions for the fit parameters (above) and derived scale factors (below) obtained from the one-dimensional $\Delta\chi^2$ profiles in the $(\kappa_V, \kappa_u, \kappa_d, \kappa_\ell, \kappa_g, \kappa_\gamma, \mathrm{BR}(H \to \text{inv.}))$ fit.

purposes, we thus restrict ourselves to the sector where all scale factors are positive. Furthermore, it can be illustrative to decompose κ_g and κ_γ into scale factors $\overline{\kappa}_i$ for the calculable contributions from SM particles (with rescaled couplings) appearing in the loop, as described by Eqs. (4)–(5), and a scale factor $\Delta\kappa_i$ for the genuine new physics contributions:

$$\kappa_g = \overline{\kappa}_g + \Delta\kappa_g, \tag{11}$$

$$\kappa_\gamma = \overline{\kappa}_\gamma + \Delta\kappa_\gamma. \tag{12}$$

This decomposition assumes that the unknown new physics does not alter the loop contributions from SM particles, Eqs. (4)–(5).

The one-dimensional $\Delta\chi^2$ profiles in the fit parameters are shown in Fig. 11. Their best-fit values and preferred parameter ranges are listed together with those of derived scale factors in Tab. 6. The best-fit point features a fit quality of $\chi^2_{\mathrm{min}}/\mathrm{ndf} = 79.9/74$ and thus a $\mathcal{P}$-value of $\sim 29.9\%$. Due to the dissolved dependence between the Yukawa couplings and the effective Higgs-gluon and Higgs-photon couplings, κ_u is far less accurately determined than in previous, more constrained, fits. In fact, it is now dominantly influenced by the recent CMS measurements targeting $t\bar{t}H$ production [86–88], which give a combined signal strength of $\hat{\mu}^{t\bar{t}H}_{\mathrm{CMS}} = 2.5^{+1.1}_{-1.0}$ [89]. Hence, the fit prefers slightly enhanced values, $\kappa_u \sim 1.42$, albeit with very large uncertainties. The scale factors κ_g and κ_γ can now be freely adjusted to match the combined rates of Higgs production in gluon fusion and $\mathrm{BR}(H \to \gamma\gamma)$, respectively. Here we observe the same tendencies as in the previous fit, cf. Sect. 3.5. Due to the slight preference for enhanced κ_u and suppressed κ_g, the fitted new physics contribution to the Higgs-gluon coupling is quite sizable and negative, $\Delta\kappa_g \sim -0.63$. In contrast, the Higgs-photon coupling is fairly well described by the (rescaled) contributions from SM particles alone because the enhanced

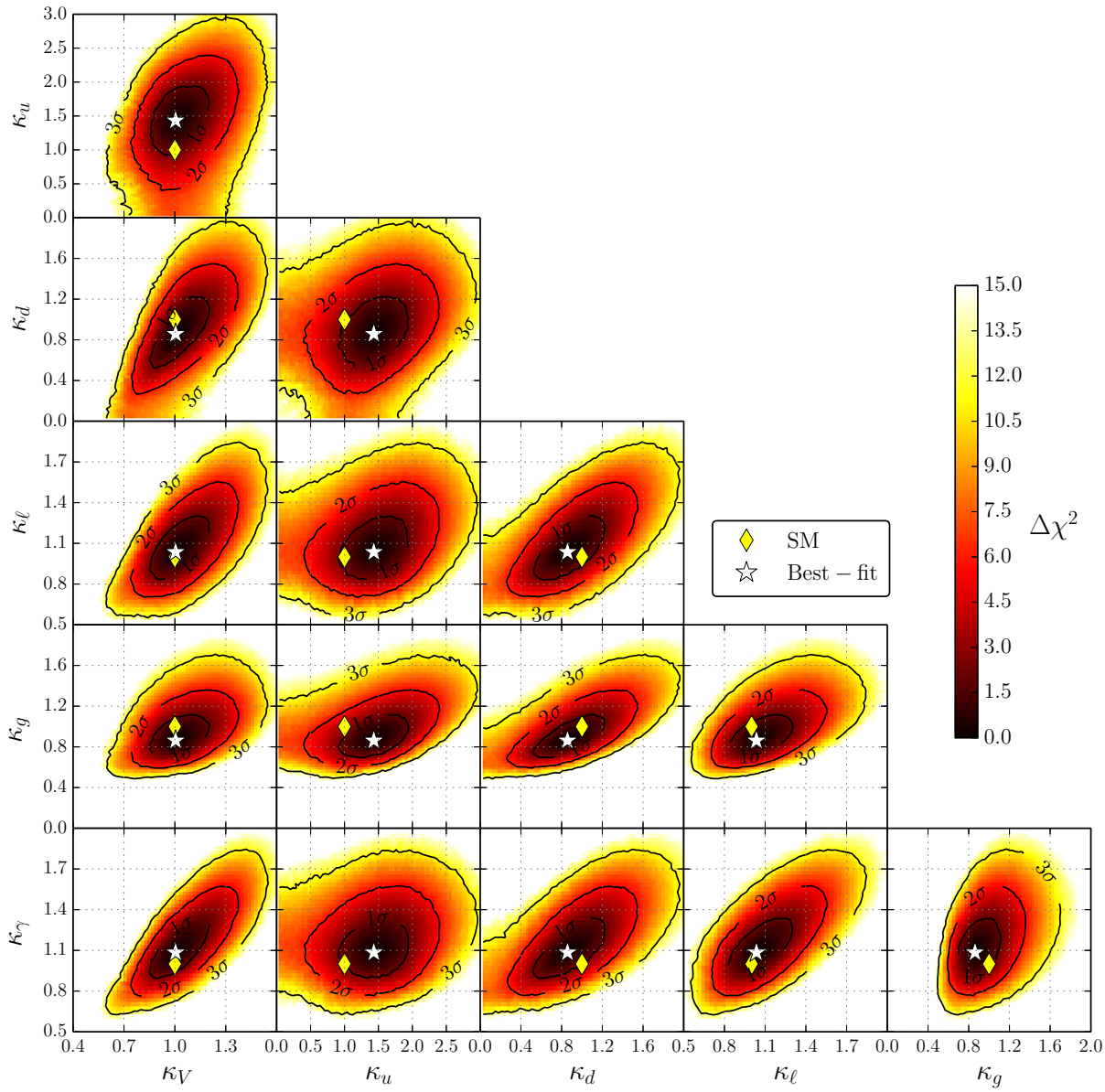

Figure 12: Two-dimensional $\Delta\chi^2$ profiles for the fitted Higgs coupling scale factors in the $(\kappa_V, \kappa_u, \kappa_d, \kappa_\ell, \kappa_g, \kappa_\gamma, \mathrm{BR}(H \to \mathrm{inv.}))$ fit.

κ_u also enhances $\overline{\kappa}_\gamma$ slightly. The favored magnitude for the genuine new physics contribution to the Higgs-photon coupling is $\Delta\kappa_\gamma \sim 0.19$.

The two-dimensional χ^2 profiles of the fitted Higgs coupling scale factors are shown Fig. 12 and their correlations with $\mathrm{BR}(H \to \mathrm{inv.})$ are given in Fig. 13. Similarly as in the fit to the Yukawa structure in Sect. 3.4, all fundamental coupling scale factors are positively correlated. However, the correlations here are much weaker due to the additional freedom introduced for the loop-induced Higgs couplings. In the projection planes for κ_V and the Higgs-fermion coupling scale factors, the ellipses tilted with respect to the previous fit in Section 3.4 towards larger slopes of the major axes, roughly

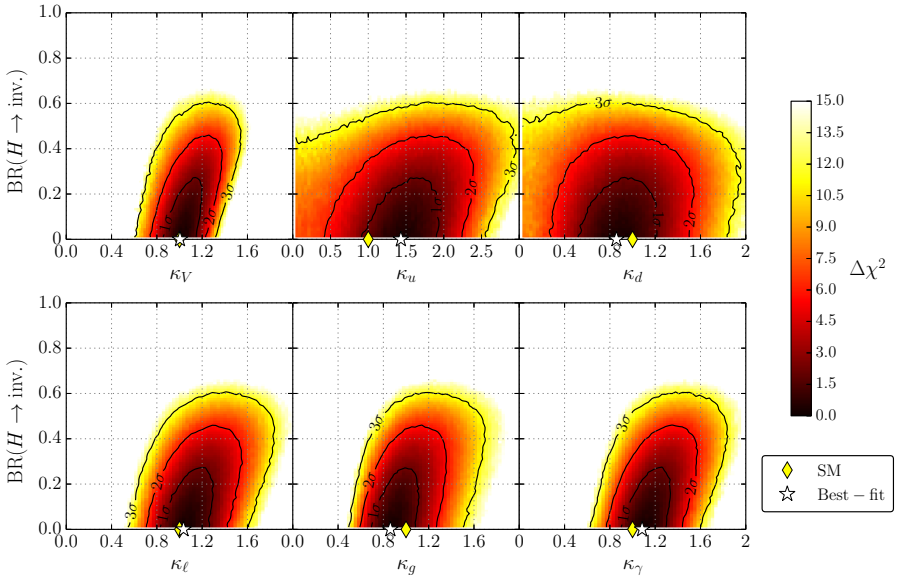

Figure 13: Two-dimensional $\Delta\chi^2$ profiles of the fitted Higgs coupling scale factors with the invisible Higgs decay mode, BR($H \to$ inv.), in the $(\kappa_V, \kappa_u, \kappa_d, \kappa_\ell, \kappa_g, \kappa_\gamma, \text{BR}(H \to \text{inv.}))$ fit.

given by 7.5, 2.5 and 2.8 for the (κ_V, κ_u), (κ_V, κ_d) and (κ_V, κ_ℓ) planes, respectively. This represents the fact that κ_u, κ_d and κ_ℓ are less accurately determined since they are now only probed by the poorly measured $t\bar{t}H$, $H \to b\bar{b}$ and $H \to \tau^+\tau^-$ rates, respectively, while κ_V is still strongly constrained by both the VBF and VH production modes and the decay modes $H \to WW^{(*)}$ and $H \to ZZ^{(*)}$.

The correlations of the fundamental coupling scale factors to the loop-induced couplings scale factors κ_g and κ_γ also turn out to be positive. Here the strongest correlation is observed among κ_g and κ_d, which govern the dominant production and decay modes, respectively. Since the decay $H \to b\bar{b}$ is not yet probed with any accuracy at the LHC, the fit allows for an enhanced decay rate if at the same time the dominant production cross section is also increased in order to compensate for the reduced branching ratios of the remaining decay modes.[7] Nevertheless, the preferred fit region is found for slightly suppressed values of both κ_g and κ_d. A strong positive correlation is also found between κ_V and κ_γ.

It should be noted that the correlation of the loop-induced couplings scale factors κ_g and κ_γ has changed with respect to the previous fit, Sect. 3.5. They now show a weak positive correlation. This is because the general parametrization features again the degeneracy of increasing scale factors and the additional decay mode, which is only broken by the BR($H \to$ inv.) constraint. This leads to a positive correlation among all κ_i which dominates over the small anti-correlations needed to adjust small tendencies in the observed signal rates. This is also reflected in Fig. 13, where all scale factors show a positive correlation with BR($H \to$ inv.).

Comparing the relative (1σ) precision on the individual scale factors obtained here with the results of an official CMS fit analysis[8] presented at the Moriond 2013 conference [5], we assert the improve-

[7] A similar correlation was found in the fit presented in Sect. 3.4 for κ_u and κ_d, because there, κ_u was dominantly influencing the derived Higgs-gluon coupling.

[8] The CMS fit parametrizes the Higgs couplings via the same scale factors as used here, however, the fit does not allow for an additional Higgs decay mode. We furthermore used the CMS fit results to validate our fit procedure, see

Fit	68% C.L. precision of the Higgs coupling scale factors [in %]					
	κ_V	κ_g	κ_γ	κ_u	κ_d	κ_ℓ
CMS Moriond 2013	20%	28%	25%	100%	55%	30%
`HiggsSignals` (LHC $\oplus$ Tev.)	12%	20%	15%	30%	35%	18%

Table 7: Comparison of the relative 68% C.L. precision of the Higgs coupling scale factors obtained by the CMS combination presented at the Moriond 2013 conference [5] and our results from the seven-dimensional scale factor fit using both LHC and Tevatron measurements. The quoted numbers are rough estimates from the (sometimes asymmetric) likelihood shapes, cf. Ref. [5] and Fig. 11.

ments (rough symmetrical estimates) listed in Tab. 7. With a common interpretation of the latest data from ATLAS and CMS (and the Tevatron experiments), a significant improvement of the scale factor determination is achieved. Moreover, the strong improvement in the precision of κ_u is due to the dedicated CMS $t\bar{t}H$ tagged analyses [86–88], which had not been included in the CMS fit. With the latest $H \to \tau^+\tau^-$ measurement by ATLAS the precision of κ_ℓ has also improved significantly. Nevertheless, for all scale factors, potential deviations within $\sim 10\%$ or even more are still allowed at the 1σ level within this benchmark model.

For this most general fit we also show the predicted signal rates for the preferred parameter space in Fig. 14. The rates $R(pp \to H \cdots \to XX)$ are idealized LHC 8 TeV signal rates where all included

Appendix A.2.

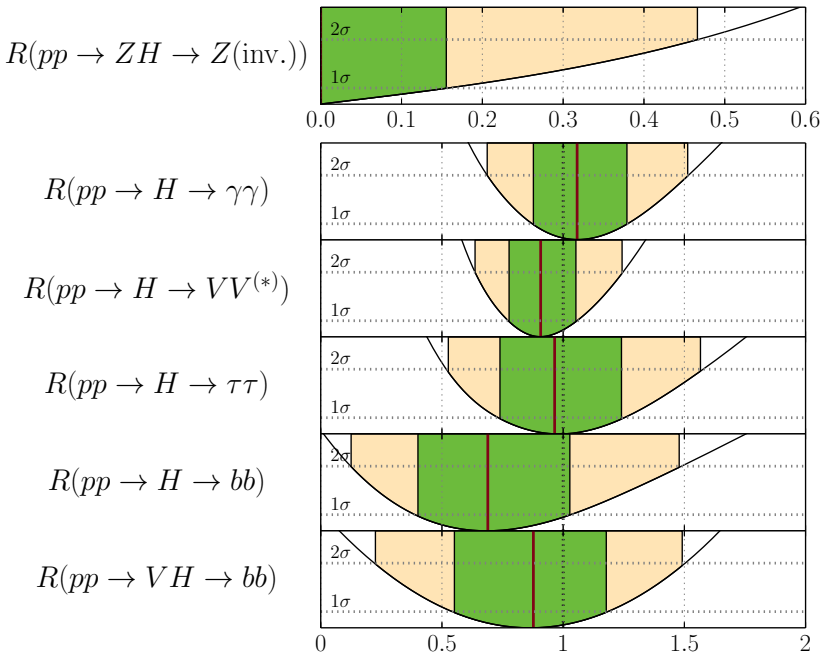

Figure 14: One-dimensional $\Delta\chi^2$ profiles from the $(\kappa_V, \kappa_u, \kappa_d, \kappa_\ell, \kappa_g, \kappa_\gamma, \text{BR}(H \to \text{inv.}))$ fit for the (idealized, SM normalized) signal rates at 8 TeV for the main LHC channels.

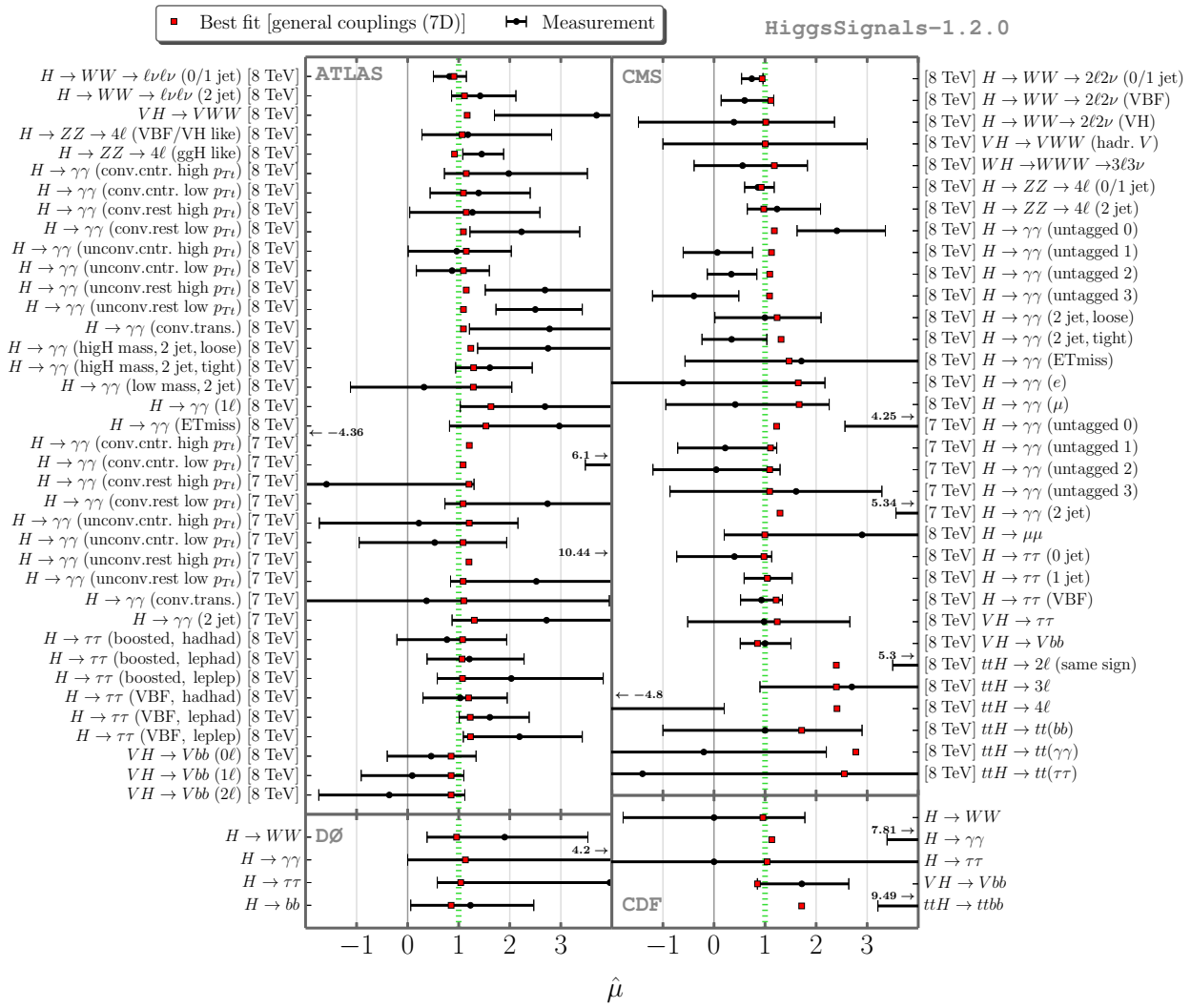

Figure 15: Comparison of the predicted signal rates of the best fit point in the general (seven-dimensional) Higgs couplings scale factor benchmark fit with the measurements from the ATLAS, CMS, CDF and DØ collaborations. The green line indicates the prediction for the SM.

channels j contribute with the same efficiency ϵ_j, i.e.,

$$R(pp \to H \cdots \to XX) \equiv \mu(pp \to H \cdots \to XX)|_{\epsilon_j=1}\,, \tag{13}$$

where μ is defined in Eq. (1). The production mode $pp \to H$ denotes inclusive production, i.e. we include all five LHC Higgs production modes at their (rescaled) SM values, whereas the rates denoted by $pp \to ZH$ [VH] include only production through Higgs-strahlung [and WH production]. It can be seen from the figure that all rates agree with the SM expectation at 68% C.L. A very weak enhancement of the $pp \to H \to \gamma\gamma$ rate is observed, while the remaining channels with fermionic or weak gauge boson final states are slightly suppressed.

Finally, in Fig. 15 we show the (actual) signal rates $\hat{\mu}$ predicted by the best fit point (depicted as red squares) compared to all 80 measurements from the Tevatron and LHC experiments (solid

black line indicating the 68% C.L. range) that went into our analysis. In the left column we show the ATLAS and DØ results, whereas in the right column the CMS and CDF observables are given. The SM (located at $\hat{\mu} = 1$) is marked as a green dashed line. It can be seen that most signal rates are predicted to be very close to the SM (where one should keep in mind the relatively large range shown for $\hat{\mu}$). An exception can be observed for the channels which comprise a substantial $t\bar{t}H$ component. Moreover, we find a slight enhancement in $H \to \gamma\gamma$ channels with a significant contribution from vector boson fusion and/or associated Higgs-weak gauge boson production. Overall, Fig. 15 demonstrates (again) that despite the large available freedom to adjust the signal rates in this very general parametrization, the preferred region agrees remarkably well with the SM. No significant improvement of the fit quality is gained by allowing the additional freedom. This implies that no significant, genuine tendencies of deviations in the SM Higgs coupling structure can be found.

3.7 Upper limits on additional undetectable Higgs decay modes

We now discuss the case where the additional Higgs decay mode(s) are not detectable with the current Higgs analyses, i.e. their final states do not lead to the missing transverse energy signature, as discussed in the beginning of Sect. 3. As discussed earlier, SM-like Higgs signal rates can be achieved even with a sizable branching fraction to undetectable final states, if at the same time the Higgs boson production rates are enhanced. In the absence of direct measurements of the Higgs total width or absolute cross sections (as will be discussed for the ILC in Sect. 4.2) the degeneracy between simultaneously increasing BR($H \to$ NP) and coupling scale factors κ_i can only be ameliorated with further model assumptions. Requiring that $\kappa_V \leq 1$ (or $\kappa_W \leq 1$ and $\kappa_Z \leq 1$), an upper limit on BR($H \to$ NP) can be derived for each investigated benchmark model without assuming that the additional decay mode leads to a missing energy signature.

Remarkably, we find that some of the six benchmark parametrizations discussed in Sect. 3.1–3.6 yield very similar limits on BR($H \to$ NP). We therefore categorize them in three Types:

Type 1: Benchmark models with universal Yukawa couplings and no additional freedom in the loop-induced couplings. This comprises the fits in Sect. 3.1–3.3.

Type 2: Benchmark models with fixed tree-level couplings but free loop-induced couplings, cf. Sect. 3.5.

Type 3: Benchmark models with non-universal Yukawa couplings, as discussed in Sect. 3.4 and 3.6.

The resulting upper limits on BR($H \to$ NP) are given in Tab. 8. The corresponding profiled $\Delta\chi^2$ distributions are displayed in Fig. 16. The most stringent limits are obtained for Type 1, where the

category	SM	Type 1	Type 2	Type 3
Fitted coupling scale factors	-	κ κ_V, κ_F $\kappa_W, \kappa_Z, \kappa_F$	κ_g, κ_γ	$\kappa_V, \kappa_u, \kappa_d, \kappa_\ell$ $\kappa_V, \kappa_u, \kappa_d, \kappa_\ell, \kappa_g, \kappa_\gamma$
BR($H \to$ NP) (68% C.L.)	$\leq 9\%$	$\leq 9\%$	$\leq 10\%$	$\leq 20\%$
BR($H \to$ NP) (95% C.L.)	$\leq 20\%$	$\leq 20\%$	$\leq 26\%$	$\leq 40\%$

Table 8: Upper limits at 68% and 95% C.L. on the undetectable Higgs decay mode, BR($H \to$ NP), obtained under the assumption $\kappa_V \leq 1$ ($V = W, Z$). All considered benchmark scenarios can be categorized into three types. The fitted coupling scale factors are given in the middle row.

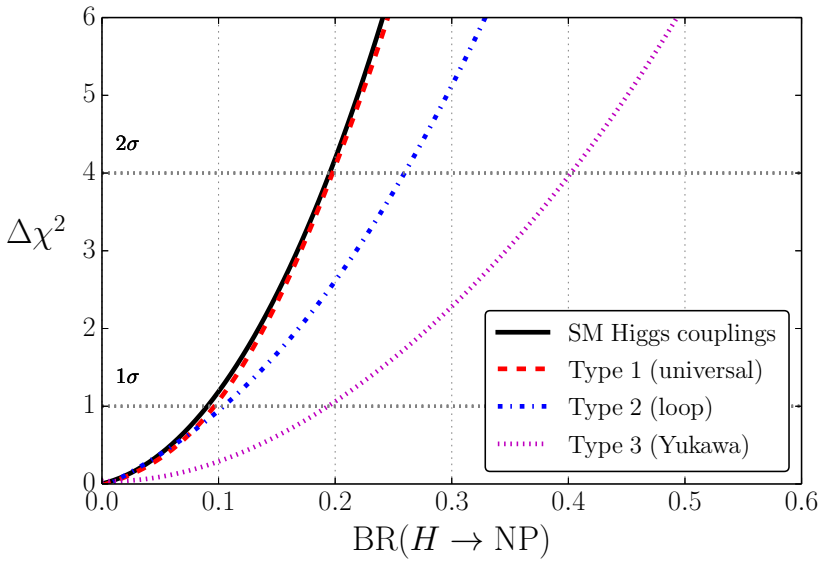

Figure 16: One-dimensional χ^2 profiles of BR($H \to$ NP) in all benchmark scenarios with the assumption $\kappa_V \leq 1$ ($V = W, Z$). The three scenario types are defined in the text.

limit is nearly identical to what is obtained with fixed SM Higgs couplings. The weakest limits are obtained for Type 3. But even in the latter, least restricted case a BR($H \to$ NP) $\leq$ 40% at the 95% C.L. is found.

4 Future precision of Higgs coupling determinations

4.1 Prospective Higgs coupling determination at the LHC

The LHC experiments ATLAS and CMS have provided estimates of the future precision for the Higgs signal rate measurements in most of the relevant channels for integrated luminosities of 300 fb^{-1} and 3000 fb^{-1} at $\sqrt{s} = 14$ TeV [90]. The first numbers (from 2012) have recently been updated [91–93]. In this section we use these updated projections to determine the accuracy of future Higgs coupling determination at the LHC. Similar studies based on the updated projections were recently performed in Refs. [94, 95], using a slightly different methodology and parametrization of the Higgs couplings. For earlier studies see also Refs. [10, 12, 30, 96].

Concerning the projected sensitivities for rate measurements from ATLAS, a detailed compilation has been provided in Refs. [91, 92] which in most cases contains information on the signal composition (efficiencies), and the projections are given with and without theoretical uncertainties. ATLAS has also provided projections for sub-channels including tags for the different production modes. Unfortunately, a projection for the important channel $H \to b\bar{b}$ is not yet available. This channel plays an important role in any global fit, since the partial decay width for $H \to b\bar{b}$ dominates the total width in the SM. Moreover, the ATLAS $H \to \tau^+\tau^-$ projection is based on an older analysis, and one could expect a potential improvement from an updated study.

CMS has provided estimates for the capabilities to measure the Higgs signal rates only for inclusive channels [93]. Unfortunately, detailed information about the signal composition is missing. We are therefore forced here to assume typical values for the signal efficiencies guided by present LHC

measurements. Moreover, we find the treatment of theoretical uncertainties in the CMS projections not very transparent.[9] CMS discusses two scenarios: Scenario 1 uses current systematic and theoretical uncertainties.[10] In Scenario 2 the theoretical uncertainties are reduced by 1/2, whereas the experimental systematic uncertainties are decreased with the square root of the integrated luminosity. No projections without theoretical uncertainties are provided by CMS. However, the Scenario 2 projections appear quite aggressive since they are of the same order as — or even more precise than — the purely experimental projections from ATLAS. Furthermore, our estimates of theoretical uncertainties, rescaled under the assumptions of Scenario 2, yield in some cases (e.g. in the $H \to \gamma\gamma, ZZ^{(*)}$ and $WW^{(*)}$ channels with 3000 fb^{-1}) already larger numbers than the CMS estimates of the total (i.e., theoretical and experimental) uncertainties of the measurements, at least when assuming that the main production mechanism for the signal is gluon fusion. Following a conservative approach, we therefore use the projected CMS rate measurements given for Scenario 2, but interpret the uncertainties as being purely experimental.[11] However, it should be noted that the dominant effect leading to differences between our results and the official CMS estimates of prospective Higgs coupling determination is the absence of (publicly available) CMS projections of the category measurements. Using only the inclusive measurements generally leads to lower precision estimates in higher-dimensional scale factor fits.

The ATLAS and CMS estimates on the (experimental) precision used in our analysis are listed in Tab. 15 (in Appendix A.3), which also gives the assumed signal composition for each channel. For both experiments we assume that the experimental precision includes a 3% systematic uncertainty on the integrated luminosity, which is treated as fully correlated among each experiment.

On top of these experimental precisions we add theoretical rate uncertainties within `HiggsSignals`. We discuss two future scenarios for the LHC-only projections: In the first scenario (S1) we take the current theoretical uncertainties as already used in the previous fits in Section 3. This scenario thus represents the rather pessimistic — or conservative — case that no improvement in the theoretical uncertainties can be achieved. With increasing integrated luminosity, however, the uncertainty from the parton density functions (PDF) can be expected to decrease [98]. Future progress can also be expected in calculations of higher-order corrections to the Higgs production cross sections and decay widths, which may further decrease the theoretical uncertainties, in particular the QCD scale dependence and remaining uncertainties from unknown electroweak (EW) corrections. Hence, in the second scenario (S2) we assume that uncertainties from the PDFs, as well as most[12] theoretical uncertainties, are halved. In both scenarios, the parametric uncertainties from the strong coupling constant, α_s, and the heavy quark masses, m_c, m_b and m_t, are unchanged. The different future scenarios considered in our analysis together with the respective assumptions on the future uncertainties and constraints are summarized in Tab. 9. The entry "100%" in Tab. 9 corresponds to the present value of the considered quantity (and accordingly, "50%" denotes an improvement by a factor of two). More details and estimates of the cross section and branching ratio uncertainties for these scenarios are given in

[9] See also Ref. [95] for a discussion of this issue.

[10] Note that improvements of systematical uncertainties that can be reduced with increasing statistics in the data control regions are however taken into account. Furthermore, even the assumption that the same systematical uncertainties as at present can be reached for the harsher experimental conditions in future is based on a projection involving a certain degree of improvement.

[11] Another way to circumvent this problem is discussed in Ref. [95], where an alternative set of projected CMS measurements is proposed.

[12] This includes uncertainties from the QCD scale and unknown EW corrections for the LHC Higgs production modes, as well as the uncertainties of all partial decay widths except the decays to W and Z bosons where higher-order EW corrections are already known with high accuracy.

Future scenario	PDF	α_s	m_c, m_b, m_t	THU[†]	BR($H \to$ inv.) constraint
LHC300 (S1)	100%	100%	all 100%	100%	conservative, Eq. (15)
LHC300 (S2, csv.)	50%	100%	all 100%	50%	conservative, Eq. (15)
LHC300 (S2, opt.)	50%	100%	all 100%	50%	optimistic, Eq. (17)
HL–LHC (S1)	100%	100%	all 100%	100%	conservative, Eq. (16)
HL–LHC (S2, csv.)	50%	100%	all 100%	50%	conservative, Eq. (16)
HL–LHC (S2, opt.)	50%	100%	all 100%	50%	optimistic, Eq. (18)
ILC250	-	50%	all 50%	50%	$\leq 0.9\%$ (cf. Tab. 16)
ILC500	-	50%	all 50%	50%	$\leq 0.9\%$ (cf. Tab. 16)
ILC1000	-	50%	all 50%	50%	$\leq 0.9\%$ (cf. Tab. 16)
ILC1000 (LumiUp)	-	50%	all 50%	50%	$\leq 0.4\%$ (cf. Tab. 16)
HL–LHC $\oplus$ ILC250 ($\sigma_{ZH}^{\text{total}}$)[‡]	50%	50%	all 50%	50%	*
HL–LHC $\oplus$ ILC250	50%	50%	all 50%	50%	*
HL–LHC $\oplus$ ILC500	50%	50%	all 50%	50%	*
HL–LHC $\oplus$ ILC1000	50%	50%	all 50%	50%	*
HL–LHC $\oplus$ ILC1000 (LumiUp)	50%	50%	all 50%	50%	*

[†] Affects the theoretical uncertainties (THU) of all partial widths except for the decay modes $H \to WW^{(*)}$ and $H \to ZZ^{(*)}$ (kept unchanged) as well as the uncertainties from QCD scale and missing EW corrections for all LHC production modes.

[‡] In this scenario only the direct ILC measurement of $\sigma(e^+e^- \to ZH)$ with 250 fb^{-1} at $\sqrt{s} = 250$ GeV is added to the HL–LHC projections to constrain the total width.

[*] For the HL–LHC $\oplus$ ILC combinations we do not use the assumption BR($H \to$ NP) $\equiv$ BR($H \to$ inv.).

Table 9: List of all future scenarios considered. Given are for each scenario the assumptions on uncertainties (relative to the current values, i.e. the entry "100%" denotes the current value, while the entry "50%" denotes an improvement by a factor of two) from parton distribution functions (PDF), the strong coupling α_s, the quark masses (m_c, m_b, m_t), and theoretical uncertainties (THU) on the predictions for the LHC Higgs cross sections and partial decay widths. The last column gives for each scenario the constraint that is employed *if* the additional Higgs decay(s) are assumed to be invisible. The considered integrated luminosities for the three energy stages 250 GeV, 500 GeV and 1 TeV of the ILC for a baseline scenario and for a luminosity upgrade (LumiUp) are specified in Section 4.2, based on Ref. [97]. The various ILC scenarios include the projected measurements from the preceding stages.

Appendix C.

ATLAS and CMS also provide projections for the 95% C.L. upper limit on the rate of an invisibly decaying Higgs boson in the Higgs-strahlung process, $pp \to ZH$. Assuming, like we have done in Sect. 3.1–3.6, that an additional Higgs decay mode gives rise to a purely invisible final state (as is stated explicitly in Tab. 9), these constraints are incorporated in our fit as ideal χ^2 likelihoods of the form

$$\chi^2 = 4 \cdot \tilde{\sigma}^2 / \tilde{\sigma}^2_{95\%\text{C.L.}}. \tag{14}$$

The quantity $\tilde{\sigma}$ corresponds to the product $\kappa_Z^2 \text{BR}(H \to \text{inv.})$, i.e the cross section of $pp \to ZH \to Z(\text{inv.})$ normalized to the SM cross section for $pp \to ZH$. Both ATLAS and CMS consider two

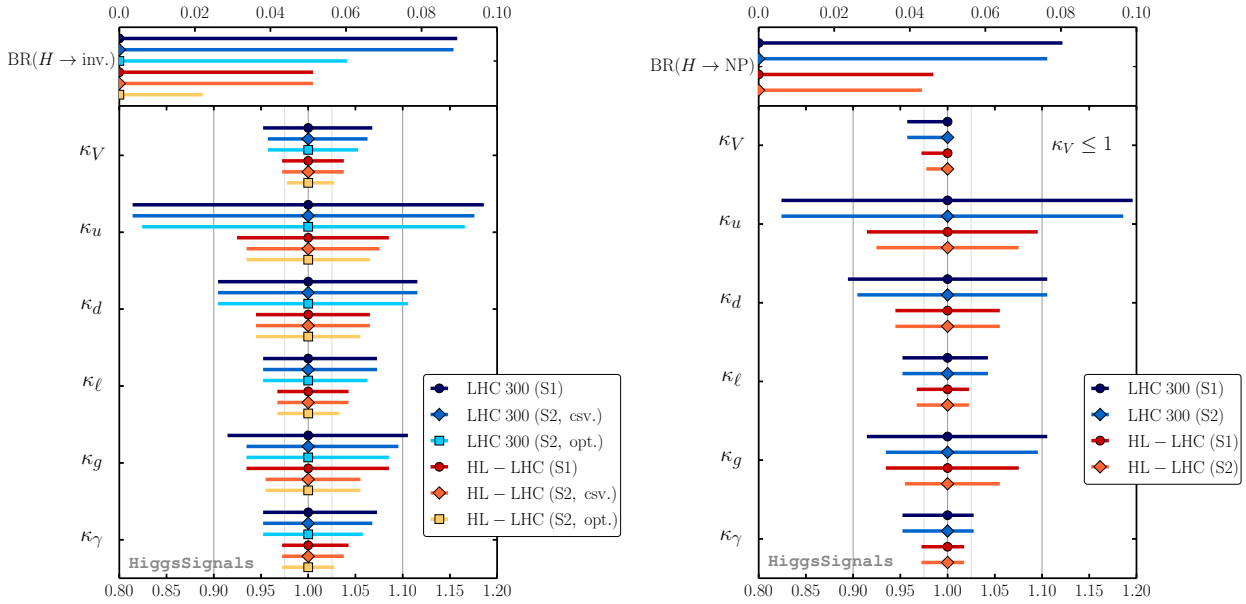

(a) Assuming BR($H \to$ NP) $\equiv$ BR($H \to$ inv.).

(b) Assuming $\kappa_V \leq 1$.

Figure 17: Projected future precision for the determination of Higgs coupling scale factors at the LHC with integrated luminosities of 300 fb^{-1} and 3000 fb^{-1} (HL–LHC).

scenarios for the projected limits [92, 93]: The conservative (csv.) scenario,

$$\text{LHC 300 fb}^{-1}: \quad \tilde{\sigma}_{95\%\text{C.L.}} = 0.32 \text{ (ATLAS)} \quad \tilde{\sigma}_{95\%\text{C.L.}} = 0.28 \text{ (CMS)} \tag{15}$$

$$\text{LHC 3000 fb}^{-1}: \quad \tilde{\sigma}_{95\%\text{C.L.}} = 0.16 \text{ (ATLAS)} \quad \tilde{\sigma}_{95\%\text{C.L.}} = 0.17 \text{ (CMS)} \tag{16}$$

and the optimistic (opt.) scenario,

$$\text{LHC 300 fb}^{-1}: \quad \tilde{\sigma}_{95\%\text{C.L.}} = 0.23 \text{ (ATLAS)} \quad \tilde{\sigma}_{95\%\text{C.L.}} = 0.17 \text{ (CMS)} \tag{17}$$

$$\text{LHC 3000 fb}^{-1}: \quad \tilde{\sigma}_{95\%\text{C.L.}} = 0.08 \text{ (ATLAS)} \quad \tilde{\sigma}_{95\%\text{C.L.}} = 0.06 \text{ (CMS)}. \tag{18}$$

We combine the projected ATLAS and CMS limits by adding their respective χ^2 contributions. For the scenario S1 we only employ the conservative constraints, Eqs. (15) and (16), whereas for the scenario S2 with reduced uncertainties we compare fits using either the conservative or the optimistic constraint. These cases are denoted by (S2, csv.) and (S2, opt.), respectively.

For the LHC projections we employ the same seven-dimensional scale factor parametrization as discussed in Sect. 3.6. The resulting 68% C.L precision estimates obtained under the assumption that the additional decay mode BR($H \to$ NP) $\equiv$ BR($H \to$ inv.) are displayed in Fig. 17(a) and listed in Tab. 10. The plot includes all six LHC-only scenarios as listed in Tab. 9.

In general the obtained 68% C.L. limit on BR($H \to$ inv.) is weaker than the limit obtained from a Gaussian combination of the limits in Eqs. (15)–(18), because the fit has the freedom to adjust $\kappa_Z (\equiv \kappa_V)$ to values < 1. Improvements in the theoretical uncertainties will mostly affect the effective Higgs-gluon coupling. At an integrated luminosity of 300 fb^{-1} we obtain a precision estimate for the

	68% C.L. Higgs coupling scale factor precision [in %]					
	LHC 300			HL–LHC		
Scenario	S1	S2, csv.	S2, opt.	S1	S2, csv.	S2, opt.
BR($H \to$ inv.)	≤ 8.9	≤ 8.8	≤ 6.0	≤ 5.1	≤ 5.1	≤ 2.2
κ_V	$^{+6.8}_{-4.8}$	$^{+6.3}_{-4.3}$	$^{+5.3}_{-4.3}$	$^{+3.8}_{-2.8}$	$^{+3.8}_{-2.8}$	$^{+2.8}_{-2.3}$
κ_u	$^{+18.6}_{-18.6}$	$^{+17.6}_{-18.6}$	$^{+16.6}_{-17.6}$	$^{+8.5}_{-7.5}$	$^{+7.5}_{-6.5}$	$^{+6.5}_{-6.5}$
κ_d	$^{+11.6}_{-9.5}$	$^{+11.6}_{-9.5}$	$^{+10.6}_{-9.5}$	$^{+6.5}_{-5.5}$	$^{+6.5}_{-5.5}$	$^{+5.5}_{-5.5}$
κ_ℓ	$^{+7.3}_{-4.8}$	$^{+7.3}_{-4.8}$	$^{+6.3}_{-4.8}$	$^{+4.3}_{-3.3}$	$^{+4.3}_{-3.3}$	$^{+3.3}_{-3.3}$
κ_g	$^{+10.6}_{-8.5}$	$^{+9.5}_{-6.5}$	$^{+8.5}_{-6.5}$	$^{+8.5}_{-6.5}$	$^{+5.5}_{-4.5}$	$^{+5.5}_{-4.5}$
κ_γ	$^{+7.3}_{-4.8}$	$^{+6.8}_{-4.8}$	$^{+5.8}_{-4.8}$	$^{+4.3}_{-2.8}$	$^{+3.8}_{-2.8}$	$^{+2.8}_{-2.8}$

Table 10: Estimates of the future 68% C.L. precision of Higgs coupling scale factors at the LHC under the assumption BR($H \to$ NP) $\equiv$ BR($H \to$ inv.). The values correspond to those in Fig. 17(a).

scale factor of the effective Higgs-gluon coupling of $\delta\kappa_g \sim 9.5\%$ in the more conservative scenario S1,[13] which is improved to $\delta\kappa_g \sim 7.5\%$ in the most optimistic scenario S2. At the high luminosity LHC with 3000 fb^{-1} the corresponding projections are $\delta\kappa_g \sim 7.5\%$ for the scenario S1 and $\delta\kappa_g \sim 5\%$ for the scenario S2 (irrespective of the assumed precision of the BR($H \to$ inv.) constraint). The assumed improvements of the theoretical uncertainties hence lead to a significant increase of the κ_g precision at the HL–LHC, while the precision at 300 fb^{-1} is still mostly limited by statistics.

The impact of more optimistic limits on the invisible Higgs decays, Eqs. (17)–(18), can directly be seen in the projected upper 68% C.L. limit on BR($H \to$ inv.) in Fig. 17(a). Since this improved constraint also applies to the Higgs–Z boson coupling the precision of the Higgs–vector-boson coupling scale factor, $\delta\kappa_V$, also improves from $\sim 5.3\%$ [3.3%] to $\sim 4.8\%$ [2.6%] at 300 fb^{-1} [3000 fb^{-1}], assuming the improved theoretical uncertainties of Scenario S2. The impact on the remaining scale factors is rather insignificant and results mostly from their positive correlation with κ_V and BR($H \to$ inv.). Hence, those are slightly more constrained from above if a more optimistic limit on the invisible Higgs decays can be achieved.

Taking into account the possibility that an additional Higgs decay mode may result in an undetectable final state, we show the fit results obtained under the assumption $\kappa_V \leq 1$ in Fig. 17(b) and Tab. 11. Overall, the achievable precision in the Higgs coupling scale factors with this assumption on the Higgs coupling to gauge bosons is very similar to what was obtained with the assumption of allowing only additional Higgs decays into invisible final states, cf. Fig. 17(a). A notable difference is, however, that in particular the scale factors κ_ℓ and κ_γ are more strongly constrained from above due to their positive correlation with κ_V, which is forced to be ≤ 1 by assumption in this case. The obtained 68% C.L. limit projection on BR($H \to$ NP) can be regarded as an independent limit projection inferred from the model assumption on κ_V and the chosen parametrization, see also the discussion in Section 3.7. Remarkably, the limit projections obtained here are stronger than the allowed range for BR($H \to$ inv.) in the previous fits in Fig. 17(a) where the constraints from searches for an invisibly

[13] Here (and in the following) the Higgs coupling precision (at 68% C.L.) is denoted by $\delta\kappa$. The values quoted in the text usually correspond to symmetric averages. For the exact asymmetric values see the corresponding tables, e.g. here Tab. 10.

	68% C.L. Higgs coupling scale factor precision [in %]			
	LHC 300		HL–LHC	
Scenario	S1	S2	S1	S2
BR($H \to$ NP)	≤ 8.0	≤ 7.6	≤ 4.6	≤ 4.3
κ_V	$^{+0.0}_{-4.3}$	$^{+0.0}_{-4.3}$	$^{+0.0}_{-2.8}$	$^{+0.0}_{-2.3}$
κ_u	$^{+19.6}_{-17.6}$	$^{+18.6}_{-17.6}$	$^{+9.5}_{-8.5}$	$^{+7.5}_{-7.5}$
κ_d	$^{+10.6}_{-10.6}$	$^{+10.6}_{-9.5}$	$^{+5.5}_{-5.5}$	$^{+5.5}_{-5.5}$
κ_ℓ	$^{+4.3}_{-4.8}$	$^{+4.3}_{-4.8}$	$^{+2.3}_{-3.3}$	$^{+2.3}_{-3.3}$
κ_g	$^{+10.6}_{-8.5}$	$^{+9.5}_{-6.5}$	$^{+7.5}_{-6.5}$	$^{+5.5}_{-4.5}$
κ_γ	$^{+2.8}_{-4.8}$	$^{+2.8}_{-4.8}$	$^{+1.8}_{-2.8}$	$^{+1.8}_{-2.8}$

Table 11: Estimates of the future 68% C.L. precision of Higgs coupling scale factors at the LHC under the assumption $\kappa_V \leq 1$. The values correspond to those in Fig. 17(b).

decaying Higgs boson have been applied.

Overall, we find estimates of Higgs coupling scale factor precisions within $\sim 5 - 18\%$ at 300 fb^{-1} and $\sim 3 - 10\%$ at 3000 fb^{-1} obtained under the assumption BR($H \to$ NP) $\equiv$ BR($H \to$ inv.). These estimates slightly improve if one assumes $\kappa_V \leq 1$ instead. Concerning comparisons with results in the literature based on the same projections of the future capabilities provided by ATLAS and CMS, our results agree quite well with those presented in Ref. [94]. A comparison of our results with Ref. [95] needs to take into account the different approaches of implementing the CMS projections. In view of this fact, we also find reasonable agreement with the results presented in Ref. [95].

It should be noted that this seven-parameter fit within the "interim framework" of Higgs-coupling scale factors still contains important simplifying assumptions and restrictions, which one would want to avoid as much as possible in a realistic analysis at the time when 300 fb^{-1} or 3000 fb^{-1} of integrated luminosity will have been collected, see the discussion in Refs. [8, 9].

4.2 Prospective Higgs coupling determination at the ILC

Looking beyond the LHC, an e^+e^- linear collider (LC) with a center-of-mass energy that can be raised at least up to $\sqrt{s} \sim 500$ GeV is widely regarded to be ideally suited for studying the properties of the discovered new particle with high precision. The Technical Design Report for the International Linear Collider, ILC, has recently been submitted [99], and there are encouraging signs that a timely realisation of this project may become possible due to the strong interest of the Japanese scientific community and the Japanese government to host the ILC.

The ILC offers a clean experimental environment enabling precision measurements of the Higgs boson mass, width, its quantum numbers and $\mathcal{CP}$-properties as well as the signal rates of a variety of production and decay channels, including a high-precision measurement of the decay rate into invisible final states. The highest statistics can be accumulated at the highest energy, $\sqrt{s} \sim 1$ TeV, from the t-channel process where a Higgs boson is produced in WW fusion ($e^+e^- \to \nu\nu H$). At $\sqrt{s} \sim 250$ GeV an absolute measurement of the production cross section can be performed from the Higgs-strahlung process ($e^+e^- \to ZH$) near threshold using the recoil of the Higgs boson against the Z boson (decaying via $Z \to \mu^+\mu^-$ or $Z \to e^+e^-$) without having to consider the actual pattern

of the Higgs decay. The absolute measurement of the production cross section can be exploited to obtain absolute measurements of the decay branching ratios and of the total width of the decaying particle. Consequently, no additional model assumptions are necessary to constrain the total width and thus the Higgs boson couplings. For $\sqrt{s} \sim 250$ GeV an integrated luminosity of 250 fb^{-1} will result in $\mathcal{O}(10^5)$ Higgs bosons. The ILC will provide high-precision measurements of channels that are known to be difficult (such as $H \to b\bar{b}$) or may even be impossible (such as $H \to c\bar{c}, gg$) at the LHC. At $\sqrt{s} \sim 500$ GeV the weak boson fusion process already dominates over the Higgs-strahlung process for a 126 GeV SM-like Higgs boson, and the two production channels together provide data with very high statistics. Starting from this energy, the top Yukawa coupling and, for sufficiently high luminosity, the trilinear self-coupling will become accessible.

In this section we study the capabilities of Higgs coupling determinations at the ILC. Similar studies have been performed in Ref. [12, 94, 95, 100]. We discuss fit results using prospective ILC measurements both alone and in combination with measurements from the HL–LHC. Since the two major Higgs production modes, Higgs-strahlung and WW fusion, are governed by the Higgs-Z-Z and Higgs-W-W couplings, respectively, from now on we abandon the assumption of custodial symmetry. Instead we fit individual scale factors for these couplings. Thus, we employ an eight-dimensional fit in the parameters κ_W, κ_Z, κ_u, κ_d, κ_ℓ, κ_g, κ_γ and BR($H \to$ NP).

The projected ILC measurements have been presented in Ref. [99] and recently updated in a Snowmass White paper [97]. These updated numbers, which we use in our fits, are summarized in Tab. 16 in Appendix A.3. In particular, we include the measurements of the total ZH cross section, cf. Tab. 16, which constrain the total width and enable a *model-independent* determination of the Higgs couplings. An assumed luminosity uncertainty of 0.1% and theoretical uncertainties of the $e^+e^- \to ZH$, $e^+e^- \to \nu\nu H$ and $e^+e^- \to t\bar{t}H$ cross section predictions of 0.5%, 1% and 1%, respectively, are treated as fully correlated in our fit. We assume the same improvements of the theoretical uncertainties for the Higgs decay modes as in Scenario S2 of the LHC projections. In addition, we assume that the parametric uncertainties from dependences on α_s and the heavy quark masses m_c, m_b and m_t can also be reduced by 50% with prospective ILC measurements and lattice calculations [98]. A further reduction of the top quark mass uncertainty — anticipated to improve by a factor of ~ 10 with respect to the current precision [99] — has negligible impact on the partial width uncertainties is and therefore not further considered here. A summary of all future scenarios that we consider in our analysis is given in Tab. 9. Estimates of the theoretical uncertainties on the Higgs branching ratios that we apply for the ILC scenarios are provided in Appendix C.

In our analysis of the ILC projections we consider three stages of center-of-mass energies, namely 250 GeV (stage 1), 500 GeV (stage 2) and 1 TeV (stage 3). For the integrated luminosities at those energy stages we investigate both a baseline program with integrated luminosities of 250 fb^{-1} at stage 1, 500 fb^{-1} at stage 2 and 1 ab^{-1} at stage 3, as well as a scenario corresponding to a luminosity upgrade (LumiUp). For the latter the integrated luminosities of 1150 fb^{-1} at stage 1, 1600 fb^{-1} at stage 2 and 2.5 ab^{-1} at stage 3 are assumed, see Ref. [97].

In Fig. 18 we show the estimated accuracies of the Higgs coupling scale factors at the ILC obtained under *model-dependent* assumptions, in analogy to the analyses performed above for the projections of future accuracies at the LHC: In Fig. 18(a) we assume that any additional Higgs decay results in invisible final states; accordingly we also take into account the projected ILC upper limit on BR($H \to$ inv.), cf. Tab. 16 (or Tab. 9). In Fig. 18(b) we apply the theoretical constraint $\kappa_W, \kappa_Z \leq 1$. For comparison we also show the fit results for the optimistic HL–LHC scenario (S2, opt) obtained under these assumptions.

Overall, the scale factor precisions achieved under those two assumptions are very similar to each

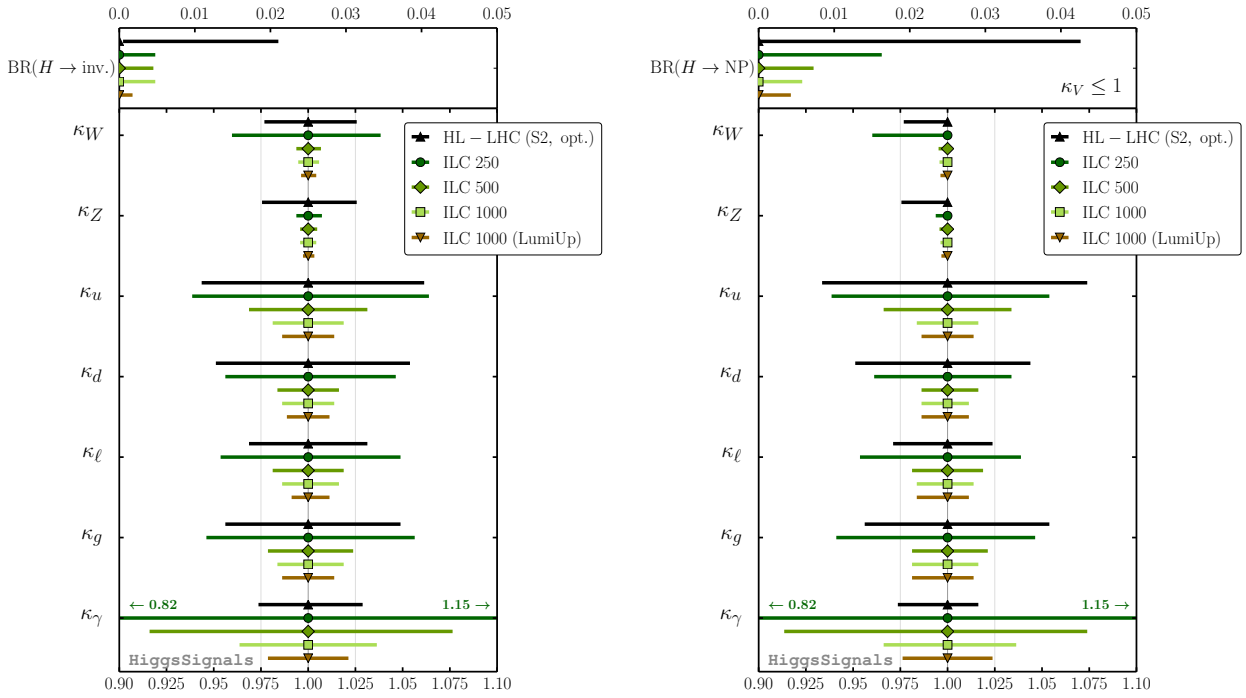

(a) Assuming BR($H \to$ NP) $\equiv$ BR($H \to$ inv.).

(b) Assuming $\kappa_W, \kappa_Z \leq 1$.

Figure 18: Prospective Higgs coupling scale factor determination at the ILC in comparison with the (optimistic) HL–LHC scenario under the same model assumptions as in Fig. 17.

other. Comparing the results of the first ILC stage, where just a 'baseline' value for the integrated luminosity of 250 fb^{-1} is assumed (ILC250), with the ultimate precision that can be reached at the LHC, we see already at this stage a substantial improvement in the precision of the scale factor κ_Z (from $\sim$ 2.5% to $\sim$ 0.7%). This is already a crucial improvement since this coupling is of central importance in the experimental test of the electroweak symmetry breaking mechanism. Furthermore, the ILC provides at this stage important measurements that are complementary to the HL–LHC measurements. For instance, the independent determination of the Higgs coupling to gluons via the decay $H \to gg$ is advantageous in order to eliminate the dependence of this quantity on the remaining PDF uncertainties of the LHC gluon fusion process. In addition, the measurement of the rate $\sigma(e^+e^- \to ZH) \times \mathrm{BR}(H \to b\bar{b})$ with 1.2% accuracy, see Tab. 16, together with the absolute cross section measurement of the ZH production process with a precision of 2.6%, give important constraints on the $H \to b\bar{b}$ decay mode, which dominantly contributes to the total width of a SM-like Higgs boson. However, the corresponding scale factors κ_Z and κ_d are still strongly correlated. Another independent measurement of the $H \to b\bar{b}$ mode with similar precision — as it is provided e.g. at the ILC stage 2 with $\sqrt{s} = 500$ GeV in WW fusion (see below) — is required to abrogate this correlation, thus allowing for a precise determination of κ_d.

The most striking improvement that the ILC already provides at the first stage with $\sqrt{s} = 250$ GeV, however, is the *model-independent* measurement of the ZH production process and correspondingly *model-independent* determinations of Higgs branching ratios. Combining this input from the ILC with the measurements performed at the HL–LHC leads to a significant improvement of the latter, as will

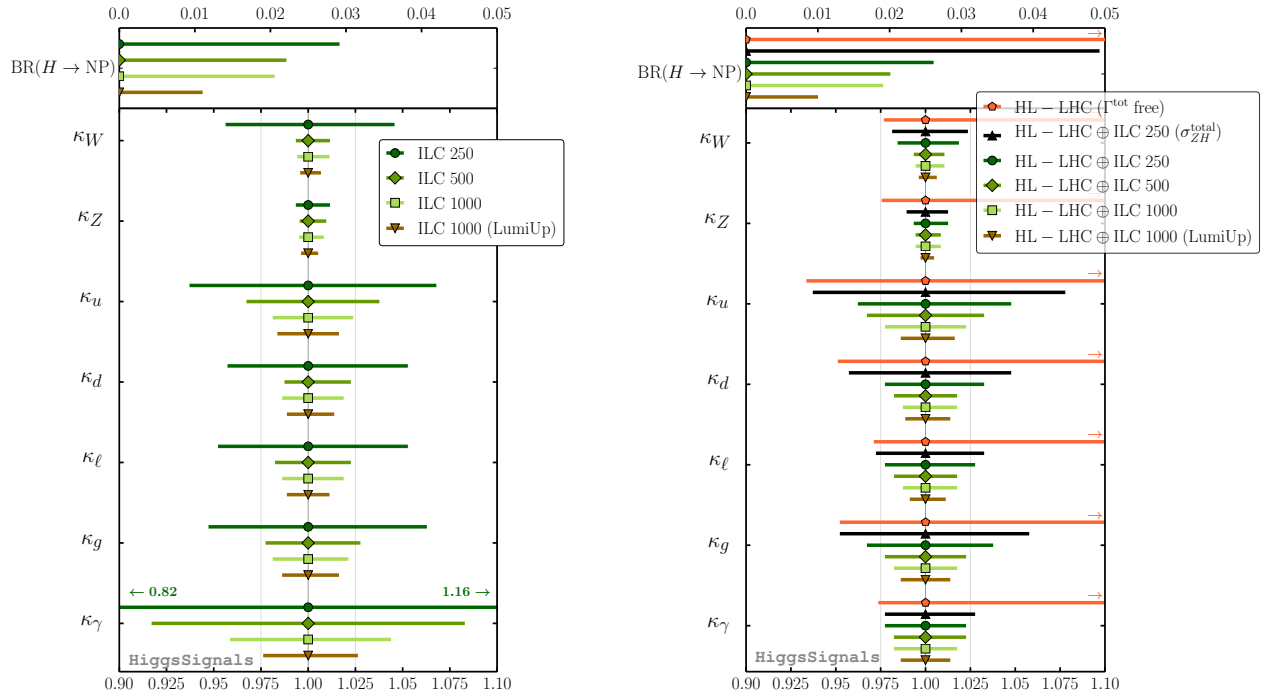

(a) ILC only.

(b) HL–LHC and combination of HL–LHC and ILC.

Figure 19: Future prospects of *model-independent* Higgs coupling scale factor determinations at the ILC alone (a) and in combination with the HL–LHC (b). For comparison, we also show the results obtained at the HL–LHC if the total width is not constrained by any assumptions on additional non-standard Higgs decay modes or limited scale factor ranges (like $\kappa_V \leq 1$).

be discussed below (see Fig. 19).

While κ_Z can be probed already quite accurately at the early ILC stage at 250 GeV due to the dominant Higgs-strahlung process, the κ_W determination is less precise, $\delta\kappa_W \sim 4.0\%$. This picture changes at the later stages of the ILC with higher centre-of-mass energies (denoted as ILC500 and ILC1000, where the 'baseline' integrated luminosities of 500 fb^{-1} and 1 ab^{-1}, respectively, have been assumed). At ILC500 and ILC1000 the WW fusion becomes the dominant production mode. Here, all scale factors in this parametrization except κ_γ can be determined to a precision of better than 2.5% using only ILC measurements. With the ultimate ILC integrated luminosity, denoted as ILC1000 (LumiUp), even the κ_γ coupling can be probed with an accuracy of $\lesssim 2.5\%$, and the remaining couplings are determined at the $\lesssim 1\%$ level, again using ILC measurements only. In the case where $\kappa_V \leq 1$ is imposed instead of assuming non-standard Higgs decays to result in invisible final states, the sensitivity for setting an upper limit on BR($H \to$ NP) inferred from the fit improves significantly at the ILC from 4.3 (8.5)% to 1.6 (3.3)% at the 68 (95)% C.L..

As stated earlier, the assumptions made in the previous fits are actually unnecessary at the ILC once the total cross section measurement of the $e^+e^- \to ZH$ process is taken into account. Therefore, *model-independent* estimates of the Higgs coupling accuracies can be obtained, which are shown in Fig. 19(a) and (b) for the ILC only and HL–LHC ⊕ ILC combined measurements, respectively. The values are also listed in Tab. 12. The estimated accuracies obtained for the ILC-only measurements

	68% C.L. Higgs coupling scale factor precision [in %]								
	ILC only				HL–LHC ⊕ ILC				
Scenario	250	500	1000	1000 (LumiUp)	250 ($\sigma_{ZH}^{\text{total}}$)	250	500	1000	1000 (LumiUp)
BR($H \to$ NP)	≤ 2.9	≤ 2.2	≤ 2.1	≤ 1.1	≤ 4.9	≤ 2.6	≤ 2.0	≤ 1.9	≤ 1.0
κ_W	$^{+4.6}_{-4.4}$	$^{+1.2}_{-0.7}$	$^{+1.2}_{-0.6}$	$^{+0.7}_{-0.4}$	$^{+2.4}_{-1.9}$	$^{+1.9}_{-1.6}$	$^{+1.1}_{-0.7}$	$^{+1.1}_{-0.6}$	$^{+0.6}_{-0.4}$
κ_Z	$^{+1.3}_{-0.7}$	$^{+1.0}_{-0.6}$	$^{+0.9}_{-0.6}$	$^{+0.5}_{-0.4}$	$^{+1.3}_{-1.1}$	$^{+1.3}_{-0.7}$	$^{+0.9}_{-0.6}$	$^{+0.9}_{-0.6}$	$^{+0.5}_{-0.3}$
κ_u	$^{+6.8}_{-6.3}$	$^{+3.8}_{-3.3}$	$^{+2.3}_{-2.3}$	$^{+1.6}_{-1.6}$	$^{+7.8}_{-6.3}$	$^{+4.8}_{-3.8}$	$^{+3.3}_{-3.3}$	$^{+2.3}_{-2.3}$	$^{+1.6}_{-1.4}$
κ_d	$^{+5.3}_{-4.3}$	$^{+2.3}_{-1.8}$	$^{+1.8}_{-1.3}$	$^{+1.4}_{-1.1}$	$^{+4.8}_{-4.3}$	$^{+3.3}_{-2.3}$	$^{+1.8}_{-1.8}$	$^{+1.8}_{-1.3}$	$^{+1.4}_{-1.1}$
κ_ℓ	$^{+5.3}_{-4.8}$	$^{+2.3}_{-1.8}$	$^{+1.8}_{-1.3}$	$^{+1.9}_{-1.6}$	$^{+3.3}_{-2.8}$	$^{+2.8}_{-2.3}$	$^{+1.8}_{-1.8}$	$^{+1.8}_{-1.3}$	$^{+1.1}_{-0.9}$
κ_g	$^{+6.3}_{-5.3}$	$^{+2.8}_{-2.3}$	$^{+2.3}_{-1.8}$	$^{+1.9}_{-1.6}$	$^{+5.8}_{-4.8}$	$^{+3.8}_{-3.3}$	$^{+2.3}_{-2.3}$	$^{+1.8}_{-1.8}$	$^{+1.4}_{-1.4}$
κ_γ	$^{+15.8}_{-17.8}$	$^{+8.3}_{-8.3}$	$^{+3.8}_{-3.8}$	$^{+2.6}_{-2.6}$	$^{+2.8}_{-2.3}$	$^{+2.3}_{-2.3}$	$^{+2.3}_{-1.8}$	$^{+1.8}_{-1.8}$	$^{+1.4}_{-1.4}$

Table 12: 68% C.L. precision estimates and upper limits for the *model-independent* determination of Higgs coupling scale factors and BR($H \to$ NP), respectively, using only ILC measurements or in combination with HL–LHC measurements. The ultimate ILC scenario at $\sqrt{s} = 1$ TeV after a full luminosity upgrade (LumiUp) is denoted as ILC 1000 (LU) here. These values correspond to those depicted in Fig. 19.

in this model-independent approach are only slightly weaker than the ones obtained above under additional model assumptions, cf. Fig. 18. At the early ILC stage (ILC250) the sensitivity for setting a *model-independent* 95% C.L. upper limit on BR($H \to$ NP) of $\lesssim 5.8\%$ is obtained from the fit. This sensitivity improves to $\lesssim 4.1-4.4\%$ at the later (baseline) ILC stages. The more precise measurement of the $e^+e^- \to ZH$ cross section at 250 GeV with the ILC luminosity upgrade improves the sensitivity further, such that BR($H \to$ NP) $\lesssim 2.2\%$ at 95% C.L. can be reached at the ultimate ILC stage at $\sqrt{s} = 1$ TeV.

For the combination of HL–LHC and ILC measurements for a model-independent Higgs coupling determination, as shown in Fig. 19(b), it is illustrative to consider first the results obtained using the HL–LHC only or with a minimal amount of ILC input, i.e. by only adding the total cross section measurement of the $e^+e^- \to ZH$ process. In the first case, as already demonstrated in Sect. 3.1, the unconstrained fit (HL–LHC (Γ^{tot} free) in Fig. 19(b)) features a degeneracy of increasing BR($H \to$ NP) and increasing scale factors κ_i, until the LHC is finally capable to observe broad width effects via off-shell Higgs production. This degeneracy manifests itself in the fact that there is virtually no precision to determine an upper limit up to very large values of the scale factors (the fact that the error bars for the case of HL–LHC only extend to values far outside of the right-hand side of the plot is indicated by little arrows in the plot).

By adding only the total $e^+e^- \to ZH$ cross section measurement from the ILC250 run (with the 'baseline' integrated luminosity of 250 fb^{-1}) to the HL–LHC observables the degeneracy is broken, leading to a very significant improvement in the determination of all Higgs coupling scale factors. Besides this effect one can see that the combination with this single input value from the ILC leads to further significant improvements affecting also the lower limits on the scale factors. In particular, the precision on the lower limit of κ_Z improves from $\sim 2.5\%$ to $\sim 1.1\%$. Moreover, the 95% C.L. upper limit on BR($H \to$ NP) inferred from this fit (without any additional assumptions) is 9.8%,

thus roughly comparable to what has been obtained under the additional model assumptions in the LHC-only fit, cf. Fig. 18(b). With the inclusion of the remaining ILC measurements at 250 GeV (with the 'baseline' integrated luminosity of 250 fb^{-1}) all scale factors except κ_u and κ_g can be measured at the $\sim 2.5\%$ level. κ_u and κ_g can be determined with a precision of $\sim 4.3\%$ and ~ 3.3, respectively. The only scale factor that is dominantly constrained by the LHC data is that for the Higgs-photon coupling, κ_γ, which remains the case even at the later ILC stages at 500 GeV and 1 TeV. With the ultimate ILC luminosity (including the upgrade) and combining all available measurements from the HL–LHC and ILC, all Higgs coupling scale factors are probed to at least a precision of 1.5%, the Higgs-weak gauge boson couplings even at the per-mille level. At this level the estimated accuracies are dominated by the assumed (reduced) theory uncertainties. We find that our estimates for the later ILC stages have a slight tendency to be more conservative than those of e.g. Refs. [94, 95], since we include (larger) theoretical uncertainties for the ILC production cross sections and their correlations.

5 Conclusions

In this paper we have investigated in detail whether the coupling properties of the discovered new particle show any significant deviations from the predictions for a SM Higgs boson at the present level of accuracies. We have further analyzed the room for potential coupling deviations, that is still consistent with the current measurements, and the associated parameter correlations. The study has been carried out within a consistent statistical framework using all available Higgs signal rate measurements from the LHC and Tevatron experiments by employing profile likelihood fits of Higgs coupling scale factors by means of the public program `HiggsSignals`. The fits have been done both for highly constrained and very generic scale factor parametrizations of the Higgs couplings. All benchmark fits allow for additional Higgs decays to non-standard final states and various assumptions are discussed for constraining the total Higgs decay width at the LHC. In contrast to other investigations in the literature, we have paid particular attention to the treatment of the general case where no constraint on the total Higgs width — or on the branching fraction of Higgs decays to potentially undetectable final states of new physics — is assumed.

We have employed the "interim framework" of Higgs coupling scale factors as a means to parametrize the relations between the physical collider observables (cross sections, branching ratios) and the possible deviations in the couplings of the new state from the predictions for a SM Higgs boson. While the scale factors probe different possible aspects of deviations from the SM predictions, their inherent simplifications and restrictions make it non-trivial to directly map the results obtained in terms of Higgs coupling scale factors onto realistic models of physics beyond the SM (which, on the other hand, typically predict certain correlations that may differ from the ones assumed for the Higgs coupling scale factors). The investigation of particular models is therefore complementary to the analysis of Higgs coupling scale factors. The tool `HiggsSignals`, which has been used in the present analysis, has been specifically designed for this purpose, and the statistical methods employed here can be directly taken over for fits of realistic new physics models.

The program `HiggsSignals` is a well-validated and accurate tool for the χ^2 evaluation based on the signal rate predictions and the currently 80 included measurements from ATLAS, CMS, CDF and DØ. It takes into account the correlations of luminosity, cross section and branching ratio uncertainties among the signal rate measurements, as well as intrinsic correlations among the cross section and branching ratio uncertainties induced by common parametric uncertainties. For this study, we have further included the correlations of the remaining major experimental systematics for the ATLAS

$H \to \tau^+\tau^-$ and CMS $H \to \gamma\gamma$ measurements. We validated the implementation against an official six-dimensional scale factor fit performed by CMS, yielding very good agreement. All these new developments, as documented here, will be provided with `HiggsSignals` version `1.2.0`.

For all considered scale factor benchmark models we find very good agreement between the LHC and Tevatron measurements and the signal rates predicted for the SM. For the SM itself (i.e., all scale factors are set to unity), we find a naive $\mathcal{P}$-value of $\sim 35.0\%$, showing good agreement between data and theory. Thus, it is not surprising that the benchmark models achieve similar $\mathcal{P}$-values, which we have found to be typically slightly lower than the SM $\mathcal{P}$-value due to the smaller number of degrees of freedom at similar minimal χ^2. The lowest $\mathcal{P}$-value of $\sim 27.8\%$ is obtained for the fit probing the Yukawa structure in Section 3.4, while the best $\mathcal{P}$-value (except for the SM $\mathcal{P}$-value) is found with $\sim 33.9\%$ for the benchmark fit probing the loop-induced Higgs couplings to gluons and photons, cf. Section 3.5.

We find no indicative hint for deviations from the SM in any of the fits. Indeed, all central values of the fitted Higgs coupling scale factors are compatible with their SM values, and also the fitted values of an additional Higgs branching fraction, $\mathrm{BR}(H \to \mathrm{NP})$, are well compatible with zero. Uncertainties on the fitted scale factors range from around 10% in the most constrained case, i.e. a fit of only one universal scaling parameter, up to 40% for the top Yukawa scale factor, κ_u, in the seven-dimensional fit discussed in Section 3.6. Comparing these results with the latest official scale factor determination performed by CMS for the Moriond 2013 conference, we find significant improvements in all scale factor precisions. This illustrates the power of a common interpretation of ATLAS and CMS (and Tevatron) measurements, as well as the importance of the recent measurements in the ATLAS $H \to \tau^+\tau^-$ and CMS $t\bar{t}H$-tagged searches.

The corresponding weakest observed limit from the fits on the invisible Higgs decay is $\mathrm{BR}(H \to \mathrm{inv.}) < 17$ [39]% at the 68% [95%] C.L., also taking into account direct searches for $\mathrm{BR}(H \to \mathrm{inv.})$ at the LHC. We furthermore find for the total signal strength to known SM final states a lower limit of $\kappa^2 \times (1 - \mathrm{BR}(H \to \mathrm{NP})) > 81\%$ at the 95% CL, employing the benchmark fit with one universal Higgs coupling scale factor κ. This limit is independent of any further assumption, such as e.g. $\kappa_{W,Z} \leq 1$. Moreover, under the assumption that $\kappa_{W,Z} \leq 1$ holds, we find from the most general fit to the present data (with seven free parameters) the limit $\mathrm{BR}(H \to \mathrm{NP}) < 40\%$ at the 95% CL.

Beyond the current measurements from the LHC and the Tevatron, we have explored the capabilities of future Higgs coupling determinations using projections of the signal rate measurements for the LHC with 300 fb^{-1} (LHC 300) and 3000 fb^{-1} (HL–LHC) at 14 TeV, as well as for various scenarios of an International Linear Collider (ILC). At the LHC 300 we find estimated precisions for the determination of the Higgs coupling scale factors within $\sim 5 - 18\%$ under the assumption $\mathrm{BR}(H \to \mathrm{NP}) \equiv \mathrm{BR}(H \to \mathrm{inv.})$. Possible improvements of theoretical uncertainties on the cross sections and branching ratios turn out to have only a marginal effect on those estimated precisions. This changes at the HL–LHC, where the achievable precision of the Higgs-gluon coupling scale factor is significantly limited by the theoretical uncertainty. The precision estimates of the remaining scale factors, however, are hardly affected by varying assumptions on the theoretical uncertainties. Overall, assuming $\mathrm{BR}(H \to \mathrm{NP}) \equiv \mathrm{BR}(H \to \mathrm{inv.})$, we find scale factor precisions of $\sim 3 - 10\%$ at the HL–LHC. If we make the model assumption $\kappa_V \leq 1$ instead of the assumption that additional non-standard Higgs decays result only in invisible final states, most of the estimated scale factor precisions marginally improve.

Concerning the prospects at the ILC, we have compared the ILC capabilities of determining Higgs couplings with those of the HL–LHC first for a model-dependent approach, i.e. using the same assumptions as for the HL–LHC analyses, namely assuming either $\mathrm{BR}(H \to \mathrm{NP}) \equiv \mathrm{BR}(H \to \mathrm{inv.})$ or $\kappa_V \leq 1$

as a means to constrain the total width. We find that already ILC measurements at 250 GeV for 'baseline' assumptions on the integrated luminosity provide significant improvements compared to the most optimistic scenario for the HL–LHC along with complementary measurements that are of similar or slightly worse accuracy compared with the projections for the HL–LHC. Starting from a center-of-mass energy of $\sqrt{s} = 500$ GeV (for the corresponding 'baseline' luminosity assumption) the ILC in fact has the potential to considerably improve upon all measurements of the HL–LHC apart from the coupling of the Higgs to photons. At $\sqrt{s} = 500$ GeV, the WW fusion channel can be measured significantly better than at 250 GeV, which leads to a significantly higher statistics for all considered quantities and in particular to a further improvement in the determination of the total width. The further improvements from ILC running at 1 TeV and from exploiting the ultimate ILC luminosity (LumiUp) turn out to be rather moderate for the considered case of a model-dependent 8-parameter fit, which is related to our fairly conservative estimates of the future theoretical uncertainties.

The impact of the ILC on improving the determination of the Higgs couplings becomes apparent most strikingly for the model-independent analyses. Without employing additional theoretical assumptions the scale factors at the LHC are essentially unconstrained from above. However, taking into account a single measurement of the ILC — the decay-mode independent recoil analysis of the total Higgs production rate at 250 GeV — in conjunction with the HL–LHC measurements already allows to perform a significantly less model-dependent (compared to the fits discussed above) and more precise fit than with the HL–LHC alone. In particular, with this ILC measurement the assumptions on the additional Higgs decay modes and on κ_V can be dropped.

From prospective measurements at the ILC up to $\sqrt{s} = 1$ TeV with the 'baseline' assumptions for the integrated luminosity together with those from the HL–LHC, we find precision estimates for *all* fitted Higgs coupling scale factors of better than 2.5%. For some scale factors a precision better than 1% is achieved. These estimates are obtained with the least amount of model assumptions and 8 free fit parameters. With the ultimate ILC luminosity (LumiUp) this precision would further increase significantly, reaching a level of better than 1.5% for all scale factors.

The Higgs coupling scale factor benchmark scenarios considered in this study typically have more freedom to adjust the predicted signal rates to the measurements than realistic models. Realistic model generally feature specific correlations among the predicted rates which furthermore depend non-trivially (and non-linearly) on the model parameters. Moreover, limits from the electroweak precision data and possibly other sectors (dark matter, collider searches, etc.) can further restrict the allowed parameter space and thus the room for Higgs coupling deviations. The fact that the exploration of the Higgs couplings with those rather general parametrizations does not improve the fit quality with respect to the SM is a clear indication of the good agreement of the data with the SM predictions. On the basis of this analysis one would not expect a significant improvement in the description of the data from a realistic model of physics beyond the SM. Thus, the full set of the present public measurements from ATLAS, CMS, CDF and DØ in the Higgs sector does not show any indications for physics beyond the SM.

Despite the lack of a concrete hint for any deviation from the SM in the current measurements, there still is ample room for future discoveries of deviations from the SM predictions for the Higgs couplings. In fact, the current uncertainties are still rather large and thus still allow for sizable deviations from the SM at the level of $\sim \mathcal{O}(10 - 40\%)$ at the 1σ level, even when making additional theory assumptions (like $\mathrm{BR}(H \to \mathrm{NP}) \equiv \mathrm{BR}(H \to \mathrm{inv.})$ or $\kappa_V \leq 1$). Comparing those accuracies with the typical deviations expected in realistic models of physics beyond the SM, a large improvement in the experimental precision will be needed in order to sensitively probe the parameter space of the most popular extensions of the SM. The measurements at an ILC-like machine (in conjunction with

the HL–LHC) will be crucial in this context for model-independent determinations of absolute Higgs couplings with precisions at the percent level or better, offering great prospects for identifying the underlying mechanism of electroweak symmetry breaking.

Acknowledgments

We thank Andre David, Ansgar Denner, Klaus Desch, Manuel Drees, Michael Duehrssen, Howie Haber, Alex Read, Björn Sarrazin, Daniel Schmeier and Tom Zirke for helpful discussions. Part of the numerical calculations were performed using the computing infrastructure [101] at the "Instituto de Física de Cantabria". This work was partially supported by the Helmholtz Alliance "Physics at the Terascale", the Collaborative Research Center SFB676 of the DFG, "Particles, Strings and the early Universe", and by the European Commission through the "HiggsTools" Initial Training Network PITN-GA-2012-316704. The work of T.S. was supported by the BMBF Grant No. 00160200 and the Bonn-Cologne Graduate School (BCGS). S.H. was supported by CICYT (Grant No. FPA 2010–22163-C02-01) and by the Spanish MICINN's Consolider-Ingenio 2010 Program under Grant MultiDark No. CSD2009-00064. O.S. is supported by the Swedish Research Council (VR) through the Oskar Klein Centre.

Since one of the authors (P.B.) is also an ATLAS member, we would like to clarify that the work presented here is the responsibility of the individual authors and does not represent an ATLAS result. This phenomenological analysis is purely based on public information.

A Experimental data

A.1 Implementation of current signal strength measurements

Tables 13 and 14 list the signal strength measurements from ATLAS, CDF, CMS and DØ as implemented in `HiggsSignals-1.2.0`; there are 80 observables in total. The tables also provide numbers for the assumed signal composition of a SM Higgs boson for all measurements. Most of these results are used directly in the fits in Section 3, except for a few cases where a more careful treatment is required as described in detail below.

For the six signal strength category measurements of the ATLAS SM $H \to \tau^+\tau^-$ search we implement additional correlations inspired by the information given in Ref. [46], following the procedure outlined in Ref. [48]. This includes

- correlated uncertainties of $\sim 5-10\%$ $(20-30\%)$ in the VBF (boosted) categories of the gluon fusion signal component, mostly representing the uncertainties of the differential p_T distribution of this signal process,
- correlated normalization uncertainties of the top and $Z \to \ell\ell$ background of $\sim 10-15\%$ among the leptonic-leptonic and leptonic-hadronic $\tau\tau$ categories,
- correlated uncertainties from hadronic τ identification of $\sim 4\%$ (12%) in the leptonic-hadronic (hadronic-hadronic) $\tau\tau$ categories,
- correlated di-hadronic τ trigger efficiency uncertainties of 7% among the two hadronic-hadronic $\tau\tau$ channels,

Analysis	energy $\sqrt{s}$	$\hat{\mu} \pm \Delta\hat{\mu}$	SM signal composition [in %]				
			ggH	VBF	WH	ZH	$t\bar{t}H$
ATL $(pp) \to h \to WW \to \ell\nu\ell\nu$ (0/1jet) [103, 104]	7/8 TeV	$0.82^{+0.33}_{-0.32}$	97.2	1.6	0.7	0.4	0.1
ATL $(pp) \to h \to WW \to \ell\nu\ell\nu$ (VBF) [103, 104]	7/8 TeV	$1.42^{+0.70}_{-0.56}$	19.8	80.2	0.0	0.0	0.0
ATL $(pp) \to h \to ZZ \to 4\ell$ (VBF/VH-like) [104, 105]	7/8 TeV	$1.18^{+1.64}_{-0.90}$	36.8	43.1	12.8	7.3	0.0
ATL $(pp) \to h \to ZZ \to 4\ell$ (ggH-like) [104, 105]	7/8 TeV	$1.45^{+0.43}_{-0.37}$	92.5	4.5	1.9	1.1	0.0
ATL $(pp) \to h \to \gamma\gamma$ (unconv.-central-low p_{Tt}) [106]	7 TeV	$0.53^{+1.41}_{-1.48}$	92.9	3.8	2.0	1.1	0.2
ATL $(pp) \to h \to \gamma\gamma$ (unconv.-central-high p_{Tt}) [106]	7 TeV	$0.22^{+1.94}_{-1.95}$	65.5	14.8	10.8	6.2	2.7
ATL $(pp) \to h \to \gamma\gamma$ (unconv.-rest-low p_{Tt}) [106]	7 TeV	$2.52^{+1.68}_{-1.68}$	92.6	3.7	2.2	1.2	0.2
ATL $(pp) \to h \to \gamma\gamma$ (unconv.-rest-high p_{Tt}) [106]	7 TeV	$10.44^{+3.67}_{-3.70}$	64.4	15.2	11.8	6.6	2.0
ATL $(pp) \to h \to \gamma\gamma$ (conv.-central-low p_{Tt}) [106]	7 TeV	$6.10^{+2.63}_{-2.62}$	92.7	3.8	2.1	1.1	0.2
ATL $(pp) \to h \to \gamma\gamma$ (conv.-central-high p_{Tt}) [106]	7 TeV	$-4.36^{+1.80}_{-1.81}$	65.7	14.4	11.0	6.2	2.8
ATL $(pp) \to h \to \gamma\gamma$ (conv.-rest-low p_{Tt}) [106]	7 TeV	$2.74^{+1.98}_{-2.01}$	92.7	3.6	2.2	1.2	0.2
ATL $(pp) \to h \to \gamma\gamma$ (conv.-rest-high p_{Tt}) [106]	7 TeV	$-1.59^{+2.89}_{-2.90}$	64.4	15.1	12.1	6.4	2.0
ATL $(pp) \to h \to \gamma\gamma$ (conv.-trans.) [106]	7 TeV	$0.37^{+3.58}_{-3.79}$	89.2	5.0	3.7	1.9	0.3
ATL $(pp) \to h \to \gamma\gamma$ (2 jet) [106]	7 TeV	$2.72^{+1.87}_{-1.85}$	23.3	75.9	0.5	0.2	0.1
ATL $(pp) \to h \to \gamma\gamma$ (unconv.-central-low p_{Tt}) [107]	8 TeV	$0.87^{+0.73}_{-0.70}$	92.0	5.0	1.7	0.8	0.5
ATL $(pp) \to h \to \gamma\gamma$ (unconv.-central-high p_{Tt}) [107]	8 TeV	$0.96^{+1.07}_{-0.95}$	78.6	12.6	4.7	2.6	1.4
ATL $(pp) \to h \to \gamma\gamma$ (unconv.-rest-low p_{Tt}) [107]	8 TeV	$2.50^{+0.92}_{-0.77}$	92.0	5.0	1.7	0.8	0.5
ATL $(pp) \to h \to \gamma\gamma$ (unconv.-rest-high p_{Tt}) [107]	8 TeV	$2.69^{+1.35}_{-1.17}$	78.6	12.6	4.7	2.6	1.4
ATL $(pp) \to h \to \gamma\gamma$ (conv.-central-low p_{Tt}) [107]	8 TeV	$1.39^{+1.01}_{-0.95}$	92.0	5.0	1.7	0.8	0.5
ATL $(pp) \to h \to \gamma\gamma$ (conv.-central-high p_{Tt}) [107]	8 TeV	$1.98^{+1.54}_{-1.26}$	78.6	12.6	4.7	2.6	1.4
ATL $(pp) \to h \to \gamma\gamma$ (conv.-rest-low p_{Tt}) [107]	8 TeV	$2.23^{+1.14}_{-1.01}$	92.0	5.0	1.7	0.8	0.5
ATL $(pp) \to h \to \gamma\gamma$ (conv.-rest-high p_{Tt}) [107]	8 TeV	$1.27^{+1.32}_{-1.23}$	78.6	12.6	4.7	2.6	1.4
ATL $(pp) \to h \to \gamma\gamma$ (conv.-trans.) [107]	8 TeV	$2.78^{+1.72}_{-1.57}$	92.0	5.0	1.7	0.8	0.5
ATL $(pp) \to h \to \gamma\gamma$ (high mass, 2 jet, loose) [107]	8 TeV	$2.75^{+1.78}_{-1.38}$	45.3	53.7	0.5	0.3	0.2
ATL $(pp) \to h \to \gamma\gamma$ (high mass, 2 jet, tight) [107]	8 TeV	$1.61^{+0.83}_{-0.67}$	27.1	72.5	0.3	0.1	0.0
ATL $(pp) \to h \to \gamma\gamma$ (low mass, 2 jet) [107]	8 TeV	$0.32^{+1.72}_{-1.44}$	38.0	2.9	40.1	16.9	2.1
ATL $(pp) \to h \to \gamma\gamma$ (E_T^{miss} sign.) [107]	8 TeV	$2.97^{+2.71}_{-2.15}$	4.4	0.3	35.8	47.4	12.2
ATL $(pp) \to h \to \gamma\gamma$ (1ℓ) [107]	8 TeV	$2.69^{+1.97}_{-1.66}$	2.5	0.4	63.3	15.2	18.7
ATL $(pp) \to h \to \tau\tau$ (VBF, had-had) [46]	8 TeV	$1.03^{+0.92}_{-0.73}$	25.1	74.9	0.0	0.0	0.0
ATL $(pp) \to h \to \tau\tau$ (boosted, had-had) [46]	8 TeV	$0.77^{+1.17}_{-0.98}$	65.1	16.1	12.5	6.3	0.0
ATL $(pp) \to h \to \tau\tau$ (VBF, lep-had) [46]	8 TeV	$1.61^{+0.77}_{-0.60}$	13.9	86.1	0.0	0.0	0.0
ATL $(pp) \to h \to \tau\tau$ (boosted, lep-had) [46]	8 TeV	$1.21^{+1.07}_{-0.83}$	68.8	16.1	10.1	5.0	0.0
ATL $(pp) \to h \to \tau\tau$(VBF, lep-lep) [46]	8 TeV	$2.19^{+1.23}_{-1.10}$	12.4	87.6	0.0	0.0	0.0
ATL $(pp) \to h \to \tau\tau$ (boosted, lep-lep) [46]	8 TeV	$2.03^{+1.80}_{-1.45}$	66.0	25.6	6.2	2.2	0.0
ATL $(pp) \to Vh \to V(bb)$ (0ℓ) [108]	7/8 TeV	$0.46^{+0.88}_{-0.86}$	0.0	0.0	21.2	78.8	0.0
ATL $(pp) \to Vh \to V(bb)$ (1ℓ) [108]	7/8 TeV	$0.09^{+1.01}_{-1.00}$	0.0	0.0	96.7	3.3	0.0
ATL $(pp) \to Vh \to V(bb)$ (2ℓ) [108]	7/8 TeV	$-0.36^{+1.48}_{-1.38}$	0.0	0.0	0.0	100.0	0.0
ATL $(pp) \to Vh \to V(WW)$ [109]	7/8 TeV	$3.70^{+1.90}_{-2.00}$	0.0	0.0	63.8	36.2	0.0
CDF $(p\bar{p}) \to h \to WW$ [110]	1.96 TeV	$0.00^{+1.78}_{-1.78}$	77.5	5.4	10.6	6.5	0.0
CDF $(p\bar{p}) \to h \to \gamma\gamma$ [110]	1.96 TeV	$7.81^{+4.61}_{-4.42}$	77.5	5.4	10.6	6.5	0.0
CDF $(p\bar{p}) \to h \to \tau\tau$ [110]	1.96 TeV	$0.00^{+8.44}_{-8.44}$	77.5	5.4	10.6	6.5	0.0
CDF $(p\bar{p}) \to Vh \to Vbb$ [110]	1.96 TeV	$1.72^{+0.92}_{-0.87}$	0.0	0.0	61.9	38.1	0.0
CDF $(p\bar{p}) \to tth \to ttbb$ [110]	1.96 TeV	$9.49^{+6.60}_{-6.28}$	0.0	0.0	0.0	0.0	100.0

Table 13: Signal strength measurements from ATLAS and CDF.

- correlated $Z \to \tau\tau$ background normalization uncertainties of $\sim 10 - 12\%$ among the hadronic-leptonic and leptonic-leptonic $\tau\tau$ categories.

The effect of including these correlations is shown in Fig. 20 for a fit in a two-dimensional scaling model. Here the gluon fusion and $t\bar{t}H$ production cross sections are scaled by $\mu_{\text{ggF+ttH}}$ and the VBF, WH and ZH production cross sections by $\mu_{\text{VBF+VH}}$. Both the original ATLAS result and the likelihood reconstructed using `HiggsSignals` are shown. It can clearly be seen that the agreement between the reconstructed and official likelihood is significantly improved by including the additional correlations.

In earlier validation fits [13] using the CMS $H \to \gamma\gamma$ [45, 102] results we found some discrepancies

Analysis	energy $\sqrt{s}$	$\hat{\mu} \pm \Delta\hat{\mu}$	SM signal composition [in %]				
			ggH	VBF	WH	ZH	$t\bar{t}H$
CMS $(pp) \to h \to WW \to 2\ell 2\nu$ (0/1 jet) [111]	7/8 TeV	$0.74^{+0.22}_{-0.20}$	83.0	11.1	3.8	2.2	0.0
CMS $(pp) \to h \to WW \to 2\ell 2\nu$ (VBF) [111]	7/8 TeV	$0.60^{+0.57}_{-0.46}$	19.8	80.2	0.0	0.0	0.0
CMS $(pp) \to h \to WW \to 2\ell 2\nu$ (VH) [111]	7/8 TeV	$0.39^{+1.97}_{-1.87}$	56.2	4.5	25.1	14.2	0.0
CMS $(pp) \to h \to WW \to 3\ell 3\nu$ (WH) [111]	7/8 TeV	$0.56^{+1.27}_{-0.95}$	0.0	0.0	100.0[1]	0.0	0.0
CMS $(pp) \to Vh \to V(WW)$ (hadronic V) [112]	7/8 TeV	$1.00^{+2.00}_{-2.00}$	59.8	4.0	24.2	12.0	0.0
CMS $(pp) \to h \to ZZ \to 4\ell$ (0/1 jet) [113]	7/8 TeV	$0.86^{+0.32}_{-0.26}$	89.8	10.2	0.0	0.0	0.0
CMS $(pp) \to h \to ZZ \to 4\ell$ (2 jet) [113]	7/8 TeV	$1.24^{+0.85}_{-0.58}$	71.2	28.8	0.0	0.0	0.0
CMS $(pp) \to h \to \gamma\gamma$ (untagged 0) [45, 102]	7 TeV	$3.88^{+2.00}_{-1.68}$	61.4	16.9	12.0	6.6	3.1
CMS $(pp) \to h \to \gamma\gamma$ (untagged 1) [45, 102]	7 TeV	$0.20^{+1.01}_{-0.93}$	87.7	6.2	3.6	2.0	0.5
CMS $(pp) \to h \to \gamma\gamma$ (untagged 2) [45, 102]	7 TeV	$0.04^{+1.25}_{-1.24}$	91.4	4.4	2.5	1.4	0.3
CMS $(pp) \to h \to \gamma\gamma$ (untagged 3) [45, 102]	7 TeV	$1.47^{+1.68}_{-2.47}$	91.3	4.4	2.6	1.5	0.2
CMS $(pp) \to h \to \gamma\gamma$ (2 jet) [45, 102]	7 TeV	$4.18^{+2.31}_{-1.78}$	26.7	72.6	0.4	0.2	0.0
CMS $(pp) \to h \to \gamma\gamma$ (untagged 0) [45]	8 TeV	$2.20^{+0.95}_{-0.78}$	72.9	11.7	8.2	4.6	2.6
CMS $(pp) \to h \to \gamma\gamma$ (untagged 1) [45]	8 TeV	$0.06^{+0.69}_{-0.67}$	83.5	8.5	4.5	2.6	1.0
CMS $(pp) \to h \to \gamma\gamma$ (untagged 2) [45]	8 TeV	$0.31^{+0.50}_{-0.47}$	91.5	4.5	2.3	1.3	0.4
CMS $(pp) \to h \to \gamma\gamma$ (untagged 3) [45]	8 TeV	$-0.36^{+0.88}_{-0.81}$	92.5	3.9	2.1	1.2	0.3
CMS $(pp) \to h \to \gamma\gamma$ (2 jet, tight) [45]	8 TeV	$0.27^{+0.69}_{-0.58}$	20.6	79.0	0.2	0.1	0.1
CMS $(pp) \to h \to \gamma\gamma$ (2 jet, loose) [45]	8 TeV	$0.78^{+1.10}_{-0.98}$	46.8	51.1	1.1	0.6	0.5
CMS $(pp) \to h \to \gamma\gamma$ (μ) [45]	8 TeV	$0.38^{+1.84}_{-1.36}$	0.0	0.2	50.4	28.6	20.8
CMS $(pp) \to h \to \gamma\gamma$ (e) [45]	8 TeV	$-0.67^{+2.78}_{-1.95}$	1.1	0.4	50.2	28.5	19.8
CMS $(pp) \to h \to \gamma\gamma$ (E_T^{miss}) [45]	8 TeV	$1.89^{+2.62}_{-2.28}$	22.1	2.6	40.6	23.0	11.7
CMS $(pp) \to h \to \mu\mu$ [114]	7/8 TeV	$2.90^{+2.80}_{-2.70}$	92.5	7.5	0.0	0.0	0.0
CMS $(pp) \to h \to \tau\tau$ (0 jet) [77, 78]	7/8 TeV	$0.40^{+0.73}_{-1.13}$	98.2	1.0	0.5	0.3	0.0
CMS $(pp) \to h \to \tau\tau$ (1 jet) [77, 78]	7/8 TeV	$1.06^{+0.47}_{-0.47}$	76.0	14.9	5.8	3.3	0.0
CMS $(pp) \to h \to \tau\tau$ (VBF) [77, 78]	7/8 TeV	$0.93^{+0.41}_{-0.41}$	17.1	82.9	0.0	0.0	0.0
CMS $(pp) \to Vh \to V(\tau\tau)$ [77, 78]	7/8 TeV	$0.98^{+1.68}_{-1.50}$	0.0	0.0	48.6[2]	26.4[2]	0.0
CMS $(pp) \to Vh \to V(bb)$ [115]	7/8 TeV	$1.00^{+0.51}_{-0.49}$	0.0	0.0	63.8	36.2	0.0
CMS $(pp) \to tth \to 2\ell$ (same-sign) [86]	8 TeV	$5.30^{+2.20}_{-1.80}$	0.0	0.0	0.0	0.0	100.0[3]
CMS $(pp) \to tth \to 3\ell$ [86]	8 TeV	$2.70^{+2.20}_{-1.80}$	0.0	0.0	0.0	0.0	100.0[4]
CMS $(pp) \to tth \to 4\ell$ [86]	8 TeV	$-4.80^{+5.00}_{-1.20}$	0.0	0.0	0.0	0.0	100.0[5]
CMS $(pp) \to tth \to tt(bb)$ [87]	7/8 TeV	$1.00^{+1.90}_{-2.00}$	0.0	0.0	0.0	0.0	100.0
CMS $(pp) \to tth \to tt(\tau\tau)$ [87]	8 TeV	$-1.40^{+6.30}_{-5.50}$	0.0	0.0	0.0	0.0	100.0
CMS $(pp) \to tth \to tt(\gamma\gamma)$ [88]	8 TeV	$-0.20^{+2.40}_{-1.90}$	0.0	0.0	0.0	0.0	100.0
DØ $(p\bar{p}) \to h \to WW$ [116]	1.96 TeV	$1.90^{+1.63}_{-1.52}$	77.5	5.4	10.6	6.5	0.0
DØ $(p\bar{p}) \to h \to bb$ [116]	1.96 TeV	$1.23^{+1.24}_{-1.17}$	0.0	0.0	61.9	38.1	0.0
DØ $(p\bar{p}) \to h \to \gamma\gamma$ [116]	1.96 TeV	$4.20^{+4.60}_{-4.20}$	77.5	5.4	10.6	6.5	0.0
DØ $(p\bar{p}) \to h \to \tau\tau$ [116]	1.96 TeV	$3.96^{+4.11}_{-3.38}$	77.5	5.4	10.6	6.5	0.0

[1] The signal is contaminated to 15.0% by $WH \to W(\tau\tau)$ in the SM.
[2] The signal is contaminated to 17.2% [9.8%] by $WH \to WWW$ [$ZH \to ZWW$] in the SM.
[3] The $t\bar{t}h \to \ell^\pm\ell^\pm$ signal is comprised of the final states WW (74.5%), ZZ (3.7%) and $\tau\tau$ (21.7%) in the SM.
[4] The $t\bar{t}h \to 3\ell$ signal is comprised of the final states WW (73.0%), ZZ (4.6%) and $\tau\tau$ (22.5%) in the SM.
[5] The $t\bar{t}h \to 4\ell$ signal is comprised of the final states WW (54.1%), ZZ (17.4%) and $\tau\tau$ (28.5%) in the SM.

Table 14: Signal strength measurements from CMS and DØ.

if only a simple χ^2 test was performed. In this case the correlations among these observables introduced by common sources of experimental systematic uncertainties are non-negligible. Guided by the information given in Ref. [45], we therefore introduce the following correlations for the CMS $H \to \gamma\gamma$ category measurements:

- Event migration of 12.5% between neighboring untagged categories for each 7 TeV and 8 TeV,
- Event migration of 15.0% between the loose and tight dijet category at 8 TeV,
- For the dijet categories, we include a dijet tagging efficiency uncertainty, corresponding to an anti-correlated uncertainty among the ggH and VBF channels, of $10-15\%$ and 30%, respectively.

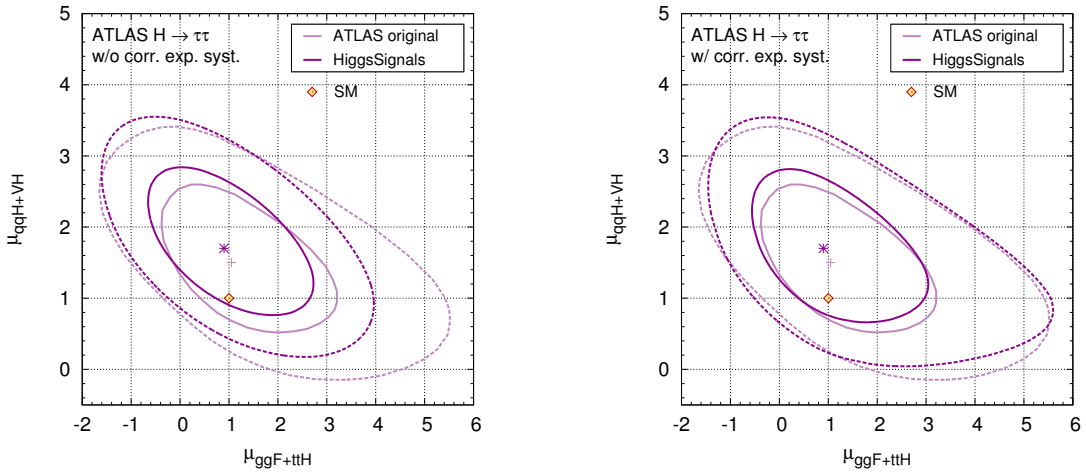

(a) Without correlations of experimental systematic uncertainies.

(b) With correlations of experimental systematic uncertainies.

Figure 20: Comparison of our fit results with official ATLAS results for rescaled production cross sections of the gluon fusion (ggF) and $t\bar{t}H$ processes vs. the vector boson fusion (qqH) and VH ($V = W, Z$) processes using the ATLAS $H \to \tau^+\tau^-$ measurements [46]. We compare the effects of neglecting or including correlations of known experimental systematic uncertainties in (a) and (b), respectively. The faint magenta curves indicates the original ATLAS results.

- E_T^{miss} cut efficiency uncertainty in the E_T^{miss} selection at 8 TeV of 15% for the ggH and VBF channels and 4% for the WH, ZH, $t\bar{t}H$ channels, respectively.

One more complication arises because the signal rate measurements in the various categories of the $H \to \gamma\gamma$ analysis are only publicly available for a mass value of $m_H = 125.0$ GeV. On the contrary, Ref. [5] provides only fit results at 125.7 GeV for the signal strengths

$$\hat{\mu}(H \to \gamma\gamma,\ \text{untagged}) = 0.70^{+0.33}_{-0.29}, \tag{19}$$

$$\hat{\mu}(H \to \gamma\gamma,\ \text{VBF tag}) = 1.01^{+0.63}_{-0.54}, \tag{20}$$

$$\hat{\mu}(H \to \gamma\gamma,\ \text{VH tag}) = 0.57^{+1.34}_{-1.34}, \tag{21}$$

combining the untagged, dijet and remaining leptonic/missing energy categories, respectively. Furthermore, the official scale factor fit results given by CMS, which can be used to validate our implementation, see Sect. A.2, assume a Higgs mass of 125.7 GeV [5]. Given the category measurements at 125.0 GeV (based on the MVA analysis), cf. Tab. 14, we repeat these fits with `HiggsSignals` to obtain

$$\hat{\mu}(H \to \gamma\gamma,\ \text{untagged}) = 0.64^{+0.32}_{-0.30}, \tag{22}$$

$$\hat{\mu}(H \to \gamma\gamma,\ \text{VBF tag}) = 0.79^{+0.58}_{-0.54}, \tag{23}$$

$$\hat{\mu}(H \to \gamma\gamma,\ \text{VH tag}) = 0.63^{+1.28}_{-1.14}. \tag{24}$$

We approximate the unknown category measurements at 125.7 GeV by rescaling the category measurements at 125.0 GeV by the ratio of the corresponding combined fit results.

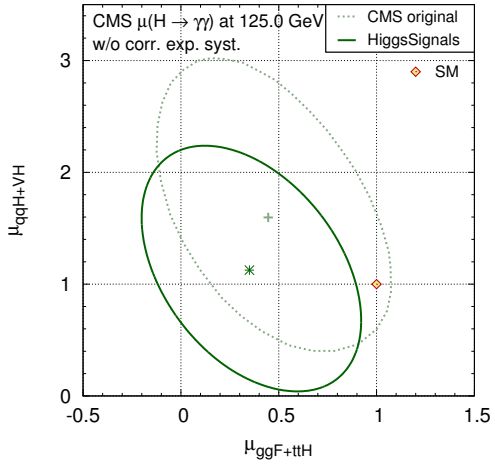

(a) Using original measurements at 125.0 GeV without correlations of experimental systematic uncertainies.

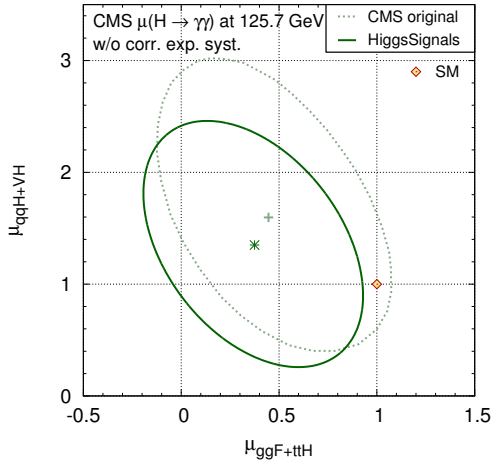

(b) Using approximated measurements at 125.7 GeV without correlations of experimental systematic uncertainies.

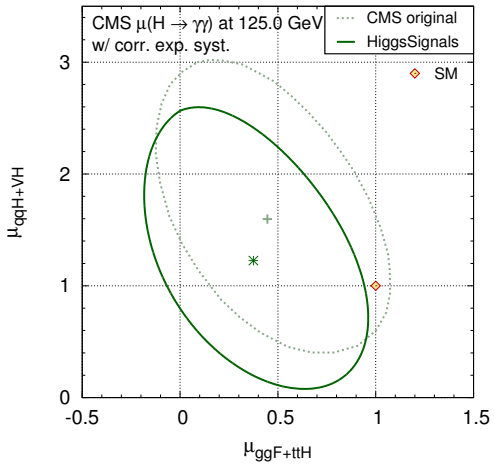

(c) Using original measurements at 125.0 GeV with correlations of experimental systematic uncertainies.

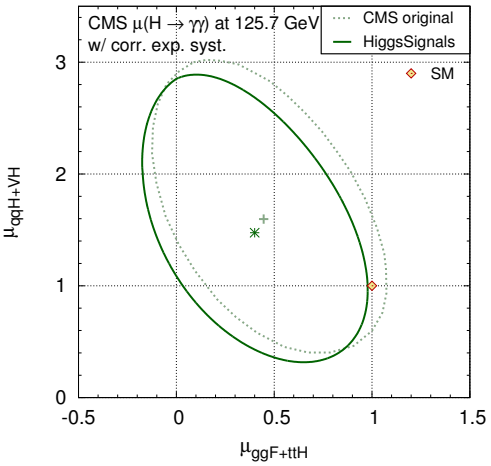

(d) Using approximated measurements at 125.7 GeV with correlations of experimental systematic uncertainies.

Figure 21: Comparison of our fit results with official CMS results for rescaled production cross sections of the gluon fusion (ggF) and $t\bar{t}H$ processes vs. the vector boson fusion (qqH) and VH ($V = W, Z$) processes using the CMS $H \to \gamma\gamma$ category measurements [45, 102]. The results have been derived using either the original measurements given at a Higgs mass of 125.0 GeV, shown in (a,c), or approximated (rescaled) measurements at 125.7 GeV, shown in (b,d). We furthermore compare the effects of neglecting or including correlations of known experimental systematic uncertainties in (a,b) and (c,d), respectively. The dotted faint green curve indicates the original CMS results obtained for a Higgs boson mass of 125.7 GeV.

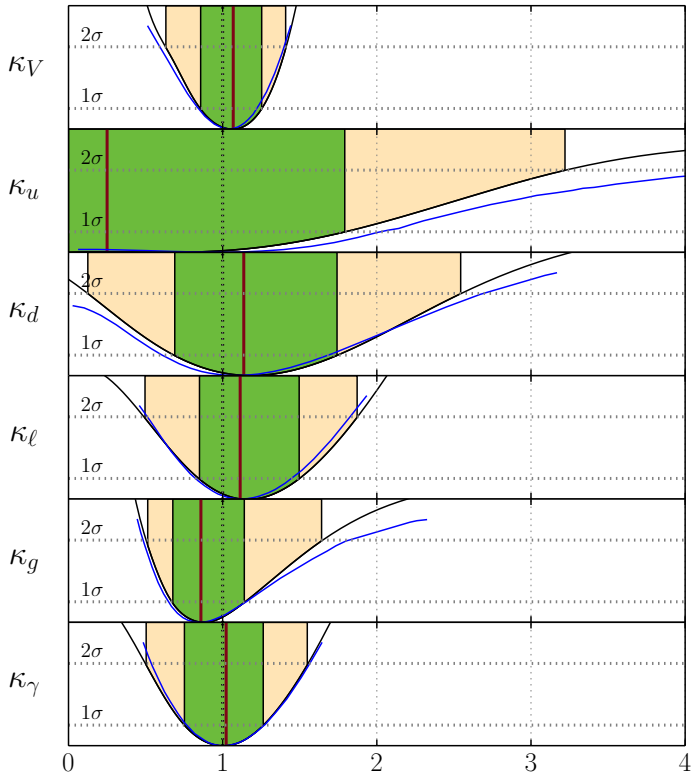

Figure 22: One-dimensional χ^2 profiles of the fitted Higgs coupling scale factors $\kappa_V, \kappa_u, \kappa_d, \kappa_\ell, \kappa_g, \kappa_\gamma$ using only the CMS Moriond 2013 results [5]. The CMS $H \to \gamma\gamma$ measurements were rescaled to a Higgs boson mass of 125.7 GeV and include correlations of some experimental systematic uncertainties. The blue curves show the original fit result obtained by CMS [5].

In Fig. 21 we show the effects of including the correlations of systematic experimental uncertainties and the rescaling of the category measurements to $m_H = 125.7$ GeV for a 2D fit to common scale factors for the gluon fusion and $t\bar{t}H$ cross section, $\mu_{\mathrm{ggF+ttH}}$, and for the vector boson fusion and VH ($V = W, Z$) cross sections, $\mu_{\mathrm{qqH+VH}}$, using only results from the CMS $H \to \gamma\gamma$ analysis [45, 102]. The original CMS result obtained for $m_H = 125.7$ GeV is overlaid in the figure. It can be seen that both effects have a sizable impact on the result. Acceptable agreement with the official CMS result can be obtained if both the correlations and the rescaling is taken into account, as shown in Fig. 21(d). We therefore use this setup of the CMS $H \to \gamma\gamma$ measurements for the fits presented in this paper.

A.2 Validation fit using CMS data only

We validate the fit procedure by performing a six-dimensional fit to the CMS Moriond 2013 data and comparing the results to the official fit results presented by CMS [5]. The model parameters are identical to the scale factors of our general fit, i.e. κ_V, $\kappa_u(\equiv \kappa_t)$, $\kappa_d(\equiv \kappa_b)$, $\kappa_\ell(\equiv \kappa_\tau)$, κ_g and κ_γ, but the total width is obtained from the rescaled effective couplings direcly (no additional Higgs decay modes). The CMS fit was performed assuming a Higgs boson mass of 125.7 GeV. The results are shown in Fig. 22, where the blue curves indicate the original CMS results [5]. With the corrected implementation of the CMS $H \to \gamma\gamma$ measurements, as discussed above, the fit shows excellent agreement.

Analysis	68% C.L. precision		Assumed signal composition [in %]				
	300 fb^{-1}	3000 fb^{-1}	ggH	VBF	WH	ZH	$t\bar{t}H$
ATL $(pp) \to h \to \gamma\gamma$ (0jet) [92]	0.12	0.05	91.6	2.7	3.2	1.8	0.6
ATL $(pp) \to h \to \gamma\gamma$ (1jet) [92]	0.14	0.05	81.8	13.2	2.9	1.6	0.5
ATL $(pp) \to h \to \gamma\gamma$ (VBF-like) [92]	0.43	0.16	39.2	58.4	1.4	0.8	0.3
ATL $(pp) \to h \to \gamma\gamma$ (VH-like) [90]	0.77	0.25	2.5	0.4	63.3	15.2	18.7
ATL $(pp) \to h \to \gamma\gamma$ ($t\bar{t}H$-like) [90]	0.54	0.16	0.0	0.0	0.0	0.0	100.0
ATL $(pp) \to h \to WW$ (0jet) [92]	0.08	0.05	98.2	1.8	0.0	0.0	0.0
ATL $(pp) \to h \to WW$ (1jet) [92]	0.17	0.10	88.4	11.6	0.0	0.0	0.0
ATL $(pp) \to h \to WW$ (VBF-like) [90]	0.20	0.09	8.1	91.9	0.0	0.0	0.0
ATL $(pp) \to h \to ZZ$ (ggF-like) [92]	0.06	0.04	88.7	7.2	2.0	1.4	0.7
ATL $(pp) \to h \to ZZ$ (VBF-like) [92]	0.31	0.16	44.7	53.2	0.7	0.4	1.0
ATL $(pp) \to h \to ZZ$ (VH-like) [92]	0.31	0.12	30.1	9.0	34.8	12.1	14.0
ATL $(pp) \to h \to ZZ$ ($t\bar{t}H$-like) [92]	0.44	0.16	8.7	1.7	1.7	3.1	84.8
ATL $(pp) \to h \to Z\gamma$ [92]	1.45	0.54	87.6	7.1	3.1	1.7	0.6
ATL $(pp) \to h \to \mu\mu$ [92]	0.45	0.15	87.6	7.1	3.1	1.7	0.6
ATL $(pp) \to h \to \mu\mu$ ($t\bar{t}H$) [90]	0.72	0.23	0.0	0.0	0.0	0.0	100.0
ATL $(pp) \to h \to \tau\tau$ (VBF-like) [92]	0.16	0.12	19.8	80.2	0.0	0.0	0.0
CMS $(pp) \to h \to \gamma\gamma$ [93]	0.06	0.04	87.6	7.1	3.1	1.7	0.6
CMS $(pp) \to h \to WW$ [93]	0.06	0.04	88.1	7.1	3.1	1.7	0.0
CMS $(pp) \to h \to ZZ$ [93]	0.07	0.04	88.1	7.1	3.1	1.7	0.0
CMS $(pp) \to h \to Z\gamma$ [93]	0.62	0.20	87.6	7.1	3.1	1.7	0.6
CMS $(pp) \to h \to bb$ [93]	0.11	0.05	0.0	0.0	57.0	32.3	10.7
CMS $(pp) \to h \to \mu\mu$ [93]	0.40	0.20	87.6	7.1	3.1	1.7	0.6
CMS $(pp) \to h \to \tau\tau$ [93]	0.08	0.05	68.6	27.7	2.4	1.4	0.0

Table 15: Projected experimental precision (i.e. without theory uncertainty) of signal strength measurements from ATLAS and CMS at $\sqrt{s} = 14$ TeV for 300 fb^{-1} and 3000 fb^{-1} (HL–LHC). The numbers from CMS correspond to Scenario 2 of their projections, however, we treat them as purely experimental precisions (see discussion in Sect. 4.1).

A.3 Projected sensitivity of future signal rate measurements

The future estimates of signal strength measurements in various channels at the LHC for integrated luminosities of 300 fb^{-1} and 3000 fb^{-1} are given in Tab. 15 for ATLAS [92] and CMS [93]. In Tab. 16 we list the estimated cross section and signal rate measurements at the ILC [97]. These values are used for the study of the LHC and ILC capabilities of Higgs coupling determination presented in Sect. 4.

B Investigating the $\mathcal{P}$-value of χ^2 fits to measured Higgs signal rates

As outlined in Sect. 2.2 and explained in detail in Ref. [13], `HiggsSignals` employs a χ^2 approximation to allow for a very fast evaluation of the model compatibility with public results from Higgs rate and mass measurements in arbitrary models. Comparisons to the results from ATLAS and CMS show that this implementation yields a good approximation to the official results [13] (see also Appendices A.1 and A.2 above). This allows for a reliable phenomenological analysis of a very large variety of models of new physics against the Higgs search results. In such studies, the $\mathcal{P}$-value, i.e. the statistical agreement of the measured results with the predictions from a theory, is of high interest. This can be evaluated using toy Monte Carlo techniques. In this section we study to what extent the specific implementation of the χ^2 evaluation in `HiggsSignals` impacts the $\mathcal{P}$-value calculation. This is also of interest for other implementations of χ^2 tests against Higgs mass and rate measurements [10–14, 20–23], which employ different levels of detail concerning the implementation of uncertainties

$\mathcal{L}$ and $\sqrt{s}$	250 fb^{-1} at 250 GeV		500 fb^{-1} at 500 GeV			1 ab^{-1} at 1 TeV	
	ZH	$\nu\bar{\nu}H$	ZH	$\nu\bar{\nu}H$	$t\bar{t}H$	$\nu\bar{\nu}H$	$t\bar{t}H$
$\Delta\sigma/\sigma$	2.6%	-	3.0%	-	-	-	-
BR($H \to$ inv.)	$< 0.9\%$	-	-	-	-	-	-
mode	$\Delta(\sigma \cdot \text{BR})/(\sigma \cdot \text{BR})$						
$H \to b\bar{b}$	1.2%	10.5%	1.8%	0.7%	28%	0.5%	6.0%
$H \to c\bar{c}$	8.3%	-	13.0%	6.2%	-	3.1%	-
$H \to gg$	7.0%	-	11%	4.1%	-	2.6%	-
$H \to WW^{(*)}$	6.4%	-	9.2%	2.4%	-	1.6%	-
$H \to \tau^+\tau^-$	4.2%	-	5.4%	9.0%	-	3.1%	-
$H \to ZZ^{(*)}$	18%	-	25%	8.2%	-	4.1%	-
$H \to \gamma\gamma$	34%	-	34%	23%	-	8.5%	-
$H \to \mu^+\mu^-$	100%	-	-	-	-	31%	-
$\mathcal{L}$ and $\sqrt{s}$	1150 fb^{-1} at 250 GeV		1600 fb^{-1} at 500 GeV			2.5 ab^{-1} at 1 TeV	
	ZH	$\nu\bar{\nu}H$	ZH	$\nu\bar{\nu}H$	$t\bar{t}H$	$\nu\bar{\nu}H$	$t\bar{t}H$
$\Delta\sigma/\sigma$	1.2%	-	1.7%	-	-	-	-
BR($H \to$ inv.)	$< 0.4\%$	-	-	-	-	-	-
mode	$\Delta(\sigma \cdot \text{BR})/(\sigma \cdot \text{BR})$						
$H \to b\bar{b}$	0.6%	4.9%	1.0%	0.4%	16%	0.3%	3.8%
$H \to c\bar{c}$	3.9%	-	7.2%	3.5%	-	2.0%	-
$H \to gg$	3.3%	-	6.0%	2.3%	-	1.4%	-
$H \to WW^{(*)}$	3.0%	-	5.1%	5.1%	-	1.0%	-
$H \to \tau^+\tau^-$	2.0%	-	3.0%	3.0%	-	2.0%	-
$H \to ZZ^{(*)}$	8.4%	-	14.0%	14.0%	-	2.6%	-
$H \to \gamma\gamma$	16.0%	-	19.0%	13.0%	-	5.4%	-
$H \to \mu^+\mu^-$	46.6%	-	-	-	-	20.0%	-

Table 16: Expected accuracies for the measurements of signal rates and absolute production cross sections at various ILC stages of the baseline program (*above*) and after a luminosity upgrade (*below*) for a Higgs boson with mass $m_H = 125$ GeV. Upper limits on BR($H \to$ inv.) are given at 95% C.L.. The numbers are taken from Ref. [97], cf. also Ref. [99].

(correlated/uncorrelated, relative/absolute, symmetric/asymmetric, etc.). In order to evaluate the impact of the calculation of uncertainties and correlations on the χ^2, we investigate the $\mathcal{P}$-value of a SM-like Higgs boson modified by a global scale parameter κ. It is tested against the latest rate measurements from ATLAS, CMS, CDF and DØ, see Appendix A for details. Using a toy Monte Carlo technique the $\mathcal{P}$-value is then evaluated from the `HiggsSignals` calculated χ^2 for sets of pseudo-measurements thrown around the best fit point and according to the covariance matrix, which we obtain at the best fit point. The exact $\mathcal{P}$-value based on the full likelihood distribution can of course only be calculated by the experimental collaborations. However, no combination of the experiments at LHC and the Tevatron is available, such that an approximate calculation is of interest.

The default treatment of uncertainties in `HiggsSignals` suggests a deviation from the ideal χ^2 distribution in both the signal strength part, χ^2_μ, and the Higgs mass part, χ^2_m. Therefore, the $\mathcal{P}$-value can only approximately be extracted from the observed χ^2 at the best fit point and the number of

degrees of freedom (ndf) assuming an ideal χ^2 distribution. Instead, toy measurements have to be employed to take into account the following effects in the $\mathcal{P}$-value evaluation:

1. The usage of asymmetric (upper and lower) uncertainties in the rate measurements instead of averaged (symmetric) uncertainties. The choice for the observed rate uncertainty entering the χ^2 evaluation, $\Delta\hat{\mu}$, is dependent on the relative position of the model-predicted signal rate μ with respect to the observed value $\hat{\mu}$:

$$\Delta\hat{\mu} = \begin{cases} \Delta\hat{\mu}^{\text{up}} & , \quad \text{if} \quad \mu > \hat{\mu} \\ \Delta\hat{\mu}^{\text{low}} & , \quad \text{if} \quad \mu < \hat{\mu} \end{cases} . \tag{25}$$

2. The usage of relative instead of absolute rate uncertainties. The luminosity uncertainty is scaled with the observed $\hat{\mu}$ value, while the theoretical rate uncertainties are scaled with the predicted μ value in `HiggsSignals`. Where the experimental systematics can not be attributed to either signal or background, they are treated as background-related and kept constant. This combination generally provides a good approximation of the experimental results.

In case that the mass is also fitted, two additional effects arise:

3. Theoretical mass uncertainties can be treated as (anti-)correlated Gaussian errors in the χ^2_m evaluation. The theory mass uncertainty of two mass observables, $\hat{m}_i$, $\hat{m}_j$, is anti-correlated if the predicted mass lies in between these measurements, $\hat{m}_i < m < \hat{\mu}_j$.

4. The automatic assignment of the Higgs boson to the observables introduces a highly non-trivial deviation from the ideal χ^2 shape in both χ^2_μ and χ^2_m. This procedure takes care that the comparison of the predicted signal rate μ (at mass m) with the measured signal strength $\hat{\mu}$ (at mass $\hat{m}$) is still approximately valid, or otherwise adds a χ^2 penalty to χ^2_μ. In the latter case, the mass measurement associated with the unassigned observable does not enter χ^2_m anymore. This issue is of course only relevant if a model with more than one Higgs boson is studied. It is not further studied in the examples below.

The items (1, 2) lead to a dependence of the covariance matrix C_μ in the χ^2_μ calculation on both the observed signal rate values, $\hat{\mu}$, and the model-predicted signal rate values, μ. Hence, it changes for each set of pseudo-measurements and depends on the tested model. The items (3, 4) are of relevance only in the case of a non-trivial model prediction of the Higgs mass. Here, we choose a fixed Higgs mass of $m_H = 125.7$ GeV. We ensure a full assignment of all observables within `HiggsSignals`, while the actual constant χ^2 contribution from the Higgs mass measurements is of no further relevance in this study. It should be noted, however, that we hereby make the approximation/assumption, that all signal rates measured by the experiments for the Higgs signal at various mass positions between 124.3 GeV and 126.8 GeV can be compared with the hypothesized Higgs state at $m_H = 125.7$ GeV.

As a simple generic toy model we employ a fit with only one free parameter, namely a global Higgs coupling scale factor κ affecting all Higgs couplings to bosons and fermions in the same way, thus the SM predictions for the Higgs boson signal rates are universally scaled by κ^2. The toy data is created using the covariance matrix constructed under the principles outlined above and evaluated at the best fit point. The resulting distributions of the minimal χ^2 from the toy experiments thrown around the best fit point in μ is shown in Fig. 23. In Fig. 23 (a), the main effects leading to a deviation from the naive χ^2-distribution are deactivated: Absolute rate uncertainties are used instead of relative ones for all statistical and systematic errors, and the experimental uncertainties are symmetrized. As

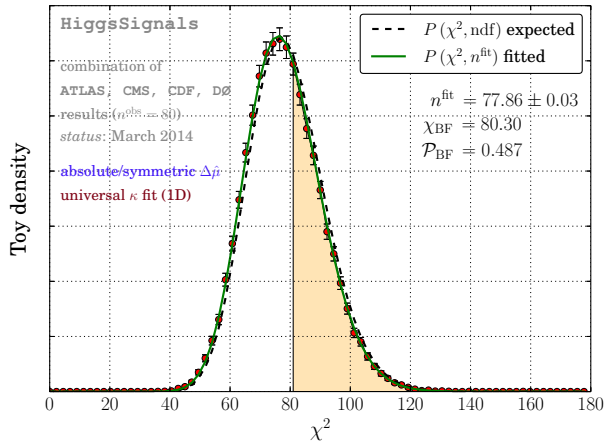

(a) Absolute and symmetrical rate uncertainties.

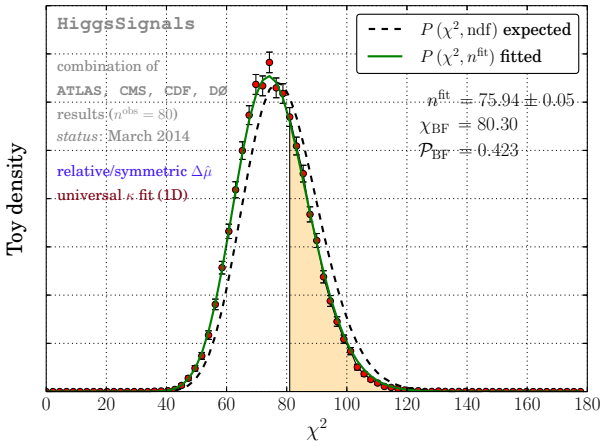

(b) Relative and symmetrical rate uncertainties

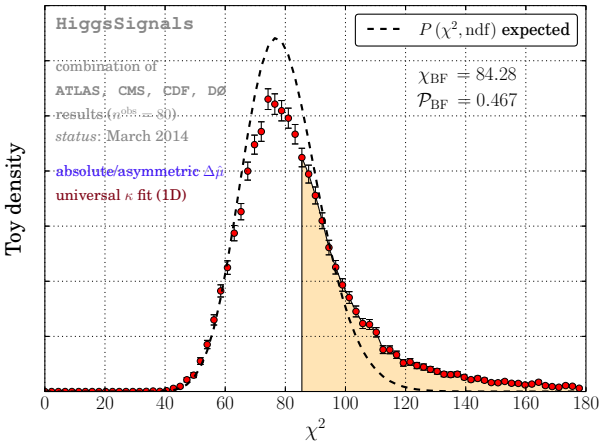

(c) Absolute and asymmetric rate uncertainties.

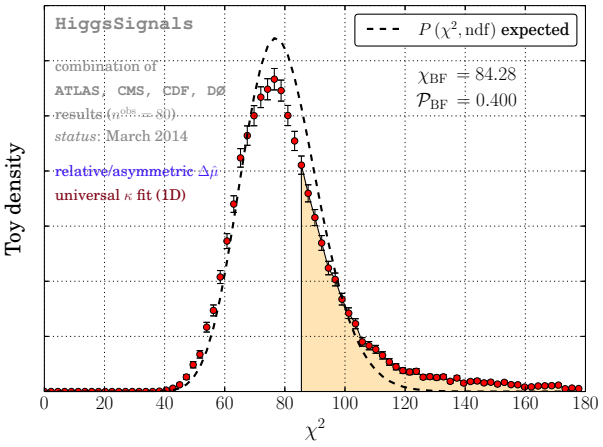

(d) Relative and asymmetric rate uncertainties.

Figure 23: χ^2 outcomes of the SM predicted Higgs rates tested against pseudo signal rate measurements in a fit setup with 80 rate measurements and one free parameter, a global scale factor κ for all Higgs couplings. The fits are performed with different `HiggsSignals` settings: In (a,c) the luminosity and theory rate uncertainties are kept at their absolute values whereas in (b,d) they are taken relative to the (pseudo-)measured signal rates as evaluated from the original measurements. In (a,b) the signal rate uncertainties $\Delta\hat{\mu}$ are implemented as averaged (symmetrical) values, while (c,d) asymmetrical upper and lower uncertainties as given in the original measurements are employed. The black dashed line shows the expected χ^2 distribution for 80 signal rate observables and one parameter. The solid, green graph shows the best-fitting χ^2 probability function to the toy outcomes. The yellow area underneath this curve as calculated from the observed best-fit χ^2 value (obtained from the original measurements) to ∞ corresponds to the $\mathcal{P}$-value.

expected, a nearly perfect χ^2 shape is obtained. The original best fit point is located at $\kappa^{\rm BF} = 0.977$ with $\chi^2_{\rm BF,abs/sym} = 80.3$. The $\mathcal{P}$-value is given by the area under the obtained χ^2 distribution for $\chi^2 \geq \chi^2_{\rm BF}$. In this treatment we obtain $\mathcal{P}^{\rm BF}_{\rm abs/sym} = 48.7\%$, indicating very good agreement of all Higgs

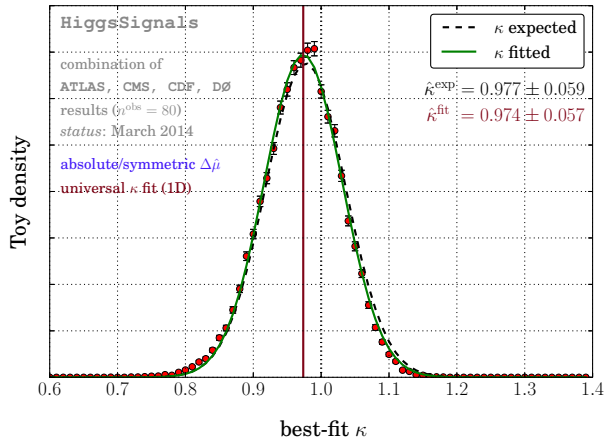

(a) Absolute and symmetrical rate uncertainties.

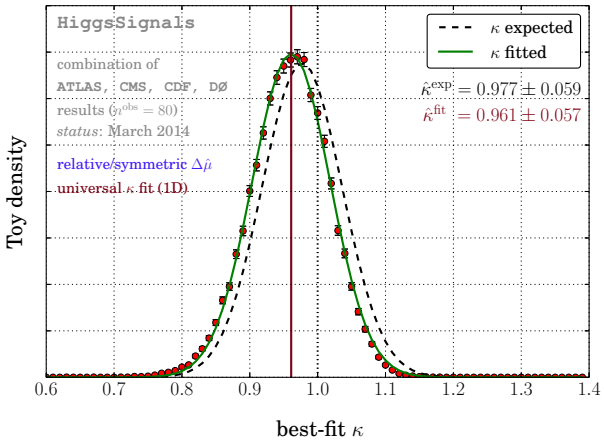

(b) Relative and symmetrical rate uncertainties

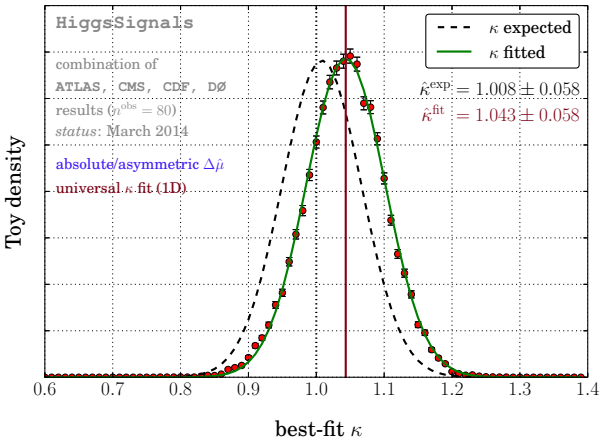

(c) Absolute and asymmetric rate uncertainties.

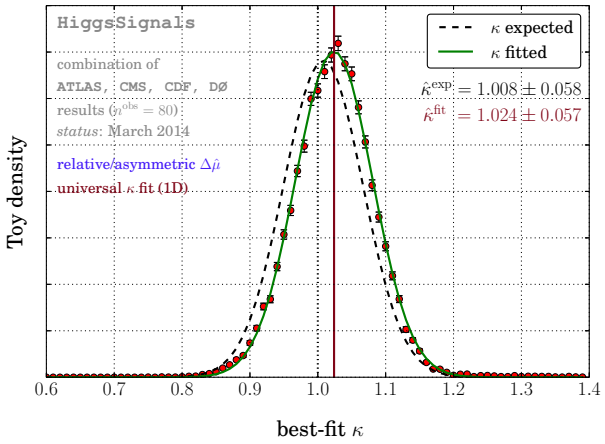

(d) Relative and asymmetric rate uncertainties.

Figure 24: Best fit values μ of the same toy fits and `HiggsSignals` settings as discussed in Fig. 23. The black dashed line shows the expected Gaussian distribution for the original best fit point and 1σ uncertainties extracted at $\Delta\chi^2=\chi^2-\chi^2_{\rm BF}=1$. The solid, green curve shows the fit of a Gaussian to the toy outcomes.

rate measurements with the toy model chosen here. Note, that the best fit point is extremely close to the SM (with $\kappa=1$), which features a $\chi^2_{\rm SM,abs/sym}=80.4$ in this treatment and thus a very similar $\mathcal{P}$-value.

The more realistic treatment of the uncertainties, however, has significant impact on the $\mathcal{P}$-value, as shown in Fig. 23(d). The full model dependence of the covariance matrix is used including relative errors and asymmetric experimental uncertainties. This is the most accurate approximation to the real likelihood distribution and thus provides a more accurate guess of the $\mathcal{P}$-value than the naive calculation above, where these effects have been ignored. The result $\mathcal{P}^{\rm BF}_{\rm rel/asym}=40.0\%$ differs from the previously obtained $\mathcal{P}^{\rm BF}_{\rm abs/sym}$. More importantly, the shape of the histogram of the obtained $\chi^2_{\rm min}$ values from the toy fits does not follow an ideal χ^2 distribution anymore. More toy outcomes

accumulate in the tail of the distribution at larger χ^2 values, thus leading to a slightly improved $\mathcal{P}$-value of the original best fit point than expected when assuming an ideal χ^2 shape. Toy MC studies like this will be of greater importance once the data is more precise, and in particular if significant deviations between the SM and the data emerge. χ^2 analyses that do not take into account the effects described above might thus lead to conclusion significantly deviating from the full results.

In order to show the origin of the deviation of the $\mathcal{P}$-value from the idealized implementation, Fig. 23(a), the two major effects yielding deviations from the naive expectation are singled out in Fig. 23(b) and (c). In Fig. 23(b), only the effect of relative errors, cf. item (2) above, is applied while the uncertainties are kept symmetrized. It can be seen that the treatment of relative uncertainties by itself has rather small effects. This is because the preferred range of the global scale factor κ is with $\Delta\kappa \sim 6\,\%$ already quite narrow. Hence, κ varies only in a small range and the impact from uncertainties varying with κ is rather insignificant. However, the picture will change in more complex models with more freedom in the variation of individual rates, including some of the benchmark scale factor fits that are discussed in Section 3.

In Fig. 23(c) the effect of asymmetric errors, cf. item (1) above, is studied. In this case we hold the values of the uncertainties fixed for every toy measurement (absolute uncertainties). It can be seen that for the $\mathcal{P}$-value this effect fully dominates the full implementation in Fig. 23(d) and should not be omitted in any implementation, since it could have a significant effect on the conclusion.

In Fig. 24 we show the toy distribution of the best fit global scale factor κ for the four different settings discussed above. Again, Fig. 24(a) shows the idealized result with absolute and symmetrized uncertainties and (d) shows the result from the full implementation of relative and asymmetric uncertainties. The same variations as explained for the $\mathcal{P}$-value can also be observed in the distribution of the best fit points. A small negative bias of about -1.6% in the universal coupling scale factor estimator κ is introduced by the relative uncertainties, as can be seen in Fig. 24(b). A much larger positive bias of the order of 3.5%, however, results from the correct treatment of asymmetric errors, cf. Fig. 24 (c). This stems from the fact that the experimental uncertainties are typically larger for variations in the upward direction as a direct consequence of the likelihood shape. As expected the full result in Fig. 24(d) is in between (b) and (c) since both biases apply, leading to an upward shift between expected and fitted universal scale factor of $\sim 1.6\%$. Note also, that the best-fit μ distribution happens to be systematically slightly narrower than what is expected from the naive χ^2 comparison, but in this case by only $\sigma_{\rm fit}/\sigma_{\rm exp} = 0.057/0.058$, which corresponds to a change of only $\lesssim 2\%$. We thus conclude that the Gaussian shape of the uncertainties is approximately preserved, and that the uncertainties derived from the profile likelihood in the main part of this paper are expected to be reliable estimates of the uncertainties obtained in a full MC toy based treatment, or even the full likelihood analysis in the experimental collaborations.

In summary, this simple toy model study shows that there are potentially significant effects affecting the evaluation of $\mathcal{P}$-values of arbitrary Higgs models tested against the signal rate measurements. These effects stem from non-Gaussian likelihood effects such as asymmetric uncertainties as well as different scaling behavior of systematic uncertainties with either the measured or predicted rates. Both effects are approximately accounted for in the χ^2 evaluation in `HiggsSignals`, leading to an outcome that does not strictly follow the naive expectation of an ideal χ^2 probability distribution with $n^{\rm dof} = n^{\rm obs} - n^{\rm par}$ due to visible changes in the $\chi^2_{\rm min}$ probability density function. In a detailed evaluation of the $\mathcal{P}$-value we therefore advice to take these effects into account by using toy experiments.

C Theoretical uncertainties of Higgs production and decay modes

The (correlated) uncertainties of the Higgs production and decay rates induced by the dependence on (common) parameters are evaluated as follows. We introduce a random variable x_i following a Normal distribution,

$$P_i(x_i;\alpha) = \frac{1}{\sqrt{2\pi}\alpha} \cdot e^{-\frac{x_i^2}{2\alpha^2}}, \tag{26}$$

for each common parametric dependence i. In particular, the following common parametric dependencies are of relevance:

- $i \in \{\alpha_s, m_c, m_b, m_t\}$ for the partial width uncertainties of *all* Higgs decay modes,
- $i = \text{PDF} + \alpha_\text{s}$ for the ggH and $t\bar{t}H$ cross section uncertainties,

The smearing of the common parameter, described by x_i, thus affects the resulting uncertainties of the corresponding production or decay modes in a fully correlated way (see also below). For the remaining parametric dependencies j, individual Normal-distributed random variables x_j^a are introduced per production or decay mode a, thus these uncertainty sources are regarded as uncorrelated. Similarly, the theoretical uncertainties corresponding to estimates of the missing higher-order corrections are described by individual (and thus uncorrelated) Normal-distributed variations, x_th^a, except in the case of WH and ZH production which are treated as fully correlated.

In Eq. (26), α is introduced as an artificial scale factor of the standard deviation of the parametric uncertainties. Usually, we choose $\alpha = 1$, corresponding to a 68% C.L. interpretation of the quoted uncertainties. For comparison, however, we define the setting 'LHCHXSWG-matched', where we adjust $\alpha = 1.5$ [1.7] for the cross section [partial width] uncertainties in order to approximately match with the uncertainty estimates given by the LHCHXSWG. Note that all (theoretical, correlated or uncorrelated parametric) variations are described by Eq. (26), hence, for simplicity, the scale factor α affects all variations in the same way.

We now employ a Monte-Carlo (MC) calculation, where each iteration k (also called "toy") is defined by throwing random numbers for the parametric and theoretical uncertainty variations, $k \equiv \{x_i, x_j^a, x_\text{th}^a\}_k$. Then, the production cross sections and partial widths predicted for this toy are evaluated as

$$\sigma_k^a = \overline{\sigma}^a + \sum_i x_i \Delta\sigma_i^a + \sum_j x_j^a \Delta\sigma_j^a + x_\text{th}^a \Delta\sigma_\text{th}^a, \tag{27}$$

$$\Gamma_k^a = \overline{\Gamma}^a + \sum_i x_i \Delta\Gamma_i^a + \sum_j x_j^a \Delta\Gamma_j^a + x_\text{th}^a \Delta\Gamma_\text{th}^a, \tag{28}$$

where $\overline{\sigma}^a$ and $\overline{\Gamma}^a$ are the central values of the production cross sections and partial widths in the SM, respectively, and $\Delta\sigma$ and $\Delta\Gamma$ their parametric or theoretical uncertainties as given in Ref. [9]. We take into account possibly asymmetric uncertainties:

$$\Delta\sigma, \Delta\Gamma = \begin{cases} \Delta\sigma^\text{upper}, \Delta\Gamma^\text{upper} & \text{for} \quad x > 0, \\ \Delta\sigma^\text{lower}, \Delta\Gamma^\text{lower} & \text{for} \quad x < 0. \end{cases} \tag{29}$$

Note, that $\Delta\sigma$ and $\Delta\Gamma$ can also be negative, depending on the response of the calculated quantity to the parameter variation. From the partial widths we can simply derive for each toy k the total decay

Mode	LHCHXSWG[1] from Ref. [9]	LHCHXSWG matched[2]	LHC-S1	LHC-S2	ILC
$\sigma(gg \to H)$ (ggH)	15.3%	15.6%	10.4%	5.2%	-
$\sigma(qq \to qqH)$ (VBF)	6.9%	5.6%	3.7%	1.9%	-
$\sigma(pp \to WH)$	3.3%	4.0%	2.7%	1.3%	-
$\sigma(pp \to ZH)$	5.7%	6.3%	4.2%	2.1%	-
$\sigma(pp \to t\bar{t}H)$	17.4%	15.6%	10.4%	5.2%	-
$\sigma(e^+e^- \to ZH)$	-	-	-	-	0.5%
$\sigma(e^+e^- \to \nu\bar{\nu}H)$	-	-	-	-	1.0%
$\sigma(e^+e^- \to t\bar{t}H)$	-	-	-	-	1.0%
Using a Gaussian-shaped parameter variation					
$\mathrm{BR}(H \to \gamma\gamma)$	4.9%	4.5%	2.7%	2.3%	1.3%
$\mathrm{BR}(H \to WW^{(*)})$	4.2%	4.3%	2.5%	2.3%	1.3%
$\mathrm{BR}(H \to ZZ^{(*)})$	4.1%	4.3%	2.5%	2.3%	1.3%
$\mathrm{BR}(H \to \tau^+\tau^-)$	5.7%	5.3%	3.1%	2.4%	1.6%
$\mathrm{BR}(H \to b\bar{b})$	3.3%	3.6%	2.1%	1.9%	1.1%
$\mathrm{BR}(H \to Z\gamma)$	8.9%	9.5%	5.6%	3.4%	2.8%
$\mathrm{BR}(H \to c\bar{c})$	12.2%	15.3%	9.0%	8.8%	4.5%
$\mathrm{BR}(H \to \mu^+\mu^-)$	5.9%	5.4%	3.2%	2.5%	1.6%
$\mathrm{BR}(H \to gg)$	10.1%	10.9%	6.4%	5.9%	3.2%

[1] Taken from Ref. [9], using (always the larger) uncertainty estimates for $\sqrt{s} = 8$ TeV, $m_H = 125.7$ GeV. Theoretical and parametric uncertainties are added linearly. In our *naive* fit, we use these numbers as maximum error estimates and neglect all correlations of common parametric uncertainty sources, total width, etc..

[2] Using an artificially enlarged range for the parametric variation of $\alpha = 1.5$ and 1.7 for the production cross section and partial width uncertainties, respectively.

Table 17: Relative theoretical uncertainties of LHC and ILC production cross sections and Higgs branching ratios for various implementations and future scenarios discussed in Tab. 9.

width, $\Gamma_k^{\mathrm{tot}} = \sum_a \Gamma_k^a$, and branching ratios, $\mathrm{BR}_k^a = \Gamma_k^a/\Gamma_k^{\mathrm{tot}}$. The covariance matrices are then given by

$$\mathrm{cov}(X)_{ab} = \langle X_a X_b \rangle - \langle X_a \rangle \langle X_b \rangle, \tag{30}$$

where $\langle\cdot\rangle$ denotes the arithmetic mean for the full toy MC sample and $X = \sigma, \Gamma$ or BR.

In Tab. 17 we give the relative uncorrelated uncertainties, given by $\mathrm{cov}(X)_{aa}/\overline{X_a}^2$, for the LHC production cross sections and Higgs branching ratios for the future scenarios 'LHC-S1', 'LHC-S2' and 'ILC' discussed in Tab. 9. These are compared with the uncertainty estimates given by the LHCHXSWG [9], where the parametric and theoretical uncertainties for a Higgs mass of $m_H = 125.7$ GeV and a (pp) center-of-mass energy of $\sqrt{s} = 8$ TeV are added linearly. For the scenario 'LHCHXSWG-matched' we employ the toy MC procedure with the artificial scale factor $\alpha = 1.5$ and 1.7 for the uncertainties of the production cross sections and branching ratios, respectively. We furthermore compared these uncertainty estimates with those obtained when using a uniform (box-shaped) smearing of the parametric and theoretical uncertainties instead of Eq. (26). The deviations found are rather small, being typically $\lesssim \mathcal{O}(10\%)$.

In order to investigate the impact of the different theoretical uncertainty implementations on the precision estimates of the Higgs coupling scale factors we perform the seven-dimensional scale factor

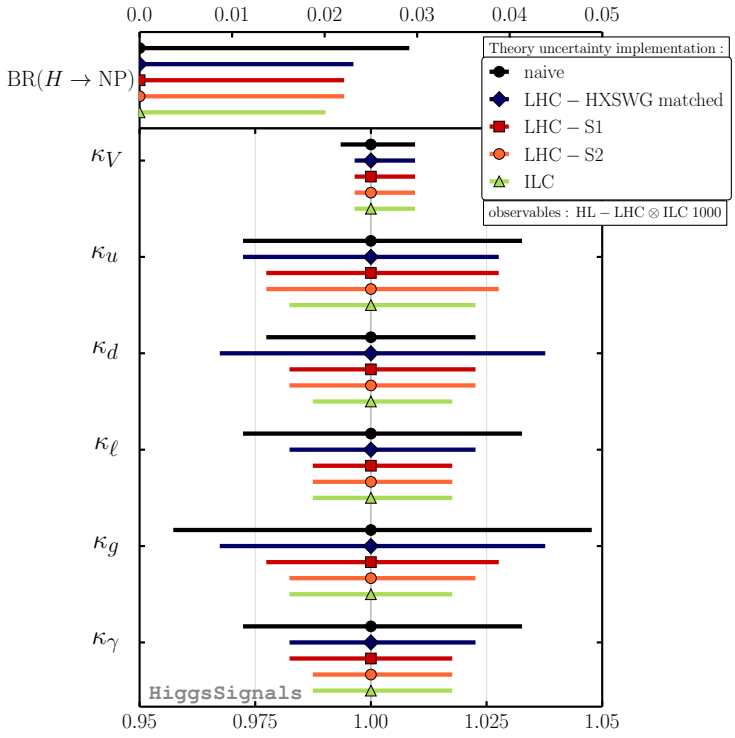

Figure 25: Comparison of Higgs coupling precision estimates obtained for various implementations of theoretical rate uncertainties. The comparison uses all available measurements from the HL–LHC and the ultimate ILC stage at 1 TeV with 1 ab^{-1} of data (and including measurements of previous ILC stages).

fit, cf. Sect. 3.6 and 4.1, to the same combined future projections for the high-luminosity LHC and all baseline ILC stages up to 1 TeV, 1 ab^{-1}, for all implementations. The result is shown in Fig. 25. Comparing the 'naive' implementation, where simply the estimates from the LHCHXSWG are taken (cf. Tab. 17) and all correlations among the cross section and branching ratio predictions are neglected, with the 'LHC-HXSWG matched' implementation, we see that for the latter, BR($H \to$ NP) and all scale factors except κ_d can be determined more precisely. Note, however, that the major effect causing these differences is actually the remaining mismatch of the uncertainty estimates, cf. Tab. 17, and not the inclusion of correlations. Nevertheless, as we have argued in this work, we find it more consistent to evaluate the covariances of the cross section and branching ratio predictions directly via the toy MC outlined above, leading to the uncertainty estimates denoted by 'LHC-S1'. Here, we find the largest differences to the 'naive' implementation in the achievable precisions of κ_d, κ_ℓ, κ_g and κ_γ, being $\mathcal{O}(1-2\%)$. As expected, in the scenarios with improved theoretical uncertainties the Higgs coupling precision is further improved, indicating that in this high-statistics scenario the theoretical uncertainties are a dominant limiting factor for the achievable precision.

References

[1] ATLAS Collaboration, G. Aad *et. al. Phys. Lett. B* **716** (2012) 1, [arXiv:1207.7214].

[2] CMS Collaboration, S. Chatrchyan *et. al. Phys. Lett. B* **716** (2012) 30, [arXiv:1207.7235].

[3] ATLAS Collaboration ATLAS-CONF-2013-034, ATLAS-COM-CONF-2013-035.

[4] ATLAS Collaboration ATLAS-CONF-2013-040, ATLAS-COM-CONF-2013-048.

[5] CMS Collaboration CMS-PAS-HIG-13-005.

[6] CMS Collaboration CMS-PAS-HIG-13-016.

[7] CDF and DØ Collaborations, T. Aaltonen *et. al. Phys. Rev. D* **88** (2013) 052014, [arXiv:1303.6346].

[8] LHC Higgs Cross Section Working Group, A. David, A. Denner, M. Duehrssen, M. Grazzini, *et. al.* arXiv:1209.0040.

[9] LHC Higgs Cross Section Working Group, S. Heinemeyer *et. al.* arXiv:1307.1347.

[10] R. Lafaye, T. Plehn, M. Rauch, D. Zerwas, and M. Duhrssen *JHEP* **0908** (2009) 009, [arXiv:0904.3866]; M. Klute, R. Lafaye, T. Plehn, M. Rauch, and D. Zerwas *Phys. Rev. Lett.* **109** (2012) 101801, [arXiv:1205.2699].

[11] T. Plehn and M. Rauch *Europhys. Lett.* **100** (2012) 11002, [arXiv:1207.6108].

[12] M. Klute, R. Lafaye, T. Plehn, M. Rauch, and D. Zerwas *Europhys. Lett.* **101** (2013) 51001, [arXiv:1301.1322]; B. A. Dobrescu and J. D. Lykken *JHEP* **1302** (2013) 073, [arXiv:1210.3342]; J. Espinosa, C. Grojean, M. Mühlleitner, and M. Trott *JHEP* **1212** (2012) 045, [arXiv:1207.1717]; G. Cacciapaglia, A. Deandrea, G. D. La Rochelle, and J.-B. Flament *JHEP* **1303** (2013) 029, [arXiv:1210.8120]; G. Belanger, B. Dumont, U. Ellwanger, J. Gunion, and S. Kraml *JHEP* **1302** (2013) 053, [arXiv:1212.5244]; J. Ellis and T. You *JHEP* **1306** (2013) 103, [arXiv:1303.3879]; A. Djouadi and G. Moreau arXiv:1303.6591; K. Cheung, J. S. Lee, and P.-Y. Tseng *JHEP* **1305** (2013) 134, [arXiv:1302.3794]; B. Holdom arXiv:1306.1564; S. Choi, S. Jung, and P. Ko *JHEP* **1310** (2013) 225, [arXiv:1307.3948].

[13] P. Bechtle, S. Heinemeyer, O. Stål, T. Stefaniak, and G. Weiglein *Eur. Phys. J. C* **74** (2013) 2711, [arXiv:1305.1933].

[14] G. Belanger, B. Dumont, U. Ellwanger, J. Gunion, and S. Kraml *Phys. Rev. D* **88** (2013) 075008, [arXiv:1306.2941].

[15] F. Caola and K. Melnikov *Phys. Rev. D* **88** (2013) 054024, [arXiv:1307.4935].

[16] J. M. Campbell, R. K. Ellis, and C. Williams *JHEP* **1110** (2011) 005, [arXiv:1107.5569].

[17] J. M. Campbell, R. K. Ellis, and C. Williams arXiv:1312.1628.

[18] J. M. Campbell, R. K. Ellis, and C. Williams arXiv:1311.3589.

[19] L. J. Dixon and Y. Li *Phys. Rev. Lett.* **111** (2013) 111802, [arXiv:1305.3854].

[20] M. R. Buckley and D. Hooper *Phys. Rev. D* **86** (2012) 075008, [arXiv:1207.1445].

[21] A. Arbey, M. Battaglia, and F. Mahmoudi *Eur. Phys. J. C* **72** (2012) 2169, [arXiv:1205.2557]; A. Arbey, M. Battaglia, A. Djouadi, and F. Mahmoudi *JHEP* **1209** (2012) 107, [arXiv:1207.1348]; S. Akula, P. Nath, and G. Peim *Phys. Lett. B* **717** (2012) 188, [arXiv:1207.1839]; J. Cao, Z. Heng, J. M. Yang, and J. Zhu *JHEP* **1210** (2012) 079, [arXiv:1207.3698]; K. Howe and P. Saraswat *JHEP* **1210** (2012) 065, [arXiv:1208.1542]; M. Drees *Phys. Rev. D* **86** (2012) 115018, [arXiv:1210.6507]; U. Haisch and F. Mahmoudi *JHEP* **1301** (2013) 061, [arXiv:1210.7806].

[22] P. Bechtle, S. Heinemeyer, O. Stål, T. Stefaniak, G. Weiglein, and L. Zeune *Eur. Phys. J. C* **73** (2013) 2354, [arXiv:1211.1955].

[23] A. Arbey, M. Battaglia, A. Djouadi, and F. Mahmoudi *Phys. Lett. B* **720** (2013) 153, [arXiv:1211.4004]; J. Ke, H. Luo, M.-x. Luo, K. Wang, L. Wang, *et. al. Phys. Lett. B* **723** (2013) 113, [arXiv:1211.2427]; A. Chakraborty, B. Das, J. L. Diaz-Cruz, D. K. Ghosh, S. Moretti, *et. al.* arXiv:1301.2745; A. Carmona and F. Goertz *JHEP* **1304** (2013) 163, [arXiv:1301.5856]; A. Arbey, M. Battaglia, and F. Mahmoudi *Phys. Rev. D* **88** (2013) 015007, [arXiv:1303.7450]; J. Cao, P. Wan, J. M. Yang, and J. Zhu *JHEP* **1308** (2013) 009, [arXiv:1303.2426]; B. Bhattacherjee, M. Chakraborti, A. Chakraborty, U. Chattopadhyay, D. Das, *et. al. Phys. Rev. D* **88** (2013) 035011, [arXiv:1305.4020]; D. Lopez-Val, T. Plehn, and M. Rauch *JHEP* **1310** (2013) 134, [arXiv:1308.1979]; A. Belyaev, M. S. Brown, R. Foadi, and M. T. Frandsen arXiv:1309.2097; J. Cao, F. Ding, C. Han, J. M. Yang, and J. Zhu *JHEP* **1311** (2013) 018, [arXiv:1309.4939]; A. Bharucha, A. Goudelis, and M. McGarrie arXiv:1310.4500; K. Cheung, J. S. Lee, and P.-Y. Tseng *JHEP* **1401** (2014) 085, [arXiv:1310.3937]; P. Bechtle, K. Desch, H. K. Dreiner, M. Hamer, M. Krämer, *et. al.* arXiv:1310.3045; J. Cao, C. Han, L. Wu, P. Wu, and J. M. Yang arXiv:1311.0678; A. Djouadi arXiv:1311.0720; R. Enberg, J. Rathsman, and G. Wouda arXiv:1311.4367; J. Cao, Y. He, P. Wu, M. Zhang, and J. Zhu *JHEP* **1401** (2014) 150, [arXiv:1311.6661]; L. Wang and X.-F. Han arXiv:1312.4759; J. Fan and M. Reece arXiv:1401.7671; G. Belanger, V. Bizouard, and G. Chalons arXiv:1402.3522; O. Stål arXiv:1402.6732.

[24] O. Stål and T. Stefaniak *PoS* **EPS-HEP** (2013) 314, [arXiv:1310.4039].

[25] J. M. Cornwall, D. N. Levin, and G. Tiktopoulos *Phys. Rev. Lett.* **30** (1973) 1268.

[26] C. Llewellyn Smith *Phys. Lett. B* **46** (1973) 233.

[27] LHC Higgs Cross Section Working Group, S. Dittmaier *et. al.* arXiv:1101.0593.

[28] LHC Higgs Cross Section Working Group, S. Dittmaier *et. al.* arXiv:1201.3084.

[29] R. V. Harlander, S. Liebler, and T. Zirke arXiv:1307.8122.

[30] M. Duhrssen, S. Heinemeyer, H. Logan, D. Rainwater, G. Weiglein, *et. al. Phys. Rev. D* **70** (2004) 113009, [hep-ph/0406323]; M. Duhrssen, S. Heinemeyer, H. Logan, D. Rainwater, G. Weiglein, *et. al.* hep-ph/0407190.

[31] P. Bechtle, O. Brein, S. Heinemeyer, G. Weiglein, and K. E. Williams *Comput. Phys. Commun.* **181** (2010) 138, [arXiv:0811.4169].

[32] P. Bechtle, O. Brein, S. Heinemeyer, G. Weiglein, and K. E. Williams *Comput. Phys. Commun.* **182** (2011) 2605, [arXiv:1102.1898].

[33] P. Bechtle, O. Brein, S. Heinemeyer, O. Stål, T. Stefaniak, *et. al. PoS* **CHARGED2012** (2012) 024, [arXiv:1301.2345].

[34] P. Bechtle, O. Brein, S. Heinemeyer, O. Stål, T. Stefaniak, *et. al. Eur. Phys. J. C* **74** (2013) 2693, [arXiv:1311.0055].

[35] S. Banerjee, S. Mukhopadhyay, and B. Mukhopadhyaya arXiv:1308.4860.

[36] I. Anderson, S. Bolognesi, F. Caola, Y. Gao, A. V. Gritsan, *et. al.* arXiv:1309.4819.

[37] A. Azatov and A. Paul arXiv:1309.5273.

[38] E. Boos, V. Bunichev, M. Dubinin, and Y. Kurihara arXiv:1309.5410.

[39] M. Chen, T. Cheng, J. S. Gainer, A. Korytov, K. T. Matchev, *et. al.* arXiv:1310.1397.

[40] G. Buchalla, O. Cata, and G. D'Ambrosio arXiv:1310.2574.

[41] S. Fichet and G. von Gersdorff arXiv:1311.6815.

[42] W. Buchmüller and D. Wyler *Nucl. Phys. B* **268** (1986) 621.

[43] R. Contino, M. Ghezzi, C. Grojean, M. Mühlleitner, and M. Spira *JHEP* **1307** (2013) 035, [arXiv:1303.3876].

[44] A. Pomarol and F. Riva *JHEP* **1401** (2014) 151, [arXiv:1308.2803].

[45] CMS Collaboration CMS-PAS-HIG-13-001.

[46] ATLAS collaboration ATLAS-CONF-2013-108, ATLAS-COM-CONF-2013-095.

[47] F. Boudjema, G. Cacciapaglia, K. Cranmer, G. Dissertori, A. Deandrea, *et. al.* arXiv:1307.5865.

[48] P. Bechtle and T. Stefaniak *available online at* http://higgsbounds.hepforge.org.

[49] K. Cranmer, S. Kreiss, D. Lopez-Val, and T. Plehn arXiv:1401.0080.

[50] H. Haario, E. Saksman, and J. Tamminen *Bernoulli* **7** (2001), no. 2 223.

[51] A. Patil, D. Huard, and C. J. Fonnesbeck *Journal of Statistical Software* **35** (2010), no. 4 1.

[52] P. Bechtle, S. Heinemeyer, O. Stål, T. Stefaniak, and G. Weiglein *available online at* http://higgsbounds.hepforge.org.

[53] A. Denner, S. Heinemeyer, I. Puljak, D. Rebuzzi, and M. Spira *Eur. Phys. J. C* **71** (2011) 1753, [arXiv:1107.5909].

[54] CMS Collaboration arXiv:1312.5353.

[55] G. Belanger, B. Dumont, U. Ellwanger, J. Gunion, and S. Kraml *Phys. Lett. B* **723** (2013) 340–347, [arXiv:1302.5694].

[56] J. M. Cline, K. Kainulainen, P. Scott, and C. Weniger *Phys. Rev. D* **88** (2013) 055025, [arXiv:1306.4710].

[57] H. K. Dreiner hep-ph/9707435; R. Barbier, C. Berat, M. Besancon, M. Chemtob, A. Deandrea, *et. al. Phys. Rept.* **420** (2005) 1, [hep-ph/0406039].

[58] H. Georgi and M. Machacek *Nucl. Phys. B* **262** (1985) 463; M. S. Chanowitz and M. Golden *Phys. Lett. B* **165** (1985) 105; J. Gunion, R. Vega, and J. Wudka *Phys. Rev. D* **42** (1990) 1673; S. Chang *JHEP* **0312** (2003) 057, [hep-ph/0306034].

[59] A. Falkowski, S. Rychkov, and A. Urbano *JHEP* **1204** (2012) 073, [arXiv:1202.1532]; S. Chang, C. A. Newby, N. Raj, and C. Wanotayaroj *Phys. Rev. D* **86** (2012) 095015, [arXiv:1207.0493]; J. Hisano and K. Tsumura *Phys. Rev. D* **87** (2013) 053004, [arXiv:1301.6455]; S. Kanemura, M. Kikuchi, and K. Yagyu *Phys. Rev. D* **88** (2013) 015020, [arXiv:1301.7303].

[60] ATLAS Collaboration ATLAS-CONF-2013-011, ATLAS-COM-CONF-2013-013.

[61] CMS Collaboration CMS-PAS-HIG-13-018.

[62] CMS Collaboration CMS-PAS-HIG-13-028.

[63] S. Heinemeyer, W. Hollik, and G. Weiglein *Comput. Phys. Commun.* **124** (2000) 76, [hep-ph/9812320].

[64] T. Hahn, S. Heinemeyer, W. Hollik, H. Rzehak, and G. Weiglein *Comput. Phys. Commun.* **180** (2009) 1426.

[65] U. Aglietti, R. Bonciani, G. Degrassi, and A. Vicini *JHEP* **0701** (2007) 021, [hep-ph/0611266].

[66] R. Bonciani, G. Degrassi, and A. Vicini *JHEP* **0711** (2007) 095, [arXiv:0709.4227].

[67] A. Djouadi, J. Kalinowski, and M. Spira *Comput. Phys. Commun.* **108** (1998) 56, [hep-ph/9704448]; M. Spira *Fortsch. Phys.* **46** (1998) 203, [hep-ph/9705337].

[68] R. Schabinger and J. D. Wells *Phys. Rev. D* **72** (2005) 093007, [hep-ph/0509209]; B. Patt and F. Wilczek hep-ph/0605188; V. Barger, P. Langacker, M. McCaskey, M. J. Ramsey-Musolf, and G. Shaughnessy *Phys. Rev. D* **77** (2008) 035005, [arXiv:0706.4311]; V. Barger, P. Langacker, M. McCaskey, M. Ramsey-Musolf, and G. Shaughnessy *Phys. Rev. D* **79** (2009) 015018, [arXiv:0811.0393]; G. Bhattacharyya, G. C. Branco, and S. Nandi *Phys. Rev. D* **77** (2008) 117701, [arXiv:0712.2693]; S. Bock, R. Lafaye, T. Plehn, M. Rauch, D. Zerwas, *et. al. Phys. Lett. B* **694** (2010) 44, [arXiv:1007.2645]; C. Englert, T. Plehn, D. Zerwas, and P. M. Zerwas *Phys. Lett. B* **703** (2011) 298, [arXiv:1106.3097]; C. Englert, T. Plehn, M. Rauch, D. Zerwas, and P. M. Zerwas *Phys. Lett. B* **707** (2012) 512, [arXiv:1112.3007]; G. M. Pruna and T. Robens *Phys. Rev. D* **88** (2013) 115012, [arXiv:1303.1150].

[69] K. Agashe, R. Contino, and A. Pomarol *Nucl. Phys. B* **719** (2005) 165, [hep-ph/0412089]; R. Contino, L. Da Rold, and A. Pomarol *Phys. Rev. D* **75** (2007) 055014, [hep-ph/0612048]; G. Giudice, C. Grojean, A. Pomarol, and R. Rattazzi *JHEP* **0706** (2007) 045, [hep-ph/0703164].

[70] G. Altarelli and R. Barbieri *Phys. Lett. B* **253** (1991) 161; M. E. Peskin and T. Takeuchi *Phys. Rev. D* **46** (1992) 381.

[71] M. Baak, M. Goebel, J. Haller, A. Hoecker, D. Kennedy, *et. al. Eur. Phys. J. C* **72** (2012) 2205, [arXiv:1209.2716]; M. Ciuchini, E. Franco, S. Mishima, and L. Silvestrini arXiv:1306.4644.

[72] T. Lee *Phys. Rev. D* **8** (1973) 1226; S. L. Glashow and S. Weinberg *Phys. Rev. D* **15** (1977) 1958; N. G. Deshpande and E. Ma *Phys. Rev. D* **18** (1978) 2574; J. F. Donoghue and L. F. Li *Phys. Rev. D* **19** (1979) 945; H. Haber, G. L. Kane, and T. Sterling *Nucl. Phys. B* **161** (1979) 493; L. J. Hall and M. B. Wise *Nucl. Phys. B* **187** (1981) 397; J. F. Gunion and H. E. Haber *Phys. Rev. D* **67** (2003) 075019, [hep-ph/0207010]; G. Branco, P. Ferreira, L. Lavoura, M. Rebelo, M. Sher, *et. al. Phys. Rept.* **516** (2012) 1, [arXiv:1106.0034].

[73] T. Cheng and M. Sher *Phys. Rev. D* **35** (1987) 3484.

[74] H. E. Haber and G. L. Kane *Phys. Rept.* **117** (1985) 75–263; J. Gunion and H. E. Haber *Nucl. Phys. B* **272** (1986) 1; J. Gunion and H. E. Haber *Nucl. Phys.* **278** (1986) 449; J. F. Gunion, H. E. Haber, G. L. Kane, and S. Dawson *Front. Phys.* **80** (2000) 1.

[75] F. Mahmoudi and O. Stål *Phys. Rev. D* **81** (2010) 035016, [arXiv:0907.1791]; A. Crivellin, C. Greub, and A. Kokulu *Phys. Rev. D* **86** (2012) 054014, [arXiv:1206.2634]; A. Crivellin, A. Kokulu, and C. Greub *Phys. Rev. D* **87** (2013) 094031, [arXiv:1303.5877].

[76] R. Hempfling *Phys. Rev. D* **49** (1994) 6168; L. J. Hall, R. Rattazzi, and U. Sarid *Phys. Rev. D* **50** (1994) 7048, [hep-ph/9306309]; M. S. Carena, M. Olechowski, S. Pokorski, and C. Wagner *Nucl. Phys. B* **426** (1994) 269, [hep-ph/9402253].

[77] CMS Collaboration CMS-PAS-HIG-13-004. Updated results (dated Dec 2013) taken from TWiki page: https://twiki.cern.ch/twiki/bin/view/CMSPublic/Hig13004TWikiUpdate.

[78] CMS Collaboration, S. Chatrchyan *et. al.* arXiv:1401.5041.

[79] CMS Collaboration, S. Chatrchyan *et. al.* arXiv:1401.6527.

[80] M. Carena, S. Gori, N. R. Shah, and C. E. Wagner *JHEP* **1203** (2012) 014, [arXiv:1112.3336]; M. Carena, S. Gori, N. R. Shah, C. E. Wagner, and L.-T. Wang *JHEP* **1207** (2012) 175, [arXiv:1205.5842]; L. Basso and F. Staub *Phys. Rev. D* **87** (2013) 015011, [arXiv:1210.7946].

[81] M. Carena, S. Heinemeyer, O. Stål, C. Wagner, and G. Weiglein *Eur. Phys. J. C* **73** (2013) 2552, [arXiv:1302.7033].

[82] K. Schmidt-Hoberg and F. Staub *JHEP* **1210** (2012) 195, [arXiv:1208.1683]; M. Hemeda, S. Khalil, and S. Moretti arXiv:1312.2504.

[83] P. Posch *Phys. Lett. B* **696** (2011) 447, [arXiv:1001.1759]; A. Drozd, B. Grzadkowski, J. F. Gunion, and Y. Jiang *JHEP* **1305** (2013) 072, [arXiv:1211.3580]; A. Cordero-Cid, J. Hernandez-Sanchez, C. Honorato, S. Moretti, M. Perez, *et. al.* arXiv:1312.5614.

[84] A. Arhrib, R. Benbrik, and N. Gaur *Phys. Rev. D* **85** (2012) 095021, [arXiv:1201.2644]; A. Goudelis, B. Herrmann, and O. Stål *JHEP* **1309** (2013) 106, [arXiv:1303.3010]; M. Krawczyk, D. Sokolowska, P. Swaczyna, and B. Swiezewska *JHEP* **1309** (2013) 055, [arXiv:1305.6266]; M. Krawczyk, D. Sokolowska, P. Swaczyna, and B. Swiezewska *Acta Phys. Polon. B* **44** (2013) 2163, [arXiv:1309.7880].

[85] A. Djouadi *Phys. Lett. B* **435** (1998) 101, [hep-ph/9806315]; M. S. Carena, S. Heinemeyer, C. Wagner, and G. Weiglein *Eur. Phys. J. C* **26** (2003) 601, [hep-ph/0202167].

[86] CMS Collaboration CMS-PAS-HIG-13-020.

[87] CMS Collaboration CMS-PAS-HIG-13-019.

[88] CMS Collaboration CMS-PAS-HIG-13-015.

[89] CMS Collaboration, https://twiki.cern.ch/twiki/bin/view/CMSPublic/ttHCombinationTWiki.

[90] European Strategy for Particle Physics Preparatory Group, R. Aleksan *et. al.*

[91] ATLAS Collaboration arXiv:1307.7292.

[92] ATLAS Collaboration ATL-PHYS-PUB-2013-014.

[93] CMS Collaboration arXiv:1307.7135.

[94] S. Dawson, A. Gritsan, H. Logan, J. Qian, C. Tully, *et. al.* arXiv:1310.8361.

[95] M. E. Peskin arXiv:1312.4974.

[96] D. Zeppenfeld, R. Kinnunen, A. Nikitenko, and E. Richter-Was *Phys. Rev. D* **62** (2000) 013009, [hep-ph/0002036].

[97] D. Asner, T. Barklow, C. Calancha, K. Fujii, N. Graf, *et. al.* arXiv:1310.0763.

[98] J. Campbell, K. Hatakeyama, J. Huston, F. Petriello, J. R. Andersen, *et. al.* arXiv:1310.5189.

[99] H. Baer, T. Barklow, K. Fujii, Y. Gao, A. Hoang, *et. al.* arXiv:1306.6352.

[100] T. Han, Z. Liu, and J. Sayre arXiv:1311.7155.

[101] I. Campos *et. al. Eur. Phys. J. C* **73** (2013) 2375, [arXiv:1212.4784].

[102] CMS Collaboration CMS-PAS-HIG-12-015.

[103] ATLAS Collaboration ATLAS-CONF-2013-030, ATLAS-COM-CONF-2013-028.

[104] ATLAS, G. Aad *et. al. Phys. Lett. B* **726** (2013) 88, [arXiv:1307.1427].

[105] ATLAS Collaboration ATLAS-CONF-2013-013, ATLAS-COM-CONF-2013-018.

[106] ATLAS Collaboration ATLAS-CONF-2012-091, ATLAS-COM-CONF-2012-109.

[107] ATLAS Collaboration ATLAS-CONF-2013-012, ATLAS-COM-CONF-2013-015.

[108] ATLAS collaboration ATLAS-CONF-2013-079, ATLAS-COM-CONF-2013-080.

[109] ATLAS collaboration ATLAS-CONF-2013-075, ATLAS-COM-CONF-2013-069.

[110] CDF Collaboration, T. Aaltonen *et. al. Phys. Rev. D* **88** (2013) 052013, [arXiv:1301.6668].

[111] CMS Collaboration, S. Chatrchyan *et. al.* arXiv:1312.1129.

[112] CMS Collaboration, C. Collaboration CMS-PAS-HIG-13-017.

[113] CMS Collaboration CMS-PAS-HIG-13-002.

[114] CMS Collaboration CMS-PAS-HIG-13-007.

[115] CMS Collaboration CMS-PAS-HIG-13-012.

[116] DØ Collaboration, V. M. Abazov *et. al. Phys. Rev. D* **88** (2013) 052011, [arXiv:1303.0823].